The Role of Metabolic Reprogramming in the Pathogenesis of Idiopathic Pulmonary Fibrosis

Dr Brintha Selvarajah

A thesis submitted to University College London for the degree of Doctor of Philosophy

Centre for Inflammation and Tissue Repair
UCL Respiratory
Division of Medicine
University College London

Acknowledgements

I am incredibly grateful to my academic supervisors Professor Rachel Chambers, Dr Paul Mercer and Dr Dimitrios Anastasiou for all the invaluable knowledge, fantastic support and guidance that you have provided throughout my studies. My experience with you has cemented my passion for science, changed the way I practise as a doctor and I hope will lead to a future career as an academic clinician.

A special thanks to Dr Ilan Azuelos, my fellow investigator, clinician and dear friend. I will be forever grateful for your knowledge, kindness and patience.

To all my colleagues in the Chambers group, I thank you for your expert knowledge, support and most importantly wonderful friendship.

I am grateful to our collaborators at GSK, especially Andy and Adam, for their expert support during my studies.

Thank you to the Crick-NIHR-BRC for their funding of my PhD.

Finally, a huge thank you to my family especially Oli and my parents for their unconditional love and support.

Declaration

I, Brintha Selvarajah confirm that the work presented in this thesis is my own. Where information has been derived from other sources, I confirm that this has been indicated in the thesis.

Abstract

Idiopathic pulmonary fibrosis (IPF) is a progressive fibrotic interstitial lung disease of unknown aetiology. It conveys a poor median survival of 3.5 years, a prognosis worse than many cancers. The pathomechanisms that contribute to IPF are not fully elucidated and treatment options remain limited.

Transforming growth factor-β (TGF-β) is a critical pro-fibrotic cytokine that drives fibroblast to myofibroblast differentiation resulting in excessive collagen deposition in the lung parenchyma. Subsequent distortion of the lung architecture leads to respiratory failure and ultimately death.

Metabolic reprogramming underlies many diseases including cancer and akin to cancer, enhanced 18F-FDG-PET has recently been observed in IPF patients, suggesting altered glucose metabolism may also be a feature of IPF pathology.

There is emerging evidence that alterations in the metabolism of myofibroblasts may be critical in fibroproliferative pathobiology. Recent work from our laboratory has shown that activation of the mTOR axis, a key metabolic regulator, is critical for regulating myofibroblast collagen synthesis.

This thesis identifies that TGF-β_1 enhances the production of activating transcription factor 4 (ATF4), the transcriptional master regulator of amino acid metabolism, to supply glucose-derived glycine to meet the amino acid requirements associated with

enhanced collagen production in response to myofibroblast differentiation.

Dissection of signalling pathways involved show that TGF-β_1 induced ATF4 production depends on the cooperation between canonical TGF-β_1 signalling through Smad3 and activation of mechanistic target of rapamycin complex 1 (mTORC1) and its downstream target eukaryotic translation initiation factor 4E-binding protein 1 (4E-BP1). ATF4, in turn promotes the transcription of genes encoding enzymes of the *de novo* serine-glycine biosynthetic pathway and glucose transporter 1 (GLUT1).

Taken together, this work identifies the TGF-β_1-mTORC1-ATF4 axis as a potential novel therapeutic target pathway for interfering with myofibroblast function in fibrosis.

Impact statement

Of all the fibrotic conditions, idiopathic pulmonary fibrosis (IPF) represents the most rapidly progressive and fatal, with a dismal median survival of just 3.5 years from diagnosis for patients not receiving anti-fibrotic therapy. The aetiology of IPF remains incompletely understood. The approval of pirfenidone and the successful repurposing of the oncology drug, the triple tyrosine kinase inhibitor, nintedanib for the treatment of IPF, represented a watershed moment in the development of anti-fibrotic agents. However, although these drugs slow lung function decline over time, they do not halt disease progression or significantly improve survival, so there remains a pressing need to develop new anti-fibrotic strategies.

Metabolic reprogramming underlies many diseases such as in cancer and there is emerging evidence suggesting that altered myofibroblast metabolism may also drive the fibroproliferative responses in IPF. Therefore the manipulation of altered metabolic signatures in IPF may represent a potential novel therapeutic strategy for this disease.

The work presented in this thesis describes the role of metabolic reprogramming during TGF-β_1 induced myofibroblast differentiation and collagen synthesis in the context of idiopathic pulmonary fibrosis.

In this study, I have identified a novel mechanistic model whereby the mTOR-ATF4 axis reconfigures the fibroblasts biosynthetic and

metabolic network to meet the collagen synthetic demands of TGF-β_1-induced myofibroblasts, the key effector cells in fibrosis.

Optimism is growing for the implementation of metabolism-targeting therapeutic strategies, including inhibiting glycolytic enzymes and kinase regulators of metabolism e.g mTOR, with a number of recent trials reporting good tolerability and efficacy in the oncology settings. The findings within this thesis, support the notion that targeting altered metabolic signatures might present novel therapeutic opportunities for the treatment of IPF and potentially other fibrotic conditions.

The work presented in this thesis has been presented at conferences nationally and internationally, opening discussions among researchers about the potential links between cellular metabolism and fibrosis. I have also won prizes locally and internationally as result of presenting these results. The data demonstrated in this thesis has also been published in open-access format in the peer–reviewed journal, Science Signaling.

Table of Contents

List of Figures

List of Tables

CHAPTER 1: INTRODUCTION

1.1 Idiopathic Pulmonary Fibrosis

Idiopathic pulmonary fibrosis (IPF) is a devastating, progressive fibrotic interstitial lung disease of unknown aetiology. It commonly affects males and is primarily seen in older adults between the ages of 40 and 70 years. The overall incidence in the UK is 4.6 per 100,000 per year with an annual increase in incidence of 11% between 1991 and 2003 *(1, 2)*. There is therefore an estimated 5000 new cases of IPF being diagnosed per year in the U.K. with a current prevalence of approximately 15000 cases. It conveys a poor prognosis with a median survival of only 3.5 years from diagnosis for patients not receiving anti-fibrotic therapy *(2)*. Approximately 5000 patients die per year from the disease and to put this into context with other fatal conditions, more people with IPF die each year than patients with lymphoma, ovarian cancer or leukaemia (2). Patients with IPF ultimately die of respiratory failure and pulmonary hypertension and in addition to premature death; patients suffer from considerable morbidity with marked and progressive exertional dyspnoea and cough.

1.1.1 Clinical and Pathological Features

IPF should be considered in all patients who present symptomatically with a chronic dry cough and exertional

breathlessness and clinically, with classical fine end-inspiratory bi-basal crackles on auscultation. International guidelines have defined diagnostic criteria for IPF, utilising specific clinical, radiological and histopathological features to aid physicians to use a multidisciplinary approach to achieve effective diagnosis and management of patients suspected with IPF.

As defined by the 2018 joint statement by the ATS/ERS/JRS/ALAT, the presence of a usual interstitial pneumonia (UIP) pattern, on radiology and histology, is essential for the diagnosis of IPF *(3)*. UIP classically presents with temporal and spatial heterogeneity. Radiologically, high resolution computed tomography (HRCT) will display reticular markings with cyst like 'honeycombing' abnormalities in a bi-basal, subpleural distribution *(3)*. Histologically, the fibrotic foci are the hallmark lesions in IPF, which are distributed alongside areas of normal lung parenchyma. The fibrotic foci are dense collections of alpha smooth muscle actin (αSMA) positive myofibroblasts embedded in a collagen type I rich extracellular matrix, overlaid by a damaged hyperplastic epithelium *(4)* (Figure 1.1).

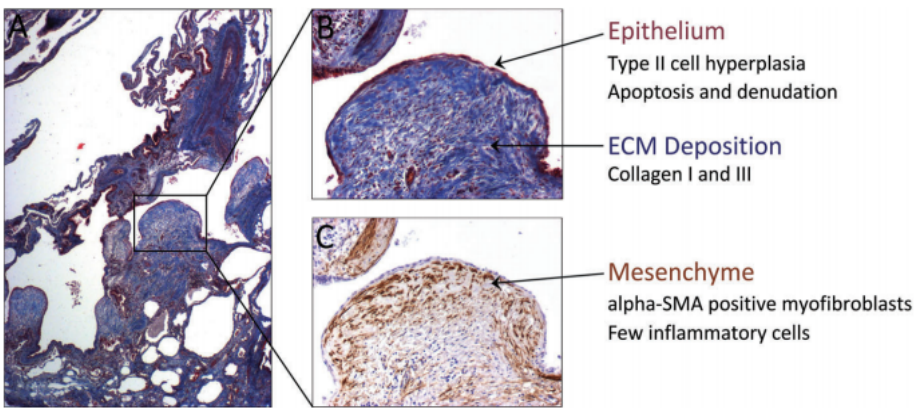

Figure 1.1 Fibrotic foci are the histological hallmark of IPF (**A**) Histological appearance of parenchymal lung tissue from an IPF patient. (**B**)

and (**C**) Fibrotic foci significantly distort lung architecture and are characterised by dense aggregation of αSMA positive myofibroblasts and collagenous extracellular matrix, overlaid with a hyperplastic epithelial layer. Image from (4), reproduced with permission from the publisher.

1.1.2 Current therapies

Unfortunately despite the clinical burden of IPF, there remains a paucity of effective treatments. For many years, the 'gold standard' triple therapy of prednisolone, azathioprine and N-acetyl cysteine (NAC) was used to address the inflammatory component of the disease. However the PANTHER trial in 2012 (clinicaltrials.gov identifier NCT00650091) revealed these drugs individually and in combination increased adverse events, hospital admissions and mortality in IPF patients *(5)*.

Two drugs have now been approved in the United States and Europe by the Food and Drug Administration (FDA) for the treatment of IPF: Pirfenidone and Nintendanib. Three large phase III randomised control trials, ASCEND (Pirfenidone) and INPULSIS-1/INPUSLSIS-2 (Nintendanib), demonstrated a reduction in the decline of forced vital capacity (FVC) annually, a marker of disease progression, in the treatment arm *(6, 7)*. Pirfenidone further increased progression-free survival with pooled data analysis demonstrating that treatment with pirfenidone for one year had a significant effect on mortality *(8)*. On a cellular and molecular level, pirfenidone has been shown to reduce growth factor-driven fibroblast proliferation and extracellular matrix production *in vitro (9)*. *In vivo*, pirfenidone decreases bleomycin induced pulmonary fibrosis in animal models *(10)*. The specific

molecular targets of this drug however remain unclear. Nintendanib was originally developed as an anti-angiogenic therapy in cancer and is a triple tyrosine kinase inhibitor that targets the receptors for vascular endothelial growth factor (VEGF), platelet derived growth factor (PDGF) and fibroblast growth factor (FGF), key pro-fibrotic mediators that have been implicated in IPF.

Although the discovery of pirfenidone and nintedanib represented a watershed moment for the development of anti-fibrotic therapeutics, these agents slow down progression rather than halt disease or reverse fibrotic changes in IPF. Furthermore, only patients with mild to moderate lung function (FVC between 50-80% expected) are eligible for these therapies, whereas 30% of the IPF population present with much worse lung function and therefore have no therapies currently available to them. Therefore there is a pressing clinical need to further our understanding of the molecular mechanisms that underlie the pathogenesis of IPF to reveal novel therapeutic targets.

1.2. Pathogenesis of IPF

As the name suggests, the aetiology of IPF is unknown and for many decades was thought to represent the end-result of chronic inflammation. However the recent observations of increased mortality and lack of efficacy with the use of immunosuppressive therapies has shifted this paradigm. The current consensus proposes that persistent and repetitive damage to the epithelium in

a genetically susceptible individual leads to a cycle of dysregulated wound healing.

The cause of injury is unclear and there are a number of potential injurious risk factors which have been implicated, including cigarette smoking *(11)*, gastro-oesophageal reflux *(12)*, type 2 diabetes *(13)*, exposure to occupation and environmental toxins *(14, 15)* and viral infections *(16)*.

A single nucleotide polymorphism (SNP) in the promoter of mucin 5B (MUC5B) gene has been identified as being significantly associated with sporadic and familial IPF *(17)*. MUC5B encodes a member of the mucin family of proteins, which contributes to the lubricating and viscoelastic properties of lung mucus. It is therefore important in airway host defence but the mechanism through which it contributes to fibrosis is not clear. Interestingly this SNP is associated with increased survival in IPF compared to patients who do not carry the gain of function variant *(18)*. In one cohort of IPF patients, enhanced bacterial load was noted in bronchoalveolar lavages (BALs) compared to control patients, however patients with MUC5B had significant lower bacterial burden, therefore potentially explaining the increased survival in these patients *(19, 20)*.

Familial IPF has been identified as the strongest risk factor for developing IPF and rare genetic variants in genes have been identified including genetic mutations of surfactant protein C (SP-C) and protein A2 *(21)*. Retention of misfolded surfactant proteins leads to ER stress in the epithelium and increased risk of alveolar

epithelial cell (AEC) apoptosis. Mutations in genes associated with telomere biology, such as *TERT* (telomerase reverse transcriptase) and *TERC* (telomerase RNA component*)* are also described in familial and sporadic IPF, where increased telomere shortening can disrupt the lung epithelial repair mechanisms *(22, 23)*. Two large genome wide association studies (GWAS) have identified multiple common genetic variants associated with susceptibility to IPF, including genes implicated with host defence, cell-cell adhesion and DNA repair *(24, 25)*.

The endpoint of normal wound healing is marked by the restoration of tissue integrity and normal function post-injury. In IPF, the regulation of key repair pathways during wound healing are dysregulated. These include uncontrolled activation of the coagulation cascade *(26)*, increased epithelial cell apoptosis and myofibroblast persistence *(27)*, increased oxidative stress *(28)* and abnormal epithelial-mesenchymal crosstalk *(29)*. These factors lead to a persisting fibrotic environment and why IPF is sometimes described as 'the wound that never heals'.

1.2.1 The role of the epithelium in IPF

Alveolar epithelial cell injury and their susceptibility to apoptosis are thought to be the key initiating events in IPF *(30)*. Transforming growth factor-β (TGF-β), the main pro-fibrotic cytokine implicated in IPF has been shown to promote epithelial cell apoptosis *(31)*. Other factors leading to increased susceptibility to apoptosis include reactive oxygen species (ROS) production secondary to cigarette smoke *(32)*, reduced

prostaglandin E2 (PGE2) levels *(33)* and angiotensin II released by fibroblasts *(34)*. The herpes virus and familial mutations of SP-C have also been implicated in the unfolded protein response (UPR) leading to endoplasmic reticulum (ER) stress and subsequent epithelial cell apoptosis *(21)*.

Recurrent epithelial injury leads to apoptosis, loss of basement membrane integrity and abnormal re-epithelisation. This leads to the formation of hyperplastic and hypertrophic type 2 alveolar cells which are a key source of major fibrogenic mediators, including TGF-β, platelet-derived growth factor (PDGF), endothelin-1 (ET-1), tumour necrosis factor alpha (TNFα) and connective tissue growth factor (CTGF) *(4)*. The pro-fibrotic milieu triggers mesenchymal cell expansion, myofibroblast differentiation and subsequent matrix deposition within the lung parenchyma, leading to progressive distortion of the lung architecture and subsequent respiratory failure and premature death.

Complex cross-talk between epithelial cells and myofibroblasts has also been described, where fibrogenic mediators released by the epithelium, trigger myofibroblasts in the fibrotic foci to release ROS and angiotensin II which can induce epithelial cell apoptosis *(35, 36)*. This feed forward mechanism alongside activation of pro-fibrogenic signalling cascades act to perpetuate the fibrogenic response in IPF.

1.2.2 The role of the fibroblast and myofibroblast in IPF

The fibroblast is mesenchymal in origin and is normally present in the adventitia of the vascular and airway structures of the lung. There is also a small resident population of fibroblasts in the healthy lung parenchyma until an injurious event signals fibroblast expansion and myofibroblast differentiation to facilitate lung repair and regeneration.

The myofibroblast is the key effector cell involved in wound healing as well as in driving the destructive changes in IPF. The source of the myofibroblast in IPF is debatable but potential sources include, resident fibroblast to myofibroblast differentiation and recruitment of CXCR4+ bone marrow derived fibrocytes *(4)*. However, a study has shown that deletion of the type 1 collagen gene in fibrocytes did not prevent the development of bleomycin-induced fibrosis in the mouse. Evidence has also pointed to the contribution of pericytes and epithelial cells to the mesenchymal populations in fibrosis *(4)*. However there has been conflicting data to show that these cell types do not express myofibroblast markers in genetic lineage tracing studies of transgenic mice exposed to the bleomycin model of fibrosis *(37)*. This suggests that the expansion of resident fibroblasts is the main contributor to the mesenchymal pool in IPF.

Regardless of cellular origin, key factors driving fibroblast to myofibroblast differentiation include TGF-β, mechanical stress from the tractional forces of resident fibroblasts during wound healing and proto-myofibroblast derived ED-A fibronectin *(38)*.

Myofibroblast differentiation is marked by the *de novo* expression and incorporation of αSMA into stress fibres which gives rise to the contractile properties required for wound closure *(39)*. The synthesis of collagen and other extracellular matrix proteins set down the scaffold for wound repair to occur. Myofibroblast apoptosis ensues once wound closure and tissue integrity is restored. Therefore the over-activation and persistent nature of myofibroblasts are crucial events during fibrosis. In IPF, myofibroblasts appear to be resistant to apoptosis and anti-proliferative signals, and seem more invasive, demonstrated by their ability to migrate into the matrigel matrix *in vitro (4)*. Furthermore the mechanical stiffness of the deposited matrix leads to activation of TGF-β via the integrin, αvβ5, promoting a feed forward loop of fibrogenesis *(40)*. There is also an observed imbalance of tissue inhibitors of metalloproteinases (TIMPS) and metalloproteinases (MMPS) which favours matrix accumulation *(41)*. The involvement of ECM turnover in IPF progression has been recently highlighted with MMP-degraded neoepitopes recently reported as biomarkers in predicting disease progression *(42)*.

1.2.3 Collagen biosynthesis

The extracellular matrix (ECM) is a highly dynamic and interlocking network of fibrous proteins and proteoglycans. It provides an essential scaffold for the cellular constituents and initiates and responds to biochemical and biomechanical signals required for tissue development, differentiation and homeostasis. ECM turnover is under tight regulatory control during wound repair

and aberrant tissue remodelling ensues, as in IPF, when this control is disrupted. As described earlier, IPF is characterised by the excessive deposition of matrix within the lung parenchyma leading to destruction of lung architecture and respiratory failure. There is also evidence that signals from the stiffened fibrotic extracellular matrix directly affects fibroblast phenotype to promote the translation of ECM genes, resulting in a self-perpetuating feed-forward loop *(43)*.

Collagen is the most abundant fibrous protein within the interstitial ECM. There are 28 known types of collagen, although types I and III have been shown to account for 95% of the total lung parenchymal collagen *(44)*. It is known that fibroblasts synthesise both collagen I and III but collagen I is known as the major contributor to the pathological features of IPF *(45)*. Indeed recent proteomic studies examining the composition of fibrotic ECM of decellularised lungs from IPF patients have identified an enriched type I collagen matrix compared to the normal lung *(46)*.

Collagen biosynthesis is a complex multi-stage process. Collagen I is a heterotrimer of two α1(I) (*COL1A1*) chains and one α2(I) (*COL1A2*) chain each containing 3330 Gly-X-Y repeats, where X and Y are proline, alanine or hydroxyproline (GLY; glycine). Collagen I α-chain genes, *COL1A1* and *COL1A2* are transcribed to mRNA and these also encode non-collagenous N and C terminal sequences. The N-terminal sequence guides the mRNAs to translation in the lumen of the rough ER *(47)*.

Critical post-translational modifications occur in the ER, including hydroxylation of proline and lysine residues and glycosylation of

lysine and asparagine residues. These post-translational modifications together with the formation of inter-chain disulphide bonds allow the formation of the three polypeptides to form into a triple helix as procollagen. Procollagen is then packed into vesicles and transported to the Golgi body, where oligosaccharides are added and then packed into secretory vesicles to be released into the extracellular matrix. Collagen peptidases in the extracellular matrix cleave the terminal N- and C-propeptides which allows spontaneous assembly of the collagen molecules into tropocollagen triple helices *(47)*. Lysyl oxidase catalyses the formation of covalent bonds between the tropocollagen molecules to form insoluble collagen fibrils in the matrix.

1.3 The role of TGF-β in IPF

TGF-β is a ubiquitous cytokine with key roles in the control of cell growth, differentiation, inflammation, tissue remodelling and to act as a tumour suppressor. There are three known isoforms in humans, TGF-β_1, TGF-β_2 and TGF-β_3, with TGF-β_1 being the most closely associated with IPF *(48)*. TGF-β_1 is critical in regulating connective tissue synthesis due to its ability to drive fibroblast to myofibroblast differentiation, increase ECM synthesis and inhibit matrix breakdown *(4)*. TGF-β_1 also increases the production of other pro-fibrotic and proliferative cytokines, including connective tissue growth factor (CTGF), fibroblast growth factor (FGF-2) and platelet derived growth factor (PDGF) *(49–51)* which propagate fibroblast proliferation, differentiation and matrix production. It also

down-regulates matrix turnover by tipping the balance in favour of increased synthesis of TIMPS versus MMPs.

The critical role of TGF-β_1 in the pathogenesis of IPF has been highlighted in a number of studies. Increased TGF-β_1 expression has been demonstrated in mesenchymal cells and alveolar macrophages in lung sections of IPF patients *(48)*. Furthermore, over-expression of TGF-β_1 results in lung fibrosis in animal models *(52)*, whilst inhibition of TGF-β_1 attenuates bleomycin-induced fibrosis in mouse models *(53)*. Although TGF-β_1 is strongly implicated in IPF, targeting TGF-β_1 has proved to be difficult. TGF-β_1 is required to maintain a number of homeostatic functions and previously studies targeting TGF-β_1 have been faced with safety issues where inhibition of TGF-β_1 leads to an overwhelming inflammatory cell infiltrate in the lung and other organs *(54)*.

1.3.1 TGF-β activation and signalling

TGF-β is synthesised by numerous cell types notably epithelial cells, macrophages and smooth muscle cells. It is secreted in association with its latency-associated peptide (LAP) and stored in the extracellular matrix, bound to the latent TGF-β binding protein (LTBP-1) by disulphide bonds. Before TGF-β can exert its biological effects, it must be disassociated from the LAP. This can occur through proteolysis, low pH, ROS, as well as by interaction with the epithelial integrin, αvβ6 *(55–58)*. αvβ6 is exclusively expressed in epithelial cells with low levels expressed in the normal lung. Elevated levels of αvβ6 are found in IPF and these correlate with survival in IPF patients. Injurious signals such as

thrombin and lysophosphatidic acid (LPA) induce cytoskeletal changes in the AECs which are transmitted to the cytoplasmic domains of αvβ6, which binds to the RGD motif of LAP. Activation of αvβ6 allows a conformational change in LAP, releasing TGF-β to act on adjacent cells. Inhibition of TGF-β_1 activation with αvβ6 antibodies significantly decreases bleomycin induced fibrosis in mouse models *(59)*. The importance of αvβ6 for TGF-β activation is now being explored at the clinical level, with a recently completed phase 2 trial, evaluating a human monoclonal antibody against αvβ6, STX 100, in IPF (NCT01371305).

Activated TGF-β signals via a heterotetrameric complex of type I (ALK1) and type II serine threonine kinase receptors, which leads to recruitment and phosphorylation of receptor-regulated SMADs (R-SMADs): Smad2 and Smad3. The phosphorylated R-SMADs form an oligomeric complex with the co-Smad, Smad4, and translocate to the nucleus where they interact with SMAD binding elements and co-factors (p300, AP-1 and FOXO1/3) to regulate gene transcription of numerous target genes including CTGF, PDGF and ECM proteins including collagen (Figure 1.2). Canonical TGF-β signalling is terminated by Smad7 which blocks and marks the type 1 TGF-β receptor for proteosomal-mediated degradation by binding to Smad specific E3 ubiquitin protein ligase 2 (Smurf2). Smad7 has also been shown to bind to DNA elements that are also targeted by Smad4, suggesting that Smad7 directly inhibits TGF-β-induced transcriptional responses in the nucleus. TGF-β classically signals through the SMAD pathway but is also known to activate non-canonical pathways, including mitogen activated protein kinases (MAPKs), small Rho GTPases and the

phosphatidylinositol-3-kinase (PI3K)/Akt and the mechanistic target of rapamycin (mTOR) signalling cascade.

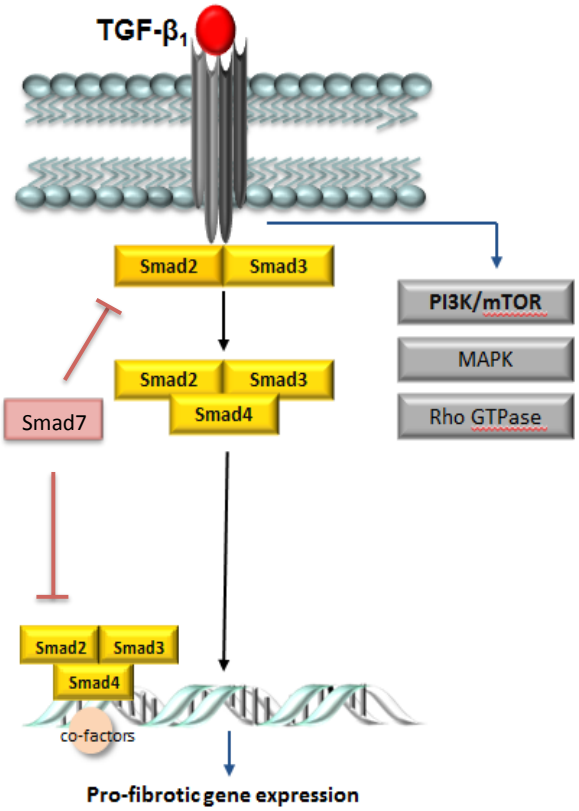

Figure 1.2 Canonical and non-canonical signalling pathways. TGF-β_1 binds to its receptor, leading to the phosphorylation of receptor-Smads 2/3, which then complex with Smad4 and translocate to the nucleus, where they interact with co-factors and induce transcriptional activation or repression of target genes. Smad7 acts to repress TGF-β_1 signalling.

1.4 The PI3K/mTOR signalling pathway

The PI3K/mTOR pathway is critically involved in a diverse range of physiological processes and aberrant activation of this pathway is associated with a number of diseases including cancer and diabetes *(60)*. Emerging evidence indicates that this pathway may also play a key role in the pathogenesis of IPF *(61)*.

1.4.1 PI3K signalling

The PI3 kinase (PI3K) family is divided into 3 classes based on their structure and substrate specificity. Class 1 PI3Ks (catalytic subunits p110α, p110β, p110γ and p110δ) are the most widely researched and defined group of PI3Ks. Traditionally, PI3Ks are activated by ligand binding to receptor tyrosine kinases (for example VEGF and PDGF), leading to receptor dimerization and autophosphorylation of tyrosine residues within the receptor and subsequent activation.

PI3 kinases phosphorylate phosphatidylinositol (PtdIns) lipid substrates, generating the lipid mediator, phosphatidylinositol-3,4,5-triphosphate (PIP_3). This phosphorylation event is negatively regulated by the tumour suppressor gene, phosphatase and tensin homolog (PTEN). PIP_3 activates a wide range of proteins containing lipid-binding pleckstrin homology domains (PH), including the serine threonine kinase, Akt. PIP_3 recruits Akt to the membrane and induces a conformational change to expose its phosphorylation sites. This allows PDK1, another serine threonine kinase, to phosphorylate Thr308, leading to partial activation of Akt and phosphorylation at Ser473 by mTORC2, leading to full activation of Akt *(62)*. The activation of Akt and other PH domain containing proteins, including tyrosine kinases (Tec family kinases), guanine exchange factors and GTPase-activating factors, facilitate a diverse range of cellular functions *(63)*.

1.4.2 mTOR signalling

The mechanistic target of rapamycin (mTOR) acts as a key metabolic rheostat that integrates intracellular and environmental cues (growth factor signalling, energy and amino acid levels) and regulates several downstream cellular events, including metabolism, autophagy and protein synthesis. mTOR has been implicated in many diseases, including cancer, genetic tumour syndromes, metabolic diseases, autoimmune diseases, neurological disorders and more recently in IPF.

mTOR forms the catalytic core of two distinct complexes known as mTOR complex 1 (mTORC1) and mTOR complex 2 (mTORC2) which are characterised by their different accessory proteins.

mTORC1 comprises mTOR, mammalian lethal with Sec13 protein 8 (mLST8), regulatory-associated protein of mTOR (RAPTOR), DEP-domain- containing mTOR interacting protein (DEPTOR) and proline rich Akt substrate 40kDA (PRAS40) proteins. RAPTOR knockout inhibits mTORC1 activity highlighting that it is a critical accessory protein for mTORC1 function. mLST8 is needed for the association of RAPTOR to mTOR and is known to enhance mTORC1 activity, whilst DEPTOR and PRAS40 are negative regulators of mTORC1.

The mTORC2 complex comprises mTOR, protein observed rictor-1 (PROTOR), DEPTOR, mLST8, different isoforms of mammalian stress activated protein kinase interacting protein (mSIN1) and rapamycin-insensitive companion of mTOR (RICTOR). RICTOR,

mLST8 and mSIN1 are necessary for the stability of mTORC1 whilst DEPTOR negatively regulates mTORC2 activity. The role of PROTOR remains unclear (Figure 1.3).

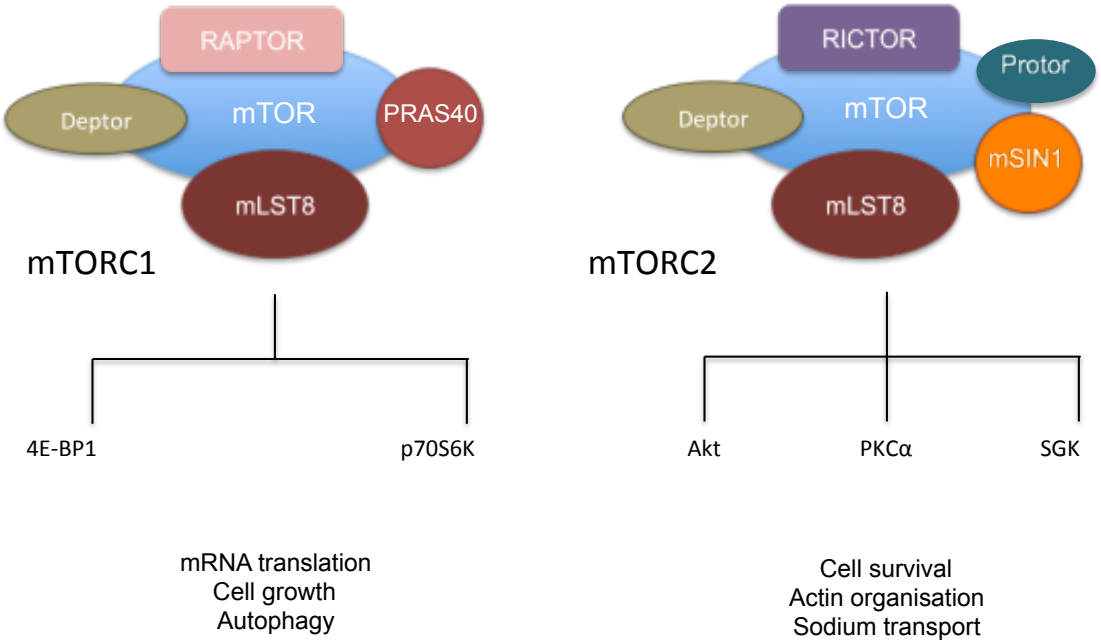

Figure 1.3 The distinct mTOR complexes. mTOR exists in 2 distinct complexes, mTORC1 and mTORC2, integrating upstream signals into unique downstream biological functions.

The mTOR complexes also differ in their regulation, downstream effectors and sensitivity to rapamycin. mTORC1 integrates a wide range of upstream signals, including growth factor signalling, energy status, nutrient availability and oxygen levels. mTORC2 is less well understood with regards to its upstream regulation and is largely insensitive to nutrient availability and energy *(64)*. It is postulated that activation may occur by growth factors and amino acid signalling via PI3K, however the precise mechanisms leading to mTORC2 stimulation are not fully understood.

Tuberous sclerosis complex (TSC) plays a key role in integrating environmental cues to regulate mTORC1. TSC is a heterodimer of TSC1 and TSC2 subunits, which acts as a GTPase-activating protein towards the small GTPase, RHEB (Ras Homolog Enriched in Brain), which inactivates RHEB and inhibits mTORC1 activity. Akt phosphorylates and inactivates TSC2, leading to RHEB activation and stimulation of mTORC1 activity. AMPK, a sensor of low cellular energy, also modulates mTORC1 activity through TSC2 phosphorylation leading to phosphorylation of RAPTOR to allosterically inhibit mTORC1 function *(65–67)*.

Independently of TSC1/2, increased levels of amino acids are known to activate mTORC1 through the Ragulator complex on the lysosomal membrane, which activates the RAG GTPases, RagA, RagB, RagC and RagD, which form heterodimeric complexes to recruit mTORC1 to the lysosomal membrane by binding to RAPTOR.

Activated mTORC1 drives cell growth by promoting mRNA translation and ribosome biogenesis through its downstream effectors, p70S6K and eukaryotic translation initiation factor (eIF4E) binding protein 1 (4E-BP1) and preventing autophagy via phosphorylation of ATG13 and ULK1. Phosphorylation of p70S6K increases ribosome biogenesis and increases the translation efficiency of mRNAs with complex 5'UTRS (untranslated region) through the phosphorylation of eIF4B to resolve the secondary structure*(68)*. 4E-BP1 is a critical regulator of the initiation phase of cap-dependent translation of the majority of eukaryotic mRNAs.

A 5' 7-methylguanosine (m7GTP) cap is co-transcriptionally added to the beginning of the 5'UTR of these mRNAs, which is recognised by eIF4F, a protein complex that regulates the initiation phase of cap-dependent translation. mTORC1 activation and subsequent phosphorylation of 4E-BP1, a negative regulator of cap-dependent translation is required to control the levels of eIF4F and binding to m^7GTP cap. At baseline, 4E-BP1 is phosphorylated on threonine 37, 46 and 70, bound to eIF4E and is therefore unavailable to bind to eIF4F to initiate cap-dependent translation. When mTOR is activated, hyperphosphorylation of serine 65 on 4E-BP1, leads to conformational change and allows its dissociation from eIF4E, to form a complex with eIF4F and initiate cap-dependent translation.

As well as regulating cap-dependent translation, mTORC1 positively regulates cellular metabolism and energy production by regulating the translation of hypoxia-inducible factor 1α (HIF-1α) and the oxidative capacity of mitochondria *(65)*. HIF-1α increases the transcription of key glycolytic enzymes; hexokinase (HK), phosphofructokinase (PFK), pyruvate kinase (PKM) and lactate dehydrogenase (LDH) in addition to the glucose transporters 1 and 3 (GLUT1 & 3). mTORC1 also increase lipid synthesis through transcription factors (e.g. sterol regulatory element binding protein [SREBP]) controlling genes involved in fatty acid and cholesterol synthesis that may be regulated through its downstream effector protein, p70S6K *(65)*.

mTORC2 activation results in phosphorylation of downstream effector proteins SGK1, protein kinase C-α (PKCα) and Akt. mTORC2 mediated hydrophobic motif (HM) phosphorylation of SGK1 is essential for its function as a regulator of sodium transport (53). In addition, mTORC2-dependent turn motif (TM) phosphorylation is essential for PKCα stability and signalling and is thought to regulate cytoskeletal organization by regulating Rho and Rac function *(64)*.

Akt activation affects a number of cellular processes including cell survival, proliferation, cell growth and increased glucose metabolism. Akt promotes cell survival by phosphorylating and inhibiting the pro-apoptotic proteins: BAD and caspase 9. It also phosphorylates FOXO1, FOXO3a and FOXO4 transcription factors which stops transcription of the pro-apoptotic Fas ligand and BIM protein *(69, 70)*. Akt activation also stimulates cell proliferation by phosphorylation and inhibition of cyclin-dependent kinase inhibitors p21 and p27 and glycogen synthase kinase-3 (GSK3) allowing the cell to advance through the cell cycle *(71, 72)*. Akt additionally promotes cell growth via activation of mTORC1 by phosphorylation and inactivation of tuberous sclerosis complex 2, or direct phosphorylation of PRAS40, an inhibitory subunit of mTORC1 *(65)*.

Akt promotes glucose uptake by stimulating the translocation of glucose transporter, GLUT4, to the cell membrane via phosphorylation of AS160, a Rab GTPase-activating protein, and upregulating the expression of GLUT1 *(73, 74)*. Akt also regulates glucose metabolism by controlling the rate of glycogen synthesis

through GSK3 and glycolysis via activation of the glycolytic enzyme, hexokinase (HK) and glycolytic activator, 6-phosphofructo-2-kinase (PFKFB3) *(75, 76)*(Figure 1.4).

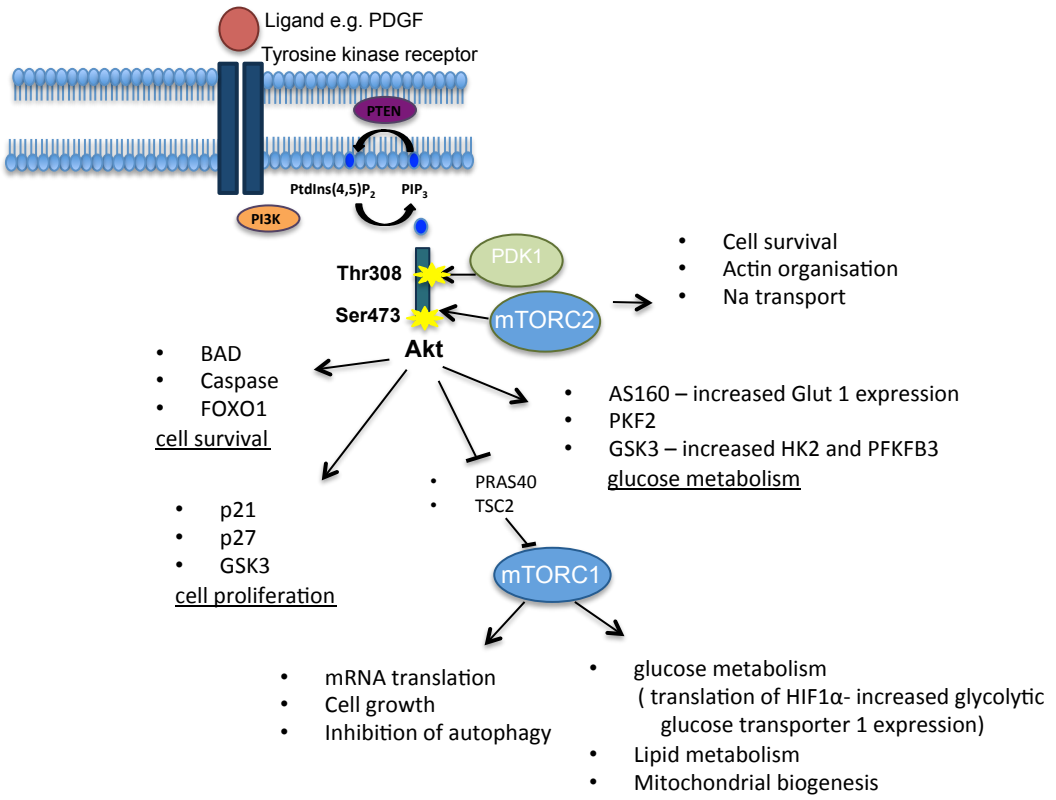

Figure 1.4 The PI3K/Akt/mTOR signalling pathway. PIP_3 recruits Akt to the plasma membrane where it is phosphorylated by PDK1 and mTORC2. Akt influences multiple downstream effects including mTORC1 activation and glucose metabolism. mTORC1 is activated upstream, by growth factors, energy status and nutrient availability whilst the mechanism through which mTORC2 is activated is less clear. Both mTOR complexes are important regulators of a number of cellular processes, protein synthesis, cell growth, proliferation and metabolism.

1.5 The role of TGF-β_1 induced PI3K/mTOR signalling in IPF

There is a wealth of evidence demonstrating a relationship between TGF-β signalling and the activation of the PI3K/mTOR pathway but the details of this interaction remain unclear *(77, 78)*. Moreover, there is conflicting evidence of the temporal kinetics of

TGF-β induced PI3K activation in fibroblasts. Whereas some studies have reported TGF-β induced SMAD activation is followed rapidly by Akt Ser473 phosphorylation *(79)*, another study displayed very delayed Akt phosphorylation in relation to Smad activation in human lung fibroblasts *(80)*. In addition, siRNA targeted knockdown of Smad3 in fibroblasts still displayed TGF-β induced Akt phosphorylation*(81)*. This suggests there are Smad dependent and independent pathways involved during TGF-β activation of PI3K signalling in fibroblasts *(79)*.

In the context of IPF, there is increased expression of class I PI3 kinase isoforms, notably p110γ, in the fibrotic foci of IPF lung tissue and fibroblast lines as well as activation of these pathways downstream of TGF-β *(82, 83)*. Immunohistochemical analysis of IPF lung sections also demonstrate evidence of Akt phosphorylation in myofibroblasts and in the hyperplastic epithelium of fibrotic foci, this is not observed in the mesenchymal cells of the normal lung parenchyma.

Low activity of the tumour suppressor, PTEN, has been demonstrated in IPF myofibroblasts and therefore may contribute to dysregulated PI3K signalling and fibrosis in IPF *(84)*. PTEN haplo-insufficient mice develop exaggerated pulmonary fibrosis in response to bleomycin injury and a specific PI3Kγ inhibitor has been shown to attenuate bleomycin-induced fibrosis in rodents *(85–87)*. PI3K inhibition also abolishes the protective effect of TGF-β against FAS mediated apoptosis of fibroblasts and apoptosis secondary to serum deprivation or loss of cell adhesion *in vitro*, maintaining the persistence of a pro-fibrotic mileu *(79, 88,*

89). Non-specific PI3K inhibition has also been shown to significantly reduce αSMA expression and the secretion of soluble collagen by TGF-β *(90, 91)*.

A pan PI3K/mTOR inhibitor, Omipalisib, which is being assessed in a phase 1 oncology clinical trial has been evaluated in a now completed proof of mechanism trial in IPF (https://clinicaltrials.gov/ct2/show/NCT01725139). Omipalisib has been shown to potently inhibit serum-induced proliferation of control and IPF fibroblasts, as well as significantly inhibit TGF-β induced collagen production by primary human lung fibroblasts. Furthermore, Omipalisib reduced collagen formation markers in *ex-vivo* slices of IPF lung tissue *(92)*. The phase 1 trial revealed acceptable tolerability of Omipalisib in subjects with IPF *(93)*.

Enhanced mTOR activation specifically has also been reported in TGF-β_1- activated normal human lung and IPF derived fibroblasts *(94–96)*. The mTOR pathway is also activated in pulmonary fibrosis with increased mTOR expression reported in hyperplastic AECs, mesenchymal cells in IPF lung tissue and in fibroblast cell lines. Furthermore, mTOR expression correlates with the degree of fibrosis and disease progression in a small study of IPF patients *(97)*. Our laboratory went on to dissect the contribution of the PI3K/mTOR signalling pathway to TGF-β_1-induced collagen synthesis and identified rapamycin-insensitive mTORC1-4E-BP1 signalling as critical for the response in control and IPF derived fibroblasts while PI3K/Akt activation was dispensable *(78)*. These data contrast with other studies that report a role for PI3K signalling in TGF-β- induced collagen synthesis *(98–100)*.

However the data was derived using PI3K inhibitors with broad actions on PI3K associated proteins, including mTOR *(101)*.

The most widely used mTOR inhibitors are rapamycin and the rapalogs (rapamycin analogs), but several adenosine 5′-triphosphate (ATP)–competitive mTOR inhibitors are also in advanced clinical development.

Rapamycin is historically known as an mTORC1 inhibitor that binds to the FKB12-rapamycin binding domain of mTOR to restrict the access of substrates to its catalytic site. However rapamycin insensitive mTORC1 signalling is now apparent. The avidly phosphorylated mTORC1 site on 4E-BP1 (Thr 37/46) is insensitive to rapamycin, but rapamycin readily inhibits the weakly phosphorylated mTORC1 sites (P70S6K [Thr38] and 4E-BP1 [Ser 65]). In contrast, the ATP-competitive dual mTOR inhibitor, AZD8055, can block all mTOR phosphorylation sites *(78, 102)*.

Whether mTOR contributes to the development of fibrosis as a result of its well-recognized immunomodulatory functions or by influencing fibroblast ECM deposition directly *in vivo* is still unclear.

1.6 Metabolic reprogramming and disease

Metabolic reprogramming underlies many diseases such as in cancer and diabetes and there is growing evidence suggesting that altered myofibroblast metabolism may also drive the fibroproliferative responses in IPF *(103, 104)*. Therefore the

manipulation of altered metabolic signatures in IPF may represent a potential novel therapeutic strategy for this disease.

Metabolic reprogramming, in its simplest terms, describes the process by which cells rewire their metabolic networks to support the requirements of exponential growth and proliferation and protect against oxidative stress. This can be a consequence of nutrient and oxygen availability but also downstream of signalling pathway activation. However, there is increasing evidence that changes in metabolism can also regulate signalling pathways and gene expression.

Protein acetylation of lysine residues and protein oxidation of cysteine resides are important regulators of cellular signalling pathways. Acetylation and protein oxidation require acetyl CoA and ROS respectively which are products generated in the mitochondria *(105)*. Epigenetic changes including methylation of histones involve donation of methionine through one carbon metabolic pathways and demethylation requires the TCA metabolite, α-ketoglutarate, for α-ketoglutarate dependent dioxygenases *(106)*. Metabolic pathways therefore can play a critical role in dictating a wide array of biological outcomes.

Almost a century ago, Otto Warburg and colleagues made the landmark discovery that cancer cells dramatically increased the uptake of glucose and that despite normoxic conditions, glucose was largely converted into lactate rather than used for oxidative phosphorylation; a phenomenon known as aerobic glycolysis or the “Warburg effect”*(107)*. Major advances in our understanding of

this phenomenon over the last decade culminated in the recognition that metabolic reprogramming is a key hallmark feature of cancer and that key oncogenic signalling pathways converge to adapt tumour cell metabolism, in order to support their growth and survival. As well as enhanced glucose uptake identified as distinctive and an early marker of malignant transformation, oncogene and growth factor (e.g. c-Myc, PI3K/Akt/mTOR, AMPK) induced expression of the ubiquitous glucose transporter type 1 (GLUT1) has been associated with increased glucose uptake observed in cancer *(108)*. The glucose-addicted nature of cancer cells is exploited clinically by the use of 18F-FDG PET/CT scans to detect cancers. 18F-FDG PET/CT measures glucose uptake by coupling the positron emitting 18F to glucose analog (FDG) which is taken up by cells but not subject to further metabolism. The reliance of cancer cells on increased glucose uptake has significantly improved tumour detection and monitoring.

Beyond the setting of cancer cell function, the recent study of immunometabolism has highlighted the role of metabolic reprogramming in shaping the innate and adaptive immune system. Characterising metabolic changes during the activation and differentiation of macrophages, T cells and dendritic cells has provided new insights into how these cells adapt their metabolic pathways to meet the demands of their function. It is also becoming increasingly evident that metabolic reprogramming can govern the phenotype of immune cells by controlling transcriptional and post-transcriptional events as well as their energy, anabolic and catabolic requirements *(109, 110)*. Activated T lymphocytes increase their glycolysis rates up to 50-fold compared to

unstimulated T lymphocytes. This is accompanied by increased expression of glucose transporters and glycolytic enzymes under the regulation of mTOR signalling *(109)*. Interestingly, increased glycolysis has been shown to influence cytokine translation during T cell activation. Glyceraldehyde-3-phosphate (GAPDH) is a glycolytic enzyme that converts D-glyceraldehyde 3-phosphate (G3P) into 3-phospho-glycerate during glycolysis. GAPDH can also regulate interferon-γ (IFN-γ) mRNA by binding to AU rich elements within the 3'UTR of IFN-γ mRNA, inhibiting its translation. Increasing glycolysis in activated T cells diverts GAPDH away from its inhibitory effect on IFN-γ mRNA translation and thereby promoting effective T cell cytokine production*(111)*.

There is also now growing evidence that metabolic reprogramming may therefore contribute to the pathogenesis of important non-oncological conditions, including Alzheimer's disease, obesity, cardiovascular disease, diabetes, ageing and notably, fibrosis. It is also appreciated that there is considerable mechanistic overlap, including some shared metabolic signatures observed between cancer and IPF *(112, 113)*.

1.6.1 Emerging role for altered metabolism in fibrosis

There is a growing body of evidence suggesting that altered myofibroblast metabolism may also drive fibroproliferative responses in IPF *(103, 114)*. Moreover, it is becoming apparent that IPF patients have a co-existing metabolic syndrome, which includes the combination of abdominal obesity, hypertension,

hyperlipidemia and insulin resistance. IPF patients are more likely to have diabetes and hypertension at diagnosis and metabolic syndrome is associated with mTOR activation *(115–118)*. Therefore, the manipulation of altered metabolic signatures in IPF may represent a potential and novel therapeutic strategy for managing this disease.

Glycolysis

Glycolysis describes the ten-step process through which glucose is broken down into pyruvate, with the free energy released used to generate the high-energy molecule, adenosine triphosphate (ATP), and the coenzyme, reduced nicotinamide adenine dinucleotide (NADH) (Figure 1.5). In the presence of oxygen, pyruvate is usually oxidised in the mitochondria to form ATP and CO_2 through the process of oxidative phosphorylation (OXPHOS). In contrast, under hypoxic conditions, pyruvate is reduced to lactate in the cytosol, a process referred to as anaerobic glycolysis. Despite OXPHOS generating approximately 18 times more ATP per glucose molecule compared to glycolysis, rapidly proliferating cancer cells even in the presence of sufficient oxygen demonstrate high rates of glucose uptake and lactate secretion (aerobic glycolysis). Otto Warburg proposed that this feature of aerobic glycolysis in cancer cells was a consequence of primary mitochondrial defects, which could be overcome by increasing glycolytic flux. However, this hypothesis has now been largely refuted based on the evidence that cancer cells have been shown to have intact mitochondrial function and generate ATP from both

glycolysis and oxidative phosphorylation, with the majority coming from the latter *(119)*.

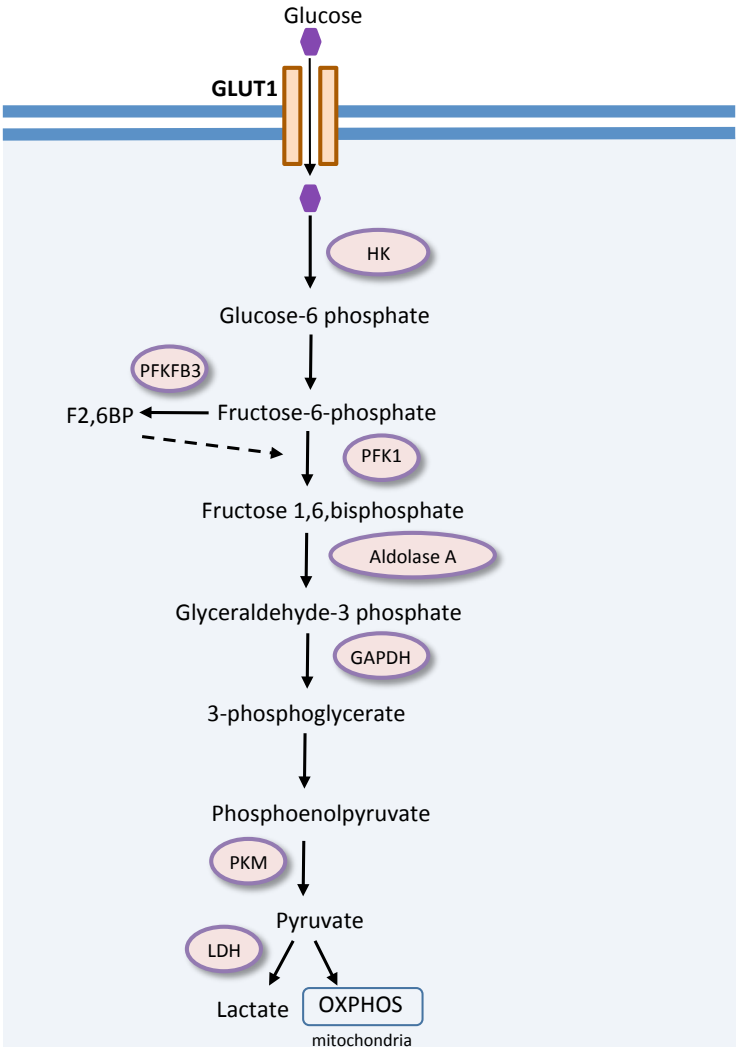

Figure 1.5 Glycolysis – Modified diagram of the key steps during glycolysis. Three irreversible steps are catalysed by HK (hexokinase), PFK1 (phosphofructokinase 1) and PKM (pyruvate kinase M). Fructose 2,6,bisphosphate is a potent stimulator of PFK1 and therefore glycolysis. Aerobic glycolysis is the preferential diversion of glucose into lactate production rather than oxidative phosphorylation despite oxygen-replete conditions. LDH; lactate dehydrogenase. GAPDH; glyceraldehyde-3-phosphate dehydrogenase. PFKFB3; 6-phosphofructo-2-kinase. OXPHOS; oxidative phosphorylation. GLUT1; glucose transporter 1.

Indeed, it was widely held that the high rates of glycolysis observed in cancer cells allows for a plentiful supply of glycolytic intermediates to feed macromolecular biosynthesis pathways in

rapidly proliferating cells *(107, 120)*. However a recent carbon labelling study in non-small lung cancer cell lines called this view into question by revealing that amino acids rather than glucose account for the majority of carbon mass in proliferating cells and that glucose represents an important source of ribose for nucleic acid replication and contributes to biomass by providing non-carbon materials, such as energy and reducing equivalents *(121)*. Additionally, there is now evidence supporting the "reverse Warburg phenomenon" in cancer cells, where surrounding stromal cells, notably cancer associated fibroblasts (CAFs), exhibit high rates of aerobic glycolysis resulting in the secretion of carbon rich intermediates, including lactate, to neighbouring cancer cells and thereby fuel oxidative phosphorylation and anaplerotic reactions *(122)*. Furthermore, increased lactate production creates a favourable tumorigenic environment by promoting tumour invasion and metastases through activation of MMPs and subsequent basement membrane disruption *(123)*.

The glucose-addicted nature of cancer cells has been exploited with the use of 18F-FDG PET/CT scans to detect certain cancers and monitor treatment response by coupling the positron emitting 18F to a glucose analogue (FDG) which is taken up by cells but not subject to further metabolism. The first clue indicating that enhanced glycolysis may also be a feature of IPF came from studies performed at University College London (UCL) demonstrating that 18F-FDG uptake is increased in the lungs of patients with IPF. The signal was further localised to areas associated with honeycombing, a radiological hallmark feature of IPF on high-resolution computed tomography (HR-CT)(87),

suggesting that these areas are metabolically active and may share the glycolytic phenotype of cancer. Interestingly, the FDG signal was subsequently also found to be higher in non-fibrotic areas of IPF lungs compared to control lungs, suggesting a global metabolic change may occur in IPF before radiological features of fibrosis are apparent *(124)*. Further work revealed that 18F-FDG PET uptake can potentially be used as a clinical biomarker to assess therapeutic response in fibrosis. For instance, pirfenidone was found to significantly reduce 18F-FDG uptake in the bleomycin murine model of lung fibrosis in mice *(125)*. Moreover, 18F-FDG PET uptake was found to predict progression-free survival in IPF and was independently associated with increased risk of mortality *(126, 127)*. In contrast, 18F-FDG uptake in the lungs of IPF patients did not appear to change over 3 months of currently approved anti-fibrotic treatment (nintedanib or pirfenidone) *(125)*. The interpretation of these findings however remains at the centre of an interesting debate around the potential confounding effect of increased lung density on the measured PET signal (tissue-fraction effect or TFE). Different methods of TFE correction have produced opposing observations with a recent study using dynamic imaging reporting that the 18F-FDG PET signal in the fibrotic areas of IPF patients is reduced when corrected for TFE *(128, 129)*. In contrast, a recent experimental medicine study focused on assessing the tolerability of the pan-PI3K/mTOR inhibitor, omipalisib, revealed an exposure-dependent reduction in 18F-FDG uptake in fibrotic areas of the lung *(93)*.

Further work is now required to improve current understanding of the signal and biological process underlying the uptake of 18F-

FDG PET in IPF and to identify which cell type(s) are responsible for the enhanced 18F-FDG PET signal. These clinical observations therefore prompted considerable research efforts aimed at furthering current understanding of the underlying mechanisms responsible for altered glycolysis, with a particular focus on (myo)fibroblast function.

Glucose uptake marks the first rate-limiting step of glycolysis, which is enhanced by the increased expression of glucose transporters. GLUT1 is the most commonly expressed glucose transporter in the lung and has found to be over expressed and promote tumorigenesis in non-small cell lung cancer *(130)*. IPF is classically described as a characteristic disease of the aging population, where overlap of perturbed cellular processes in aging and IPF contribute to accelerated fibrogenesis. Pulmonary fibrosis is enhanced in response to bleomycin injury in aged versus young mice and this was shown to be associated with increased GLUT1 mRNA and protein levels (105–107). GLUT1 expression has been reported to be raised in lung tissue from IPF patients and in the bleomycin model *(131–133)*.

Glycolysis culminates in the production of pyruvate, which can either be shuttled into the TCA cycle or converted into lactate by lactate dehydrogenase (LDH). Lactate excretion is therefore used as a surrogate marker of enhanced glycolytic flux and can be measured by commercially available kits, mass spectrometry or nuclear magnetic resonance (NMR). Extracellular flux analysis (e.g. Seahorse^{TM} Bioscience platform) allows the simultaneous analysis of extracellular acidification and oxygen consumption as

proxy measures of glycolysis and OXPHOS and has been used in multiple fibroblast studies. Extracellular acidification and enhanced lactic acid production has been reported to be a key feature of TGF-β_1-activated fibroblasts and critical for myofibroblast differentiation and collagen synthesis *(103, 134)*. Lactate levels are increased in IPF lung tissue *(103, 135, 136)* and in the murine model of bleomycin-induced fibrosis *(134, 137)*, however whether this reflects increased lactate production and glycolysis by myofibroblasts, at least in part, is not known.

It is also worth commenting that although many studies support the notion that TGF-β_1 stimulation of fibroblasts leads to an overall increase in lactate production and therefore glycolytic flux, this was not a universal finding. Indeed, one study demonstrated that IPF-derived senescent fibroblasts have a tendency towards reduced glycolysis, by demonstrating a reduced rise in the extracellular acidification rate (ECAR) of the surrounding tissue culture media, upon TGF-β_1 stimulation when compared to normal lung fibroblasts *(138, 139)*. However, whether this observation is restricted to a specific senescent IPF fibroblast population within the IPF lower lung lobes from which these particular fibroblasts were isolated remains unknown. It is also not clear if the conflicting data obtained in different laboratories might be reflective of cells representing different stages of the disease. By combining metabolomic and microarray analysis, a recent study recently reported that levels of glycolytic metabolites, including fructose 1,6-bisphosphate and phosphoenolpyruvate, were lower in IPF whole lung tissue relative to control lung and were accompanied by a decrease in the expression of PFK and PFKFB3. The same

study reported increased lactate levels, suggesting that glycolytic products might be funnelled into lactate production. Conversely, using a mass spectrometry-based metabolomics approach, others reported increased levels of glycolytic intermediates, which would suggest that there is either increased glycolysis or decreased glucose derived carbon utilisation in the IPF lung. Further investigation involving approaches such as metabolic flux analysis, is now clearly needed to reconcile these somewhat disparate findings. It is also worth bearing in mind that whole lung tissue studies in IPF represent a combined profile of resident and recruited immune cells, so that spatial-temporal heterogeneity of the disease process and the contribution of individual cell types, may be important factors influencing the data obtained *(135, 140)*.

The first study in this disease setting demonstrating that lactate levels are increased also reported that LDH5, one of the five LDH isoenzymes with the highest efficiency *(141)* to influence the conversion of pyruvate to lactate, was elevated at both the mRNA and protein levels during TGF-β_1-induced myofibroblast differentiation in control and IPF derived lung fibroblasts as well as in IPF lung tissue. Moreover, non-selective pharmacological inhibition of LDH using gossypol and siRNA silencing of LDH5, attenuated the TGF-β_1-induced increase in αSMA protein synthesis in control and fibrotic lung fibroblasts *(142)*. Gossypol not only prevented the development of fibrosis but also halted progression of fibrosis in the murine model of bleomycin-induced fibrosis *(137)*. The study investigators proposed that increased lactate production may provide a feed-forward loop for the activation of latent TGF-β_1 via a pH-dependent mechanism to drive

myofibroblast differentiation *(103)*. However, it is worth commenting that in anti-cancer trials gossypol was found to exert unspecific cytotoxic and genotoxic effects in mammalian cell types *(143)*. This lead to a study examining the effect of a specific small molecule inhibitor of LDH5, Tool Compound 408 (Genentech) on TGF-β_1-stimulated differentiation of primary human lung fibroblasts. Selective inhibition of LDH5 failed to decrease fibronectin, collagen and αSMA expression despite inhibiting the TGF-β_1-induced increase in lactate production. Additionally, neither knockdown of *LDHA* nor of *LDHB* (which encode gene products in varying combinations to generate all LDH1-5 isoforms) by siRNA inhibited fibroblast differentiation. In contrast, gossypol did exert an anti-fibrotic effect but by acting detrimentally on cell viability rather than through a specific effect on LDH5 *(137)*. Therefore, the role of increased lactate production during fibrogenesis remains unclear.

As discussed earlier, the mTOR axis has a number of critical functions including regulating glucose metabolism. Furthermore, there is now evidence that aberrant activation of the mTOR pathway plays a role in the pathogenesis of IPF (Section 1.5). In support of the potential translational significance of this finding, Omipalisib was found to induce an exposure-dependent reduction in 18F-FDG uptake in fibrotic areas of IPF lungs *(93)*. Understanding the interplay between glucose metabolism, the mTOR signalling axis and TGF-β induced fibrosis, may allow the development of selective targeted therapies in IPF.

1.7 Hypothesis and Aims

There is emerging evidence for potentially altered metabolic profiles and mTOR signalling within the primary lesions of the IPF lung. The key molecular mechanisms central to these biosynthetic alterations are poorly understood in the setting of IPF, and the tractability of therapeutic targets in this pathway is unexplored.

This thesis will examine the hypothesis that **mTOR plays a key role in promoting TGF-β_1 induced myofibroblast differentiation and extracellular matrix deposition in the setting of IPF by influencing glucose metabolism.**

In order to address this hypothesis I aim to:

- Examine the effect of TGF-β_1 on glucose metabolism in primary human lung fibroblasts.

- Determine the role of mTOR in regulating TGF-β_1-induced myofibroblast differentiation and collagen I deposition by primary human lung fibroblasts.

- Evaluate the role of mTOR in regulating glucose metabolism during TGF-β_1 induced collagen synthesis.

CHAPTER 2: MATERIALS AND METHODS

2.1 Chemical solvents and tissue culture materials

All chemicals were of analytical grade and obtained from Sigma Aldrich (UK) unless otherwise stated. All water used for the preparation of buffers was distilled and deionised using a Millipore Water Purification System (Milipore R010 followed by Milli-Q Plus, Milipore Ltd, UK). All sterile tissue culture media, sterile tissue culture grade trypsin/EDTA, antibiotics (penicillin/streptomycin) and fetal calf serum (FCS) were purchased from Thermo Fisher Scientific (UK). Bovine serum albumin was obtained from Merck Millipore (UK). Sterile tissue culture flasks, plates and disposable pipettes were obtained from Nunc (Denmark). Sterile polypropylene centrifuge tubes were obtained from Falcon (New Jersey, USA).

2.2 Cytokines

Transforming growth factor β_1 (TGF- β_1) was purchased from R&D Biosystems (UK) and was reconstituted in 4mM HCl/ 0.1% BSA (w/v) to 10 μ g/ml and stored in aliquots at -20° C.

2.3 Primary human fibroblast culture

Primary human fibroblasts (pHLFs) were grown from explant cultures of healthy control lung tissue, as previously described *(144)*. Human tissues were sourced ethically, and their research use was in accord with the terms of informed consents.

Institutional research ethics committee approval for this work was obtained from the University College London (UCL) Research Ethics Committee (12/EM/0058).

To avoid exposing cells to supra-physiological glucose and glutamine concentrations in standard Dulbecco's modified Eagle's medium (DMEM), pHLFs (passages 4 to 8) were cultured in glucose and glutamine-free DMEM (Thermo Fisher Scientific) that was supplemented with 10% fetal calf serum (FCS) (Sigma-Aldrich), 5 mM glucose, 0.7 mM glutamine (Thermo Fisher Scientific), and 1% penicillin (100 U/ml)– streptomycin (100 µg/ml) (Thermo Fisher Scientific). The RNA sequencing experiment utilised fibroblasts cultured in standard Dulbecco's modified Eagle's medium (DMEM) (Thermo Fisher Scientific) which contains 25mM glucose and 2mM glutamine. Table 2.1 lists the DMEM composition of low glucose and glutamine DMEM, standard DMEM and serum like DMEM.

	SMEM (serum like DMEM) (uM)	Low glucose (uM)	Standard (uM)
l-alanine	510		
Arginine	64	39	398
l-asparagine	41		
l-aspartic acid	6		
l-citrulline	55		
l-cystine	65	201	200
l-histidine	120		200
l-glutamic acid	98		
l-glutamine	650	700	2000
l-glycine	330	400	400
l-isoleucine	140	801	802
l-leucine	170	801	802
l-lysine	220	797	798
l-methionine	30	201	201
l-ornithine	80		
l-phenylalanine	68	400	400
l-proline	360		
l-serine	140	400	400
l-threonine	240	798	798
l-tryptophan	78	78	78
l-tyrosine	74	398	397
l-valine	230	803	803
Choline chloride	7	29	29
d-calcium patothenate	2	8	8
Folic acid	2	9	9
Niacinmamide	8	32	33
Pyridoxine hydrochloride	5	20	20
Riboflavin	0	1	1
Thiamine hydrocholride	3	11	12
i-inositol	11	40	40
Calcium chloride	1800	1801	1802
Magnesium sulfate	813	814	808
Potassium chloride	5330	5330	5333
Sodium bicarbonate	44050	44047	44048
Sodium chloride	118706	110344	110345
Sodium phosp monobasic	1010	906	2868
D- glucose	5560	5000	25000
Sodium pyruvate	100		1000
Taurine	130		
l-histidine		200	

Table 2.1 Media compositions

Cells were incubated in a humidified atmosphere containing 10% CO_2. The medium was removed and the cell monolayer was incubated with 5ml of 0.05% trypsin-ETDA at 37°C until cell detachment was observed. Trypsin was neutralised with DMEM containing 10% FCS and the cell suspension was centrifuged for 5 minutes at 300g at room temperature using a bench centrifuge (MSE Mistral 3000, UK). The supernatant was discarded and cell pellet split at 1:4 ratio before being re-suspended in 10% FCS MEM and transferred to new T175 flasks.

2.4 Cell preparation for experiments

For experiments, the fibroblast monolayer was trypsinised and the cell pellet prepared as above. The supernatant was discarded and the cell pellet brought into a single cell suspension with 10ml DMEM containing 10% FCS (v/v) by gentle mixing. An aliquot of the suspension was used to determine the cell count (Scepter 2.0 Handheld Automatic Cell Counter, Millipore). For each experiment, the cell density was adjusted with DMEM/10% FCS (v/v) to reach a concentration of $1x10^5$/ml, unless otherwise stated. Cells were grown to confluence and serum-starved for 12-24 hours prior to experimentation. Before each experiment, the serum-free medium was removed and replaced with fresh serum-free DMEM, with or without cytokines or inhibitors for a selected length of time.

All fibroblast cultures tested negative for mycoplasma. A pHLF cell line expressing a dominant-negative mutant form of 4E-BP1 was generated as described previously *(78)*. Cells were selected with puromycin (2 μg/ml) (Sigma-Aldrich) for 4 days.

Expression of the mutant 4E-BP1 was induced with doxycycline (1 μg/ml) (Sigma-Aldrich) for 24 hours before treatment with or without TGF-β_1. After 24 hours, pHLF lysates were analysed for ATF4 abundance by immunoblotting.

2.5 Real-time qPCR analysis of gene expression

2.5.1 RNA extraction from fibroblasts

Fibroblasts for RNA extraction were seeded into 12-well plates as previously described and samples collected at specified time-points following treatment. To minimise RNA degradation, all equipment and surfaces were cleaned thoroughly with RNaseZap (Sigma-Aldrich, UK) and filter pipette tips were used throughout. Qiagen RNeasy Mini kit was used to extract RNA. Supernatants were removed from tissue culture plates prior to the addition of 350μl /well of Buffer RLT (Qiagen). Cell lysates were then passed through a filter pipette tip several times, transferred to 1.5ml microcentrifuge tubes and frozen at -80°C if RNA was not immediately extracted.

If frozen, samples were thawed on ice and then placed at room temperature for 5 minutes before being centrifuged at 13200 rpm and 4°C for 2 minutes to remove any lysate from the lid of the tube. To each sample, 350 μl of 70% ethanol was added. The tubes were mixed thoroughly for 5-10 seconds using a vortex. 700μl of the sample was placed in a RNeasy Mini spin column and centrifuged for 15s at >8000 x g. The flow-through was discarded and 700 μl of Buffer RW1 (Qiagen) was added to the spin column

and centrifuged again. Flow-through was discarded and 500 μ l Buffer RPE (Qiagen) was added to the column and re-centrifuged. Flow-through was again discarded and the above step repeated. 30-50 μ l RNase-free water was added directly to the spin column and centrifuged to elute RNA.

2.5.2 DNase treatment

Contaminating genomic DNA was removed using the Precision DNase kit (Primer Design). RNA concentration and protein contamination were quantified on a Nanodrop spectrophotometer (Thermo Fisher Scientific) by measuring the A_{260} and $A_{260/280}$ ratios respectively. The $A_{260/280}$ ratio was used as a guide as the purity of the RNA sample; ratios between 1.7 and 2.0 were considered acceptable.

2.5.3 cDNA synthesis

cDNA was prepared by reverse transcription using qScript cDNA Supermix kit (Quanta Biosciences, USA). Up to 1µg of RNA sample was added to 4µl of qScript cDNA Supermix (5X reaction buffer containing optimized concentrations of MgCl2, dNTPs (dATP, dCTP, dGTP, dTTP), recombinant RNase inhibitor protein, qScript reverse transcriptase, random primers and oligo (dT) primers). A final volume of 20µl was achieved by the addition of nuclease free water. Samples were incubated for 5 minutes at 25°C, 30 minutes at 42°C and 5 minutes at 85°C.

2.5.4 Quantitative RT-PCR

Quantitative real-time polymerase chain reaction (qRT-PCR) was performed using the Power SYBR® Green PCR Master Mix (ThermoFisher Scientific, UK). 2 μ l of cDNA and forward and reverse primers were added at a final concentration of 800nM. Samples were run as duplicates on the Mastercycler EP Realplex (Eppendorf, Germany). Specific primers were designed to detect the expression of various genes (Table 2.2). PCR amplification was carried out for 40 cycles at a melting temperature of 95^{o}C for 15s and an annealing temperature of 60^{0}C for 60s. A dissociation curve was analysed for each PCR experiment to assess primer-dimer formation or contamination.

COL1A1 (F)	5’-ATGTAGGCCACGCTGTTCTT-3’
COL1A1 (R)	5’-GAGAGCATGACCGATGGATT-3’
ACTA2 (F)	5’-AATCCTGTGAAGCAGCTCCAG-3’
ACTA2 (R)	5’-TTACAGAGCCCAGAGCCATTG-3’
HKII (F)	5’-GGTGGAGTGGAGATGCACAA-3’
HKII (R)	5’-GAGGATGCTCTCGTCCAGG-3’
ATF4 (F)	5'-GCTAAGGCGGGCTCCTCCGA-3'
ATF4 (R)	5'-ACCCAACAGGGCATCCAAGTCG-3'
LDHA (F)	5’-GGAGATTCCAGTGTGCCTGT-3’
LDHA (R)	5’-GTCCAATAGCCCAGGATGTG-3’
LDHB (F)	5’-GGGAAAGTCTCTGGCTGATGAA-3’
LDHB (R)	5’-CTGTCACAGAGTAATCTTTATCGGC-3’
PFKFB3 (F)	5’-AAAAGTGTTCAACGTCGGGG-3’
PFKFB3 (R)	5’-CATGGCTTCCTCATTGTCGG-3’
PHGDH (F)	5’-GGAGGAGATCTGGCCTCTCT-3’
PHGDH (R)	5’-GTCATTCAGCAAGCCTGTCG-3’
PSAT1 (F)	5’-GCGGCCATGGAGAAGCTTAG-3’
PSAT1 (R)	5’-ATGCCTCCCACAGACACGTA-3’
PSPH (F)	5’-GAGGACGCGGTGTCAGAAAT-3’
PSPH (R)	5’-GGTTGCTCTGCTATGAGTCTCT-3’
SHMT1 (F)	5’-GTGACCACCACCACTCACAA-3’
SHMT1 (R)	5’-ACAGCAACCCCTTTCCTGTAG-3’
SHMT2 (F)	5’-GCTGCCCTAGACCAGAGTTG-3’
SHMT2 (R)	5’-GCAGAGGCCGAGCCG-3’
SLC2A1 (F)	5’-ACTGTCGTGTCGCTGTTTGT-3’
SLC2A1 (R)	5’-GATGGCCACGATGCTCAGAT-3’

Table 2.2 Primer sequences

Relative expression was calculated using $2^{-\Delta Ct,}$ and Δ Ct was calculated from the mean of two reference genes, ATP5B and β2 microglobulin (PrimerDesign Ltd.).

2.6 Immunoblotting

Adherent fibroblasts were washed with ice-cold phosphate-buffered saline and then lysed using PhosphoSafe extraction reagent (Merck Millipore) supplemented with protease inhibitor (Merck Millipore). Equal protein quantities of lysate were separated by SDS–polyacrylamide gel electrophoresis (SDS-PAGE) and transferred to nitrocellulose, and protein levels were assessed by Western blotting with the following antibodies: p70S6K [Cell Signaling Technology (CST) #9202], phospho-p70S6K Thr389 (CST #9234), 4E-BP1 (CST #9644), phospho-4E-BP1 Ser65 (CST #9451), SMAD3 (CST #9523), Rictor (CST #2114), Raptor (CST #2280), GLUT1 (Abcam #EPR3915), PHGDH (CST #13428), PSAT (Thermo Fisher Scientific #PA522124), PSPH (Insight Biotechnology #GTX109163-S), SHMT2 (CST #12762), ATF4 (CST #11815), α-tubulin (CST #9099), phospho-eIF2α (Ser51) (CST #3597), and eIF2α (#9722).

The dilutions of primary and secondary antibodies were according to the manufacturer's instructions. Tunicamycin (2 μg/ml; MP Biomedicals) was used as a positive control for immunostaining of p-eIF2α. Protein band intensity was measured by densitometry in ImageQuant TL v8.1 (GE Healthcare) after

electrochemiluminescence. All densitometries are presented relative to α-tubulin unless otherwise stated.

2.7 Determination of collagen type I deposition by high-content imaging

Extracellular collagen biosynthesis was measured in 96-well format by a high-content imaging–based macromolecular crowding assay as described previously *(78)*. pHLFs were seeded in a black-walled 96-well plate (Corning, USA) in 10% FCS DMEM (v/v) on day 1. On day 2, the medium was changed to DMEM containing 0.4% FCS (v/v). Macromolecular crowding medium was prepared by diluting ascorbic acid (final concentration 17µg/ml) in 0.4% FCS DMEM containing Ficoll 70 (37.5 mg/ml) and Ficoll 400 (25mg/ml) (Sigma Aldrich, UK) as molecular crowding agents. The medium was filter-sterilised with a 0.2µM filter (Thermo Fisher Scientific, UK). The medium on the wells was discarded to waste and replaced with 100µl of crowding medium. After serum starvation for 24 hours, pHLFs were treated in the presence or absence of TGF-β_1 (1 ng/ml) (R&D Systems) with compounds AZD8055 (1µM used unless otherwise stated; supplied by GSK), rapamycin (100 nm used unless otherwise stated; Millipore), NCT-503 (20 μM; Sigma-Aldrich), GSK2656157 (Cambridge Bioscience), 2DG (3 mM used; Sigma-Aldrich), or vehicle (0.1% DMSO). For rescue experiments, glycine (450µM; Sigma-Aldrich) and serine (Sigma-Aldrich) were used. Inhibitor concentrations were prepared by serially diluting 100% DMSO

10mM stock solution in crowding medium before application to the cells unless otherwise stated. The final DMSO concentration was 0.1% in all wells, including that of vehicle controls. Cells were incubated at 37°C in 10% CO_2 prior to stimulation with TGFβ_1 (1ng/ml) for 48 hours. pHLFs were fixed in ice cold methanol (VWR, UK), permeabilised with 0.1% (v/v) Triton-X-100 in PBS (Sigma Aldrich, UK) and stained with primary antibody specific for human collagen I (Sigma, C2456) or αSMA (Thermo Fisher Scientific, M085101-2) overnight at 4°C. Plates were washed three times with 0.05% (v/v) Tween-20 in PBS, followed by the addition of fluorescent Alex Fluor488 secondary antibody (Life Technologies, A11001) and nuclear DAPI to counterstain for cell count. Plates were incubated for 1 hour at room temperature followed by three final washes with 0.05% (v/v) Tween-20 in PBS. 200µl PBS was added to each well and the plates were stored at 4°C before imaging. Fluorescent signal was captured and quantified using ImageXpress Micro XLS high-content imaging system at 20X magnification (Molecular Devices), with four fields of view imaged per well and signal intensity normalized to cell count.

2.8 Histology and immunohistochemistry

All human samples were obtained with informed signed consent and with research ethics committee approval (10/H0504/9, 10/H0720/12, and 12/EM/0058). Patients with IPF were diagnosed in accordance with current international guidelines (61). Immunostaining for ATF4 and αSMA was conducted on 10 μ m

formalin-fixed paraffin-embedded serial sections of human lung biopsy material (n = 3 patients with IPF and n = 2 control subjects). Confocal dual immunofluorescence for ATF4 (Sigma, WH0000468M1) was enhanced with streptavidin conjugated with Alexa Fluor 488 (Thermo Fisher Scientific) and colocalized with primary goat polyclonal αSMA (Thermo Fisher Scientific #PA5–18292) labelled with donkey anti-goat Alexa Fluor 647 (Abcam) and counterstained with DAPI. Digitized images were captured on a Leica DM6000 CS microscope fitted with a Leica TCS SP8 confocal head and the Leica LAS X software suite (Leica Microsystems GmbH). All images are representative, and final images were prepared with ImageJ. Sections prepared by Dr Pascal Durrenberger (CITR) and immunostaining optimisation carried out in collaboration with Dr Pascal Durrenberger.

2.9 NMR spectroscopy

pHLFs were seeded in six-well plates at $2x10^5$ cells/ml and incubated in growth media for 3 days. Media were then replaced with serum-free media, and cells were further cultured for 24 hours, at which point they were treated with or without at TGF-β_1 (1 ng/ml). Cell supernatant was then collected and supplemented with 10% D_2O for shift lock and 1 mM trimethylsilylpropanoic acid (TSP) standard (Sigma). Using a 500-MHz Bruker machine, 1H-spectra were obtained using presaturation method after 128 scans. The resulting spectra were analysed using ACD Labs software (Advanced Chemistry Development UK Ltd.), and integrals of the 5.2 ppm peak and 1.3 ppm peak, corresponding to glucose and lactate, respectively, were quantified relative to the internal TSP

peak (0 ppm) standard.

2.10 3H-2DG uptake

pHLFs were seeded in six-well plates at 1 x 10^5 per ml and incubated in growth media for 3 days. Media were then replaced with serum-free media for 24 hours. The next day, cells were treated with or without TGF-β_1 at 1 ng/ml. After 22 hours of stimulation, media were changed to glucose-free media for 2 hours. Cells were then washed with 0.5 ml of Krebs-Ringer-Hepes (KRH) buffer. Cells were incubated in KRH buffer (2 ml per well) that contained 5 mM 2DG and 2-deoxy-[3H]glucose (0.625 μCi per well) (PerkinElmer) for 5 min. The cells were washed four times with KRH buffer and lysed with 0.05 mM NaOH for 2 hours at 37°C. Incorporated radioactivity in the cell lysate was determined by liquid scintillation counting.

2.11 Assessment of extracellular acidification and oxygen consumption

The Seahorse™ Bioscience XFe96 extracellular flux analyzer was used to measure OCR and ECAR. Briefly, pHLFs were seeded in XFe96 microplates at 1 x 10^5 per well and incubated for 3 days in growth media. Media were then replaced with DMEM containing 0.4% FCS for 24 hours. The next day, cells were treated with or without TGF-β_1 at 1 ng/ml, in the presence (or absence) of AZD8055. The following day, media were replaced with assay media prewarmed to 37°C supplemented with 5 mM glucose, 0.7 mM glutamine, and 1 mM pyruvate (Sigma, S8636).

Measurements of OCR and ECAR were performed after equilibration in assay medium (lacking supplemental CO_2) for about 45 min. Oligomycin (Sigma, O4876), FCCP (Sigma, C2920), antimycin A (Sigma, A8674), and rotenone (Sigma, R8875) were added to perform a mitochondrial stress test as per the manufacturer's instructions. Seahorse^{TM} experiments were performed by Dr Ilan Azuelos (CITR).

2.12 Lactate colorimetric assay

Extracellular lactate production in the culture medium was quantified with a lactate assay (Biovision II, USA). After fibroblasts were treated, 2µl of media was sampled at different time points over the 48 hours of treatment. Samples were diluted in assay buffer and mixed with lactate reaction mixture for 30 min at 37°C. The optical density of the mixture in each well was measured at 570nm wavelength on a microplate reader. The lactate concentration was calculated from a standard curve.

2.13 Transcriptomic analysis by RNA-seq

Confluent fibroblast monolayers were untreated ("media alone") or stimulated with TGF-β_1 (and media) (1 ng/ml; porcine origin; R&D Systems, USA) for 24 hours with or without AZD8055 (1µM; synthesized and provided by GSK) or rapamycin (100 nM; Merck Chemicals) in standard DMEM (n = 4 biological replicates per condition). Total RNA was extracted with miRCURY RNA Isolation Kit (Exiqon). Polyadenylate-tailed RNA enrichment and library preparation were performed using the KAPA Stranded mRNA-Seq Kit with KAPA mRNA Capture Beads (KAPA Biosystems,

Wilmington, MA, USA). Paired-end RNA-seq was performed with the NextSeq sequencing platform (Illumina, San Diego, CA, USA). Read preprocessing and alignment to the genome (Homo sapiens UCSC hg19) were performed using STAR aligner. Counts were normalized using the R package DESeq2, then log2-transformed with an offset of 1, and filtered to remove genes with an average count <1 across all samples. This left 15,959 genes that were then interrogated using the WGCNA package in R. Briefly, gene coexpression similarity was estimated by generating an absolute Pearson product moment correlation matrix. Using a soft threshold of 20, an adjacency matrix was calculated and used to estimate the topological overlap and assign genes to modules. Highly correlated modules were merged usifng a cut height of 0.06 on the topological matrix dendrogram. Sixty-five modules were returned and assigned colors as names. MetaCore (Thomson Reuters) was used to run pathway enrichment analyses and interaction network analyses on each of the 65 modules. OCN analysis was performed using the MetaBase R packages licensed from Clarivate Analytics and identifies one-step away direct regulators of the dataset that are statistically overconnected with the objects from the dataset. The P value of overconnectivity was calculated using hypergeometric distribution. The RNA sequencing (RNA-seq) dataset (GSE102674) was provided by Dr Hannah Woodcock and Dr Manuela Plate (CITR) and WGCNA was performed by Dr Adam Taylor (GSK).

2.14 In silico prediction of SMAD2/3/4 binding sites in the ATF4 promoter

The ATF4 promoter sequence was obtained from the eukaryotic promoter database (EPD) (Homo sapiens version 6; https://epd.vital-it.ch/human/human_database.php) *(145)*. SMAD2/3/4 binding site prediction was performed using web-based applications: EPD Search Motif Tool (using a cutoff P value of 0.001), PROMO (http://alggen.lsi.upc.es/cgibin/promo_v3/promo/promoinit.cgi?dirDB=TF_8.3) *(146)* (selecting eukaryote for factor's and site's species), and ConTra V3 (http://bioit2.irc.ugent.be/contra/v3/#/step/1) *(147)* (selecting visualization as type of analysis, human as reference organism, and ATF4 sequence under identification number NM_182810). The consensus binding site was obtained from the JASPAR database (http://jaspar.genereg.net/matrix/ MA0513.1/).

2.15 ATF4 protein stability

Lysates were prepared from pHLFs stimulated with TGF-β_1 (1 ng/ml) for 13 hours before pre-treatment with DMSO or lactimidomycin (LTM; 1 μM; Merck Millipore #506291) for 5 min, followed by exposure to DMSO or AZD8055 (1 μM) for 0, 10, 20, 30, or 60 min before lysis. Immunoblotting was used to analyse the abundance of ATF4 normalized to α-tubulin.

2.16 RNA interference

For the determination of collagen deposition by molecular crowding assay, pHLFs were grown to confluence in our standard growth media in 96-well plates. During the serum starvation period in growth media containing 0.4% FCS, cells were transfected with 10nM siRNAs (Dharmacon, SMARTpool) targeting *ATF4*, *PHGDH*, and *SMAD3* using RNAiMAX Lipofectamine (Invitrogen) according to the manufacturer's instructions. The following day, the media were replaced by Ficoll-containing media, and the macromolecular crowding assay was performed as described above.

For Western blotting and qPCR experiments, confluent pHLFs in 12-well plates were starved in serum-free media and transfected with 10 nM siRNA (Dharmacon) using RNAiMAX Lipofectamine (Invitrogen) according to the manufacturer's instructions. The following day, the media were replaced with fresh serum-free media with or without TGF-β_1 (1 ng/ml) for the indicated time points.

2.17 CRISPR-Cas9 gene editing

Our protocol was based on published protocol on CRISPR-Cas9 genome editing of primary human lung fibroblasts *(148)*. Performing gene editing in low-passage primary fibroblasts is difficult due to an inability of the cells to proliferate indefinitely from a single cell and not amenable to monoclonal selection or clonal expansion following gene editing. Therefore the above protocol was used, which uses a pool of edited cells (bulk cell culture) and high editing efficiency was evaluated by western blotting. Mix 1μL

of crRNA with 1μL tracrRNA plus 2μL IDT duplex buffer in a 0.5mL eppendorf tube. Anneal the RNAs at 95°C for 5 mins. Mix 2.9μL of annealed RNA with 1μL Cas9. Incubate for 10min. Put in a 15mL falcon tube, 2.5 x 10^5 cells per gRNA. Add PBS to reach 5mL and centrifuge. Add 0.6μL of electroporator enhancer to the Cas9/RNA complex and leave for at least 10 minutes. Remove the PBS, add 5mL of PBS again and centrifuge again. Remove PBS. Resuspend the cells in 15.5μL Nucleofactor solution P3/ per gRNA. Add 15.5μL of cells to the RNP complex. pHLFs were electroporated with the CRISPR ribonucleoprotein (RNP) complex using the Lonza 4D Nucleofector™ system (Basel, Switzerland). The guide RNA (gRNA) sequence targeting ATF4 (AGGTCTCTTAGATGATTACCTGG), RPTOR exon 26 (CCGCGTCTACGACACAGAAGGATGG), or RICTOR exon 29 (AATATCGGCTCATCAAATTGGGG) was designed using a combination of previously published work*(149)*, the DeskGen design platform (https://www.deskgen.com/landing/#/documentation), and the Integrated DNA Technologies online tool (https://eu.idtdna.com/site/order/designtool/index/CRISPR_CUSTOM). A predesigned control gRNA sequence (Integrated DNA Technologies) was used to generate matched wild-type pHLFs. CRISPR models were generated by Dr Delphine Guillotine (CITR).

2.18 Incorporation of U-^{14}C-glucose and U-^{14}C-glycine into collagen I

pHLFs were grown to confluence in 12-well plates and quiesced in

serum-free media for 24 hours. Cells were then incubated in fresh serum-free media containing 5 mM ^{12}C-glucose with or without 2 μCi U-^{14}C-D-glucose (1 nM; PerkinElmer). For glycine tracing studies, media containing 1 mM ^{12}C-glycine, 1 mM ^{12}C-glycine plus 2 μCi U-^{14}C glycine (3.9 nM; PerkinElmer), or media alone were added to cells with either AZD8055 (1 μM) or vehicle (0.1% DMSO). For TGF-β_1–treated cells, TGF-β_1 was added at 1 ng/ml. After 48 hours, cell layers were lysed [lysis buffer: 300 mM NaCl, 10 mM tris (pH 7.4), 1% NP-40, and protease inhibitor] and precleared with protein G agarose beads (CST #37478) for 4 hours at 4°C. Cleared lysates were immunoprecipitated with 1 μg of anti-collagen α1(I) primary antibody (CST #84336) followed by protein G agarose bead incubation overnight at 4°C. Immunoprecipitated material was then eluted in lithium dodecyl sulfate (LDS)–containing sample buffer at 93°C for 5 min and incorporated radioactivity in the eluate determined by liquid scintillation counting in a Beckman Coulter LS6500 using Ecoscint A (National Diagnostics) scintillation fluid. pHLF lysates incubated with corresponding treatments in the presence of 12C-glucose or 12C-glycine were also subjected to SDSPAGE, transferred to polyvinylidene difluoride, and immunoblotted to determine collagen α1(I) abundance. To demonstrate immunoprecipitation efficiency, representative input (10%) and unbound (10%) portions were immunoblotted for collagen α1(I) alongside immunoprecipitated protein, antibody alone (0.4 μg), and beads alone (10% slurry).

2.19 Statistical analysis

All data are expressed as means +/- SEM, and figures were constructed using GraphPad Prism version 7.00. All experiments were repeated at least three times. Statistical differences between two groups were analysed using a standard two-tailed t test (assuming unpaired datasets and unequal variances). When more than two groups were compared, either one-way or two-way ANOVA was used with post hoc application of the Tukey method. Four-parameter nonlinear regression analyses were used to generate IC50 values from concentration-response curves. The alpha level was set at 0.05 for all tests (GraphPad Prism).

CHAPTER 3: RESULTS

Overview

The experimental results section of this thesis has been divided into seven sections. The first part examines the effect of the pro-fibrotic mediator, TGF-β_1 on glucose metabolism in primary human lung fibroblasts (pHLFs). The second section evaluates the role of the metabolic rheostat, mTOR, in mediating the pro-fibrotic response in human lung fibroblasts in physiological media conditions. The third section specifically delineates the role of mTOR signalling in mediating alterations in glycine-serine metabolism. The 4th section identifies and characterizes the expression of ATF4, a key transcriptional factor, during the TGF-β_1 induced increase in glycine metabolism. The 5th section examines the role that ATF4 plays during TGF-β_1 induced glycine and collagen synthesis. The 6th section investigates the role of mTOR in regulating the alterations in glucose metabolism in response to TGF-β_1. The final section interrogates the interplay between glycolysis and *de novo* glycine synthesis in mounting an mTOR dependent increase in TGF-β_1-induced collagen deposition.

3.1 The role of glucose metabolism during TGF-β_1 stimulated differentiation and collagen production in human lung fibroblasts

3.1.1 Introduction

Rewiring of metabolic pathways is not just considered a cardinal feature of many cancers but also plays a critical role in number of other pathological and non-pathological settings. In cancer, metabolic reprogramming is thought to support the requirements of exponential growth and proliferation as well as protect against oxidative stress. There is growing evidence that glucose metabolism may potentially re-configure to support pro-fibrotic processes in IPF. The following section aims to characterize the alterations that occur in glucose metabolism during TGF-β_1 stimulated differentiation and collagen production in primary human lung fibroblasts.

The vast majority of biomedical researchers use cell culture media that does not reproduce the physiological cellular environment but instead has selected nutrients such as glucose and glutamine at several fold higher concentrations than what is observed physiologically. Recent work has shown that physiological medium improves the metabolic fidelity and biological relevance of *in vitro* cancer models *(150)* and there is growing consensus for studying metabolic responses in a physiological environment. Because mTOR is sensitive to environmental signals, including energy and nutrient abundance, and in view of the profound effects of mTOR inhibition on the transcriptome of multiple metabolic

genes [reviewed in *(151)*], all studies were performed at physiological concentrations of glucose (5 mM) and glutamine (0.7 mM).

3.1.2 The effect of TGF-β_1 stimulation on type I collagen and αSMA gene and protein expression in pHLFs.

TGF-β_1 is a potent profibrotic growth factor, which mediates fibroblast to myofibroblast differentiation. This is characterised by the *de novo* expression and incorporation of αSMA into stress fibres. TGF-β_1 also promotes the synthesis of a type I collagen rich extracellular matrix. To examine the time course of TGF-β_1 induced type I collagen (*COL1A1*) and αSMA (*ACTA2*) gene expression, primary human lung fibroblasts (pHLFs) were stimulated with TGF-β_1 (1ng/ml) and the expression of *COL1A1* and *ACTA2* assessed over a 48-hour time course by RT-qPCR (Figure 3.1). Type I collagen and αSMA gene expression are significantly increased at 12 hours with a peak in expression between 24 and 32 hours, with a reduction thereafter. Expression of *COL1A1* showed a 6-fold increase ($p<0.0001$) and *ACTA2,* a 50-fold increase ($p<0.0001$) relative to baseline at the 24-hour time point (Figure 3.1).

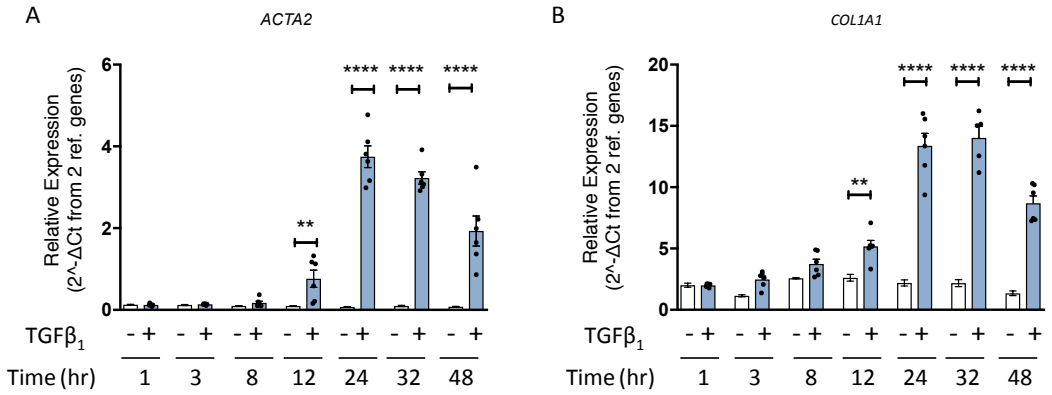

Figure 3.1 Effect of TGF-β$_1$ on type I collagen and αSMA gene expression. Confluent pHLFs were incubated in media alone or media plus TGF-β$_1$ and the relative abundance of (**A**) *ACTA2* and **(B)** *COL1A1* mRNA over time were measured by real-time quantitative polymerase chain reaction (RT-qPCR). Data are presented as means +/- SEM from six technical replicates per condition and representative of three independent experiments. Differences between groups were evaluated by two-way analysis of variance (ANOVA) test with Tukey post hoc test. **P < 0.01, ***P < 0.001 and ****P < 0.0001.

3.1.3 Glucose uptake increases during TGF-β$_1$-induced myofibroblast differentiation and collagen synthesis.

The increased ^{18}F-FDG-PET signal observed in the IPF lung suggests there is elevated glucose uptake in areas of fibrosis, however the cellular source of this signal remains unclear. During myofibroblast differentiation, ^{1}H-NMR spectroscopy of cell supernatants over 24 hours demonstrated a significantly lower levels of glucose in TGF-β$_1$-stimulated fibroblasts compared to media-only treated fibroblasts, which equated to a 2.2 fold increase in glucose uptake during TGF-β$_1$-induced differentiation ($p<0.0001$) (Figure 3.2, panel A). Glucose uptake continued to increase over 24 hours, during which the myofibroblast was actively synthesizing collagen. [3H]-2-deoxy-D-glucose ([3H]-2DG)

uptake over 5 minutes was measured after 24 hours of TGF-β_1 or media-only treatment which demonstrated a 3-fold increase in tritiated 2DG uptake after 24 hours suggesting there is a need for increased glucose uptake during collagen synthesis (p=0.0001) (Figure 3.2, panel B).

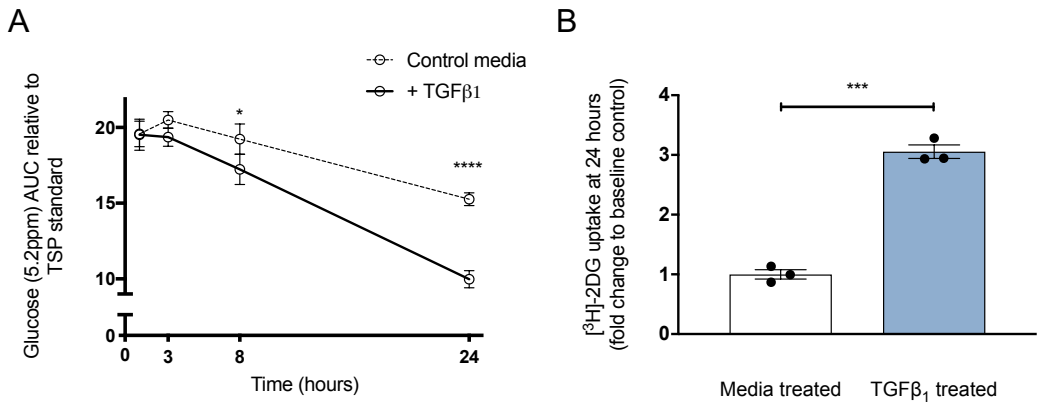

Figure 3.2 Glucose uptake increases during TGF-β_1 induced myofibroblast differentiation and collagen synthesis. (**A**) Control primary human lung fibroblasts were treated with TGF-β_1 or media over 24 hours and supernatants were collected at specified time points and extracellular glucose content was measured using 1H-NMR. Data expressed as the AUC of the corresponding glucose peak on NMR spectra relative to TSP standard. (**B**) Confluent pHLFs were incubated with or without TGF-β_1 for 24 hours and radiolabelled 2-deoxyglucose (^{3}H-2DG) uptake was measured. All data are representative of 3 independent experiments with 3 technical replicates per condition. Differences between groups were evaluated by two-way (A) ANOVA test with Tukey post-hoc test or unpaired t-test (B) *P<0.05, ***P< 0.001,****p< 0.0001.

3.1.4 Glucose transporter 1 expression increases during TGF-β_1-induced myofibroblast differentiation and collagen synthesis.

Glucose is a hydrophilic compound, which cannot pass through the lipid bilayer by simple diffusion and requires specific glucose transporters to mediate its transport into the cytosol. There are at least 13 glucose transporter isoforms differentially expressed in

mammalian tissue, with glucose transporter type 1 (GLUT1) being the most commonly expressed glucose transporter in the lung which is also known to facilitate FDG-PET uptake observed in cancer *(104, 152)*. In concordance with increased glucose uptake, there was a significant increase in GLUT1 (*SLC2A1*) gene expression from 24 hours in response to TGF-β_1 as measured by qRT-PCR. There was a peak, 3.6-fold increase in GLUT1 expression at 24 hours and a reduction in expression thereafter (Figure 3.3, panel A). Similarly, at the protein level, enhanced GLUT1 protein production was observed by western blot analysis at 24 hours (Figure 3.3, panel B).

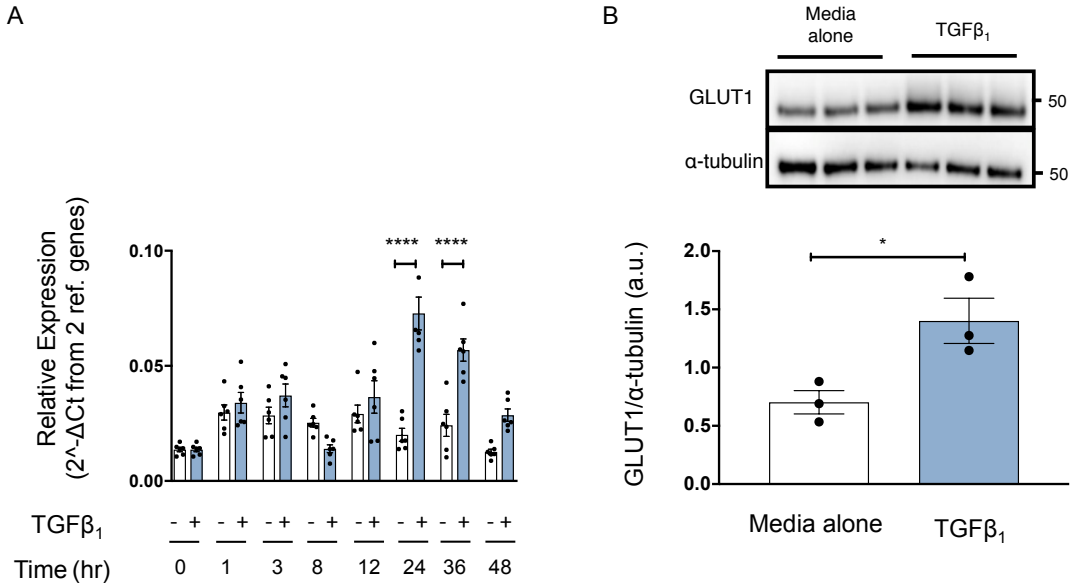

Fig 3.3 TGF-β_1 stimulation increases abundance of *SLC2A1* transcripts and GLUT1. (**A**) Relative abundance of *SLC2A1* mRNA was measured by RT-qPCR in confluent pHLFs that were stimulated with TGF-β_1 or media alone over 48 hours and (**B**) GLUT1 protein abundance in confluent pHLFs that were stimulated with TGF-β_1 or media alone. Immunoblotting and densitometric quantification of GLUT1 were performed at 24 hours. All data are representative of 3 independent experiments with at least 3 technical replicates per condition. Differences between groups were evaluated by two-way ANOVA test with Tukey post-hoc test (A) or unpaired t test (B). *P<0.05, ****P< 0.0001.

3.1.5 Extracellular lactate production increases during TGF-β_1 induced myofibroblast differentiation and collagen synthesis.

Glucose uptake is the first rate-limiting step of glycolysis, which suggests that elevated glucose uptake may potentially lead to and be part of an increase in glycolysis. Lactate production is the final step of glycolysis and therefore can act as a surrogate marker of enhanced glycolysis. Extracellular lactate production in the supernatant was therefore measured by a colorimetric assay (Biovision) to assess the role of glycolysis during TGF-β_1 induced myofibroblast differentiation. Comparing extracellular lactate production of TGF-β_1 and media-only treated primary HLFs over 48 hours, significantly elevated levels of lactate production was observed after 24 hours of TGF-β_1 stimulation which continued to rise until 48 hours. During differentiation there was a 2.3 fold increase in lactate production at 24 hours and 3.4 fold increase at 48 hours ($p=0.0063$ and $p<0.0001$ respectively) compared to baseline (Figure 3.4, panel A). The lactate: glucose ratio was measured by examining the ratio of lactate to glucose in cell-conditioned media by 1H-NMR spectroscopy over 48 hours as this was felt to be a better representation of overall glycolytic flux. Again, TGF-β_1 led to increased glucose depletion and lactate production compared to media alone treated fibroblasts resulting in an overall increase in glycolytic flux (Figure 3.4, panel B).

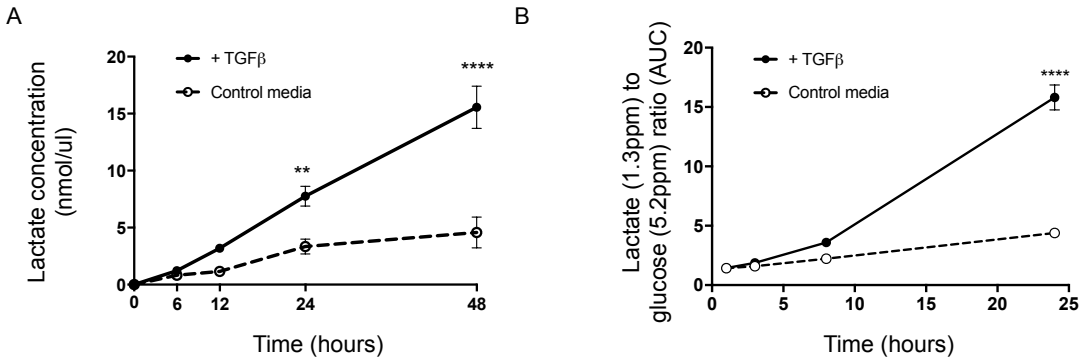

Figure 3.4 Increased extracellular lactate production during TGF-β_1 induced myofibroblast differentiation and collagen synthesis. (**A**) Confluent pHLFs were exposed to TGF-β_1 or media only over 48 hours and supernatants were collected at specified time points and extracellular lactate was measured using a Biovision assay. (**B**) Confluent pHLFs were exposed to media plus TGF-β_1 or media only for 24 hours. The area under the curve (AUC) of lactate relative to that of glucose in cell supernatants was measured by nuclear magnetic resonance (NMR) spectroscopy at the indicated time points. Data are representative of three independent experiments with three technical replicates per condition. ppm, parts per million. NMR data generated in collaboration with Dr I. Azuelos (CITR). Differences between groups were evaluated by two-way ANOVA test with Tukey post hoc test **P < 0.01 and ****P < 0.0001.

3.1.6 Glycolytic enzyme gene expression during TGF-β_1 induced myofibroblast differentiation.

Increased expression of key glycolytic enzymes with a concomitant increase in glycolysis is a well-documented characteristic for many cancers *(153)*. After demonstrating an increase in glycolysis, the gene expression of key glycolytic enzymes during TGF-β_1 induced myofibroblast differentiation was examined. mRNA levels of the key rate-limiting glycolytic enzymes, hexokinase 2 (HK2), pyruvate kinase M1 and M2 (PKM1/PKM2) and lactate dehydrogenase A and B (LDHA/ LDHB) were measured by RT-qPCR. Pyruvate kinase converts phosphoenolpyruvate (PEP) to pyruvate, which is catalysed by pyruvate kinase. PKM1 and PKM2 are formed from

alternative splicing of the PKM gene. PKM2 exists in either a low activity dimer or high activity tetramer, where the latter form shifts glucose metabolism away from oxidative phosphorylation and instead favours lactate production in many cancers.

LDH is a cytoplasmic enzyme composed of tetramers composed of two LDH subunits, M and H, which are encoded by the *LDHA* and *LDHB* genes respectively. Five LDH isoenzymes (LDH 1-5) exist and are made up of different combinations of the two subunits. *LDHA* encodes proteins that give rise to isoenzymes that favour the conversion of pyruvate to lactate, while *LDHB* encodes isoenzymes that favour the reverse reaction. The mRNA levels of 6-phosphofructo-2-kinase (PFKFB3) were also measured as this enzyme catalyses the conversion of fructose-6-phosphate to fructose-2,6,-bisphosphate, which is an allosteric activator of the glycolytic enzyme phosphofructokinase-1 (PFK1) and consequently acts as a potent stimulator of glycolysis. In response to TGF-β_1, there was no significant change in the gene expression of *HK2, LDHB, PKM2* or *PKM1*. However, mRNA levels of *PFKFB3* and *LDHA* were significantly increased (Figure 3.5, panels B and E), with peak relative expression observed at 3 hours for *PFKFB3* (6 fold increase compared to baseline, $p<0.0001$) and 8 hours for *LDHA* (1.6 fold, $p=0.0059$). These results support the notion that augmented glycolysis is enabled by enhanced gene expression of key enzymes that stimulate this process as well as increased glucose uptake. Early peak expression of *PFKFB3* is noted compared to a more sustained increase in *LDHA* suggesting potentially differing roles of these enzymes during TGF-β_1 induced myofibroblast differentiation.

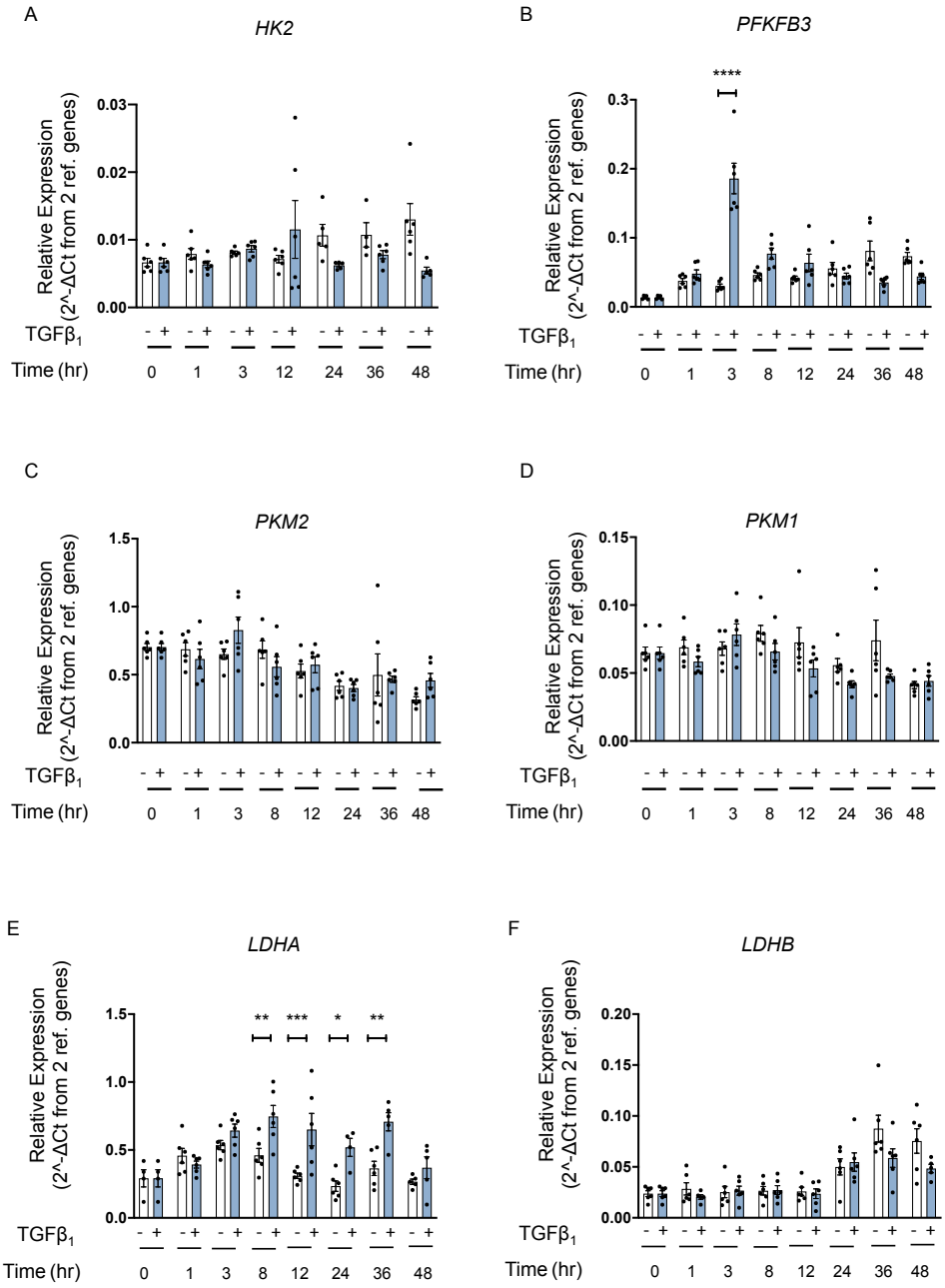

Figure 3.5 Glycolytic gene expression increases during TGF-β$_1$ induced myofibroblast differentiation. Confluent pHLFs were incubated with or without TGF-β$_1$, and the relative abundance of (**A**) *HK2*, (**B**) *PFKFB3* (**C**) *PKM2* (**D**) *PKM1* (**E**) *LDHA* and (**F**) *LDHB* mRNAs over time were measured by RT-qPCR. All data are expressed as means +/- SEM from six technical replicates per condition and representative of three independent experiments. Differences between groups were evaluated by two-way ANOVA test with Tukey post hoc test. ****P<0.0001, *** P=0.0006, ** P=0.0059, * P=0.019.

3.1.7 Effect of glucose deprivation and glycolytic inhibition during TGF-β_1-induced myofibroblast differentiation and collagen synthesis.

Having demonstrated that increased glucose metabolism accompanies TGF-β_1 induced differentiation and collagen synthesis, I next sought to determine whether augmented glucose metabolism was a requisite for the acquisition of the myofibroblast phenotype. Using a novel high content imaging based assay to measure collagen and αSMA expression*(154)*, the effects of glucose deprivation on TGF-β_1 induced differentiation and collagen synthesis were assessed.

Conventional 2-dimensional (2D) cell culture does not efficiently enable the deposition and incorporation of collagen I fibrils into an extracellular matrix. Collagen production has traditionally been quantified by using reverse-phase high-performance liquid chromotography (HPLC) quantification of hydroxyproline, and therefore does not assess the final collagen processing step into deposited collagen matrix. Furthermore, conventional monolayer culture is affected by media dilution of critical C and N terminal peptidases which results in very slow deposition of insoluble pro-collagen. Therefore investigation of the complete biosynthetic pathway of deposited collagen matrix has previously been low throughput and time-consuming. This has been addressed by the optimization of a novel fibrosis assay in our laboratory. It utilizes the concept of macromolecular crowding, where neutral macromolecules (ficoll) are introduced to create a macromolecular crowding environment in the cell culture media to mimic

physiological conditions, which allows the timely deposition of insoluble fibrillar collagen into a matrix within 48-72 hours. Fibrillar collagen can be rapidly assessed in a high throughput manner using fluorescently labelled antibodies on a high content imaging platform. This assay allows the quantification of key fibrotic end points such as the differentiation marker, αSMA, collagen I and DAPI as a marker of cell count.

Primary HLFs were incubated for 24 hours in either glucose-deplete or glucose containing media (5mM) before TGF-β_1 (1ng/ml) was added for 48 hours. In the presence of glucose containing media, there is a 2.2 fold and 2.3 fold increase in αSMA protein abundance and deposited collagen respectively in response to TGF-β_1 stimulation (Figure 3.6, panel A and B). In the absence of glucose, there was a 50% and 47% reduction in αSMA abundance and deposited collagen respectively, with no effect on baseline levels or cell count ($p<0.0001$).

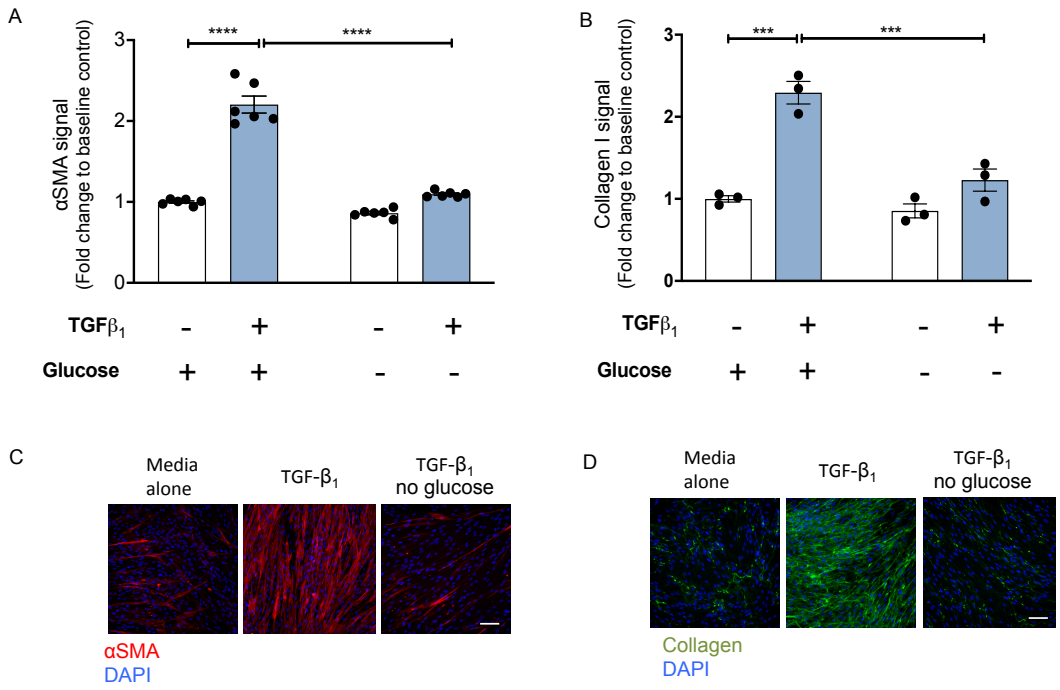

Figure 3.6 Glucose deprivation inhibits TGF-β$_1$ induced myofibroblast differentiation and collagen deposition. (**A-D**) Confluent pHLFs were deprived of glucose or incubated with glucose (5mM) for 24 hours, followed by TGF-β$_1$ stimulation for 48 hours before assessment of (**A**) αSMA and (**B**) collagen I deposition by high content imaging. Each data point shown is the mean +/- SEM of the fold change relative to baseline of at least three technical replicates per condition. Data are representative of three independent experiments. Immunofluorescence staining showing (**C**) αSMA and (**D**) collagen I deposition in pHLFs treated as in (A and B). DAPI, 4',6-diamidino-2-phenylindole. Differences between groups were evaluated by two-way ANOVA test with Tukey post hoc test. ****p<0.0001, *** p<0.0006. Scale bar, 100μm.

The effect of glucose deprivation suggests that glucose, as a nutrient source is a critical substrate required for TGF-β$_1$ induced myofibroblast differentiation and collagen synthesis. The effect of inhibiting glycolysis was next examined to see whether this notion was supported. 2 deoxy-d-glucose (2-DG) was used to interrogate this question. 2-DG is a glucose analogue that competes with glucose for uptake via the glucose transporters. The first glycolytic enzyme, hexokinase (HK), is unable to fully metabolise 2DG leading to 2-DG-6-phosphate accumulation in the cell which inhibits the 2nd glycolytic enzyme, phosphoglucose isomerase

(PGI) in a competitive, and HK in a noncompetitive manner. As expected, TGF-β_1 (1ng/ml) significantly up regulated collagen I deposition and αSMA expression after 48 hours. Collagen deposition and αSMA expression were both inhibited by 2DG in a concentration-dependent manner (IC50 values were 179μM and 299μM respectively). No reduction in cell count was observed at any concentration of 2DG. Of note, significant inhibition was achieved with sub-equimolar concentrations of 2DG (3mM) to glucose (5mM) (Figure 3.7).

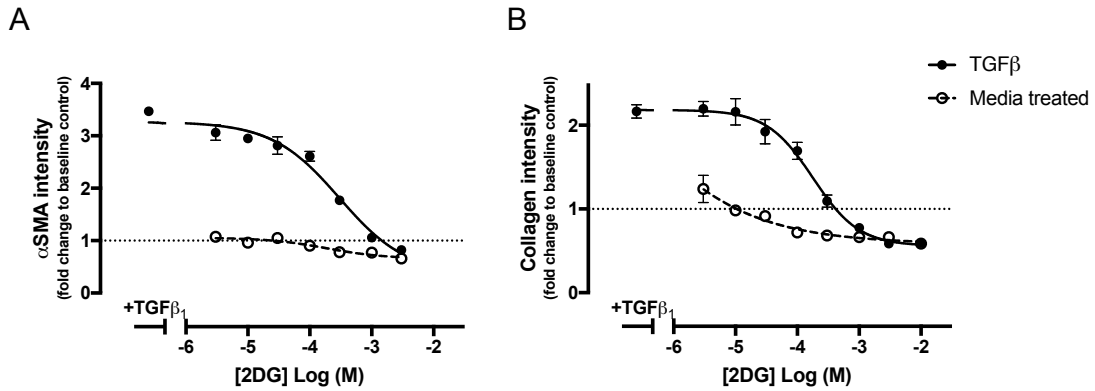

Figure 3.7 Inhibition of glycolysis with 2DG abrogates TGF-β_1 induced myofibroblast differentiation and collagen deposition. Confluent pHLFs were stimulated with TGF-β_1 in the absence or presence of the glycolysis inhibitor 2DG as indicated. (**A**) αSMA and (**B**) collagen I deposition at 48 hours were assessed by high-content imaging. Half maximal inhibitory concentrations (IC_{50}) values were calculated using four-parameter nonlinear regression. Each data point shown is the mean +/- SEM of the fold change to baseline of at least three technical replicates per condition. Data are representative of three independent experiments.

3.1.8 Effect of glycolytic inhibition on the TGF-β_1 induced increase in α-SMA and collagen gene expression.

Given that maximum inhibition of collagen and αSMA protein abundance had been achieved by 3mM [2DG], this concentration was used to treat normal HLFs to investigate the impact of

glycolytic inhibition on TGF-β_1-induced αSMA (*ACTA2*) and collagen I (*COL1A1*) gene expression (Figure 3.8). As expected, *COL1A1* and *ACTA2* mRNA levels were significantly increased in response to TGF-β_1 in fibroblasts at 24 hours and there was a significant inhibition in the presence of 2DG of collagen I and αSMA gene expression at this time point (P<0.0001). No significant effect was observed on baseline expression of αSMA or collagen I. These data suggest that glucose is required for TGF-β_1-induced collagen I and αSMA gene expression.

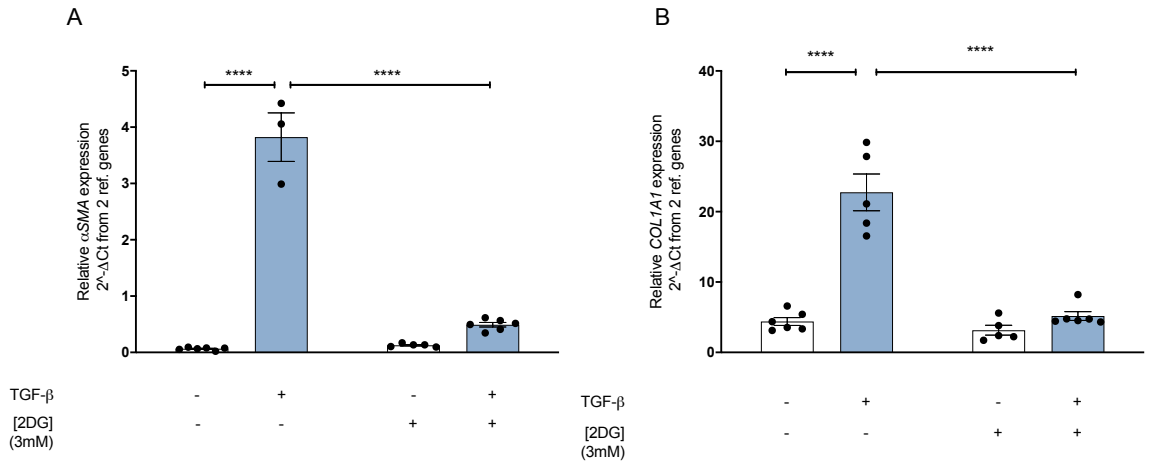

Figure 3.8 Inhibition of glycolysis with 2DG abrogates TGF-β_1 induced myofibroblast differentiation and collagen mRNA abundance. Confluent pHLFs were stimulated with or without TGF-β_1 in the absence or presence of the glycolysis inhibitor 2DG as indicated and the relative abundance of (**A**) *ACTA2* and (**B**) *COL1A1* mRNAs over time were measured by RT-qPCR. All data are expressed as means +/- SEM from at least 3 technical replicates per condition and representative of three independent experiments. Differences between groups were evaluated by two-way ANOVA test with Tukey post hoc test. ****p<0.0001.

In contrast, glucose depletion had no effect on *COL1A1* gene expression but reduced αSMA mRNA levels by 90%. This highlights the potential difference between mechanisms governing

TGF-β_1 induced differentiation and collagen production. Moreover the ability of 2DG to inhibit collagen mRNA levels at sub-equimolar concentrations to glucose suggests its mode of action with regards to inhibiting collagen and αSMA gene expression may be separate to its effect on glycolysis. Taken together, it is clear that glycolysis is required for collagen and αSMA protein expression but more work is needed to clarify the role, glucose plays at the transcriptional level.

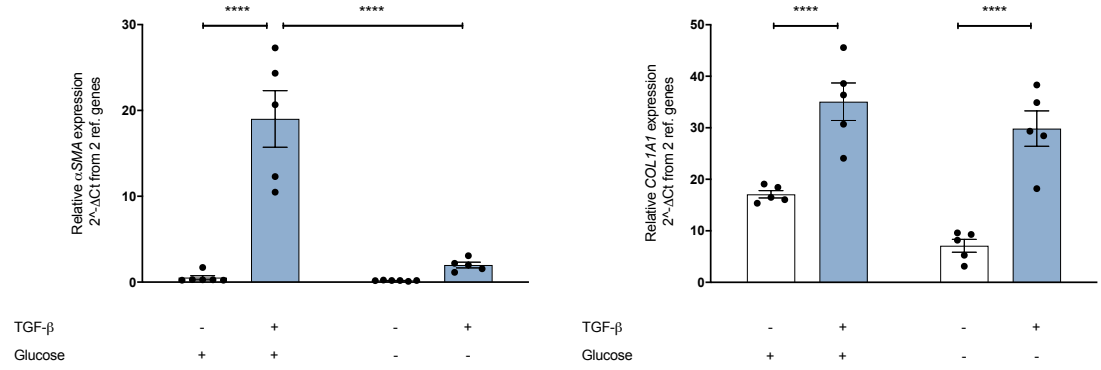

Figure 3.9 Glucose deprivation abrogates the TGF-β_1 induced increase in αSMA gene expression but not collagen I gene expression. Confluent pHLFs were deprived of glucose for 24 hours, followed by TGF-β_1 stimulation and the relative abundance of (**A**) *ACTA2* and (**B**) *COL1A1* mRNAs at 24 hours were measured by RT-qPCR. All data are expressed as means +/- SEM from at least 3 technical replicates per condition and representative of three independent experiments. Differences between groups were evaluated by two-way ANOVA test with Tukey post hoc test. ****P <0.0001.

3.1.9 Enhanced mitochondrial respiration during TGF-β_1-induced collagen synthesis in pHLFS.

Pyruvate can either be used for lactate production and/or oxidative phosphorylation (OXPHOS). My results so far have demonstrated an increase in glycolysis of HLFs in response to TGF-β_1 but concurrent work also investigated the changes in OXPHOS that

occur during TGF-β_1 collagen synthesis in myofibrolasts. The Seahorse^{TM} platform allows for the simultaneous assessment of glycolysis and oxidative phosphorylation. Glycolysis is determined by measuring the extracellular acidification rate (ECAR) of the surrounding media and is predominantly from the excretion of lactic acid while OXPHOS is assessed by measuring the oxygen consumption rate. On going work in our laboratory has previously found that TGF-β_1 causes an increase in OCR as early as 3 hours after stimulation and rising to its peak at 24 hours. A mitochondrial stress test which measures basal respiration, ATP production, maximal respiration and non- mitochondrial respiration of adherent cells also showed that TGFβ_1 stimulation caused a significant increase in basal, ATP production and maximal respiration at 24 hours (Figure 3.10, panel A). In agreement with the lactate assays (Figure 3.4, panel B), ECAR was also significantly elevated at 24 hours after TGF-β_1 stimulation (Figure 3.10, panel B).

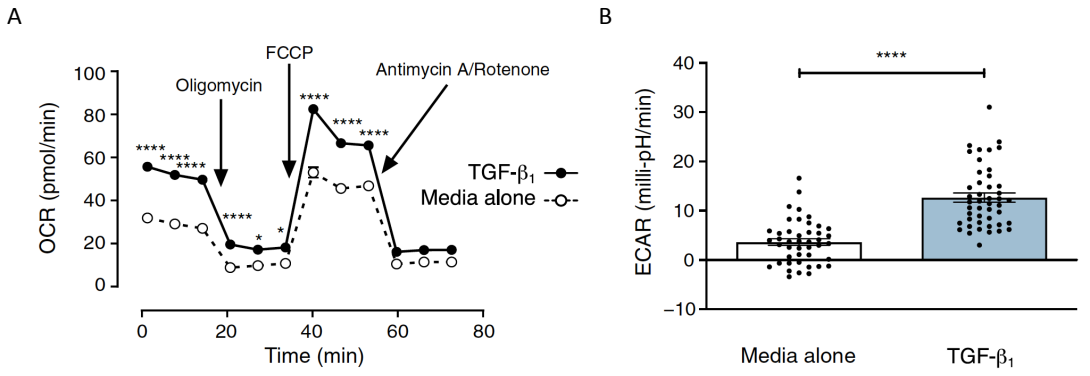

Figure 3.10 TGF-β_1 enhances oxygen consumption rate (OCR) and extracellular acidification rate (ECAR) and in pHLFs. (**A** and **B**) Confluent pHLFs were exposed to media plus TGF-β_1 or media only for 24 hours. OCR (**A**) and ECAR (**B**) were measured using the Seahorse^{TM} XFe96 assay. Data are representative of three independent experiments with 46 technical replicates per condition. FCCP, carbonyl cyanide p-trifluoromethoxyphenylhydrazone. Differences between groups were

evaluated by two-way ANOVA test with Tukey post hoc test (A) or unpaired t tests (B). ****P <0.0001, *P<0.05. Data generated by Dr. Ilan Azuelos (CITR).

An increase in mitochondrial respiration, albeit thought to be to a lesser degree to glycolysis, may potentially occur to provide ATP, TCA carbon intermediates and reactive oxygen species (ROS) to support a number of fibrogenic responses. As shown in Figure 3.10, rotenone and antimycin A, electron transport chain (ETC) I and II complex inhibitors, significantly inhibited the TGF-β_1-induced increase in OCR, so I next evaluated the effect of these compounds on TGF-β_1-induced collagen deposition in the macromolecular crowding assay. These compounds had no effect on αSMA expression or collagen deposition.

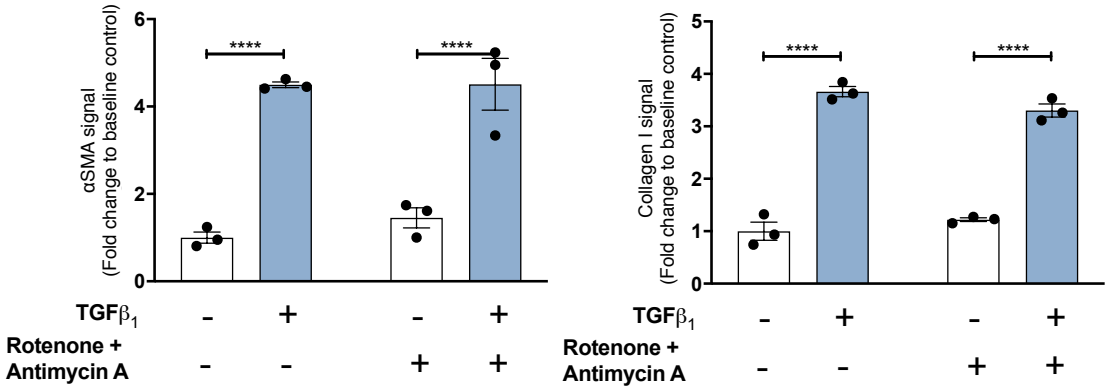

Figure 3.11 Enhanced **mitochondrial respiration is** dispensible for **TGF-β_1-i**nduced collagen synthesis**. (A** and **B**) HLFs were pre-incubated with rotenone (1μM) and antimycin A (1μM) before stimulation for 48 hours with or without TGF-β_1. (**A**) αSMA and (**B**) collagen I deposition were assessed by high-content imaging. Each data point shown is the mean +/- SEM of the fold change relative to baseline of three technical replicates per condition. Data are representative of three independent experiments. Differences between groups were evaluated by two-way ANOVA test with Tukey post hoc test. ****P < 0.0001.

Summary

The results described in this section, examining the effect of TGF-β_1 stimulation on glucose metabolism in HLFs show that:

- Glucose uptake and glucose transporter 1 gene and protein expression are increased in TGF-β_1 stimulated pHLFs.

- Enhanced glycolysis is accompanied by increased expression of key rate limiting glycolytic enzymes and lactate production in TGF-β_1 stimulated pHLFs.

- Glucose availability and glycolysis are critical for αSMA expression and collagen I deposition.

- Induced oxidative phosphorylation is not required for αSMA or collagen I deposition.

Taken together, these data support the conclusion that TGF-β_1 stimulated myofibroblasts demonstrate a glycolytic phenotype which is critical for both myofibroblast differentiation and collagen deposition.

3.2 The role of mTOR signalling in mediating the pro-fibrotic effects of TGF-β_1 in human lung fibroblasts

3.2.1. Introduction

The data presented in Section 3.1 show that HLFs are dependent on TGF-β_1-induced increases in glucose metabolism for enhanced differentiation and collagen deposition but the mechanisms underlying these changes in metabolism are unclear. The serine-threonine kinase mechanistic target of rapamycin (mTOR) plays a key role in regulating cell metabolism and is strongly implicated in coordinating metabolic reprogramming in cancer cells to optimize nutrient uptake and utilization and to meet the biosynthetic needs of proliferative cancer cells *(155–157)*. mTORC1 and mTORC2, two distinct complexes central to mTOR, integrate critical environmental and intracellular cues provided by nutrients, energy, oxygen, and growth factors [reviewed in (17)]. Previous studies have shown that inhibition of the mTOR pathway inhibits fibroblast proliferation and collagen production *in vitro (78, 84, 158)* and further dissection of this pathway by our laboratory in standard DMEM glucose and glutamine concentrations, revealed that specifically rapamycin-insensitive mTORC1 signalling is critical for TGF-β_1–induced collagen deposition *(78)*.

This next chapter aims to characterize the role of mTOR in modulating the fibrogenic effects TGF-β_1 in physiological media conditions.

3.2.2 Effect of TGF-β_1 on mTORC1 signalling in pHLFs.

Previous studies from our laboratory provided strong scientific evidence that mTORC1 and phosphorylation of its downstream substrate, 4E-BP1, are critical for TGF-β_1–induced collagen deposition in fibroblasts *(78)*. I now show that under physiological glucose and glutamine media conditions, TGF-β_1 similarly caused a marked increase in mTORC1 signalling in pHLFs as evidenced by p70S6K (Thr389) and 4E-BP1 (Ser65) phosphorylation by western blotting, with the strongest signal seen at 1 hour post TGF-β_1 stimulation (Figure 3.12)

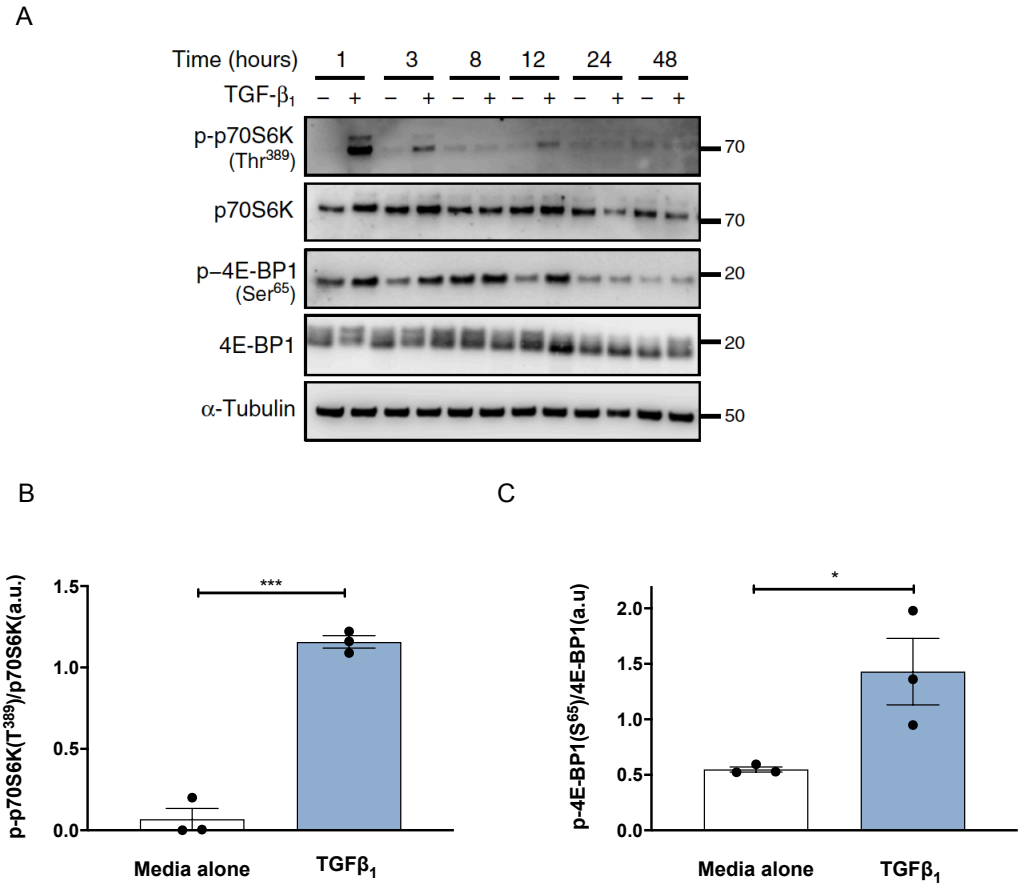

Figure 3.12 TGF-β_1 enhances mTORC1 signalling in pHLFs. (**A**) Confluent pHLFs were stimulated with media alone or media plus TGF-β_1, and extracts were immunoblotted for the indicated proteins. (**B** and **C**) Confluent pHLFs

were incubated with or without TGF-β_1 for 1 hour followed by immunoblotting and densitometric quantification of (**B**) p70S6K phosphorylated at Thr^{389} (p-p70S6K) relative to p70S6k and (**C**) 4E-BP1 phosphorylated at Ser^{65} (p-4E-BP1) relative to 4E-BP1. All data are representative of 3 independent experiments with 3 technical replicates per condition Differences between groups were evaluated by unpaired t-test. *P <0.05, ***P <0.001.

3.2.3 ATP competitive dual mTOR inhibition during TGF-β_1-induced myofibroblast differentiation and collagen synthesis.

To address the function role of mTOR during TGF-β_1 induced mTOR signalling and myofibroblast function, I assessed the effect of the ATP competitive inhibitor AZD8055. The selectivity data available for AZD8055 suggests that it is highly selective for its target and our laboratory has previously shown AZD8055 completely inhibits TGF-β_1 induced phosphorylation of downstream mTORC1 and mTORC2 substrates *(78)*. HLFs were treated with AZD8055 with concentrations ranging from 3nM to 10μM for 1 hour prior to stimulation with TGF-β_1 (1ng/ml), and collagen I deposition was assessed after a further 48 hours. TGF-β_1 increased collagen deposition by 251 ± 8.6%, as determined by high-content imaging of collagen I immunostaining at 48 hours (Figure. 3.13) *(78)* and ATP-competitive mTOR inhibition with AZD8055 attenuated TGF-β_1–induced collagen deposition in a concentration-dependent manner with an IC50 of 340 nM (Figure. 3.13, panel A). This IC50 is comparable to previously published data from our laboratory demonstrating significant inhibition of collagen in standard DMEM concentrations of glutamine and glucose *(78)*.

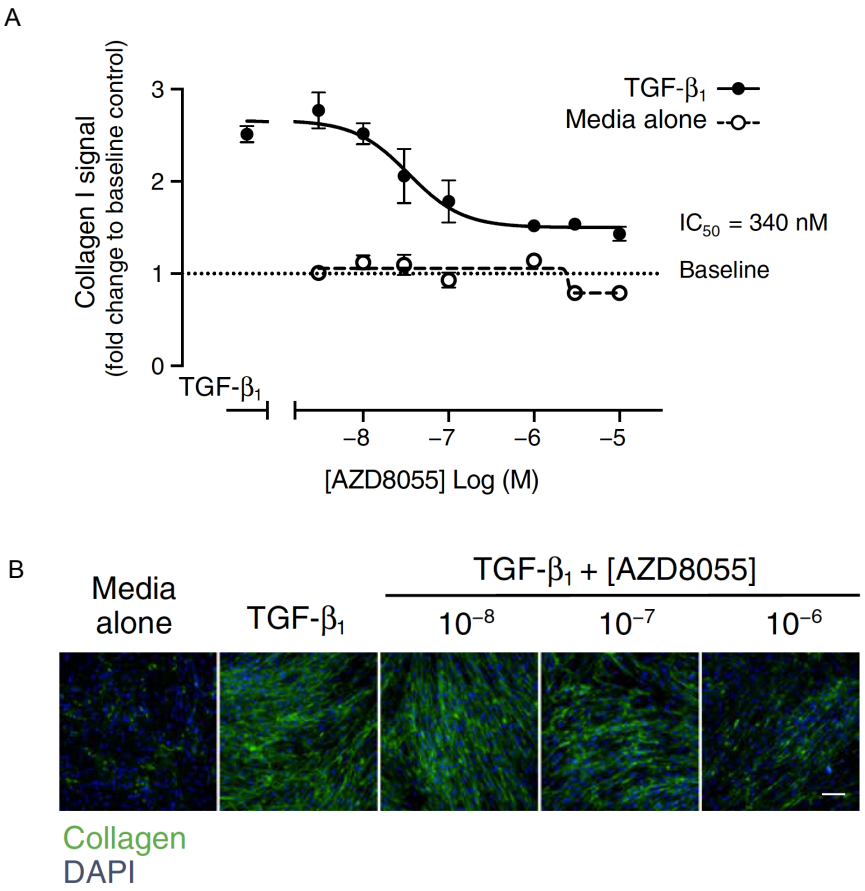

Figure 3.13 mTOR regulates TGF-β$_1$-induced collagen deposition in pHLFs. (A) Confluent pHLFs were pre-incubated with media plus vehicle [dimethyl sulfoxide (DMSO)] or AZD8055 and stimulated for 48 hours with or without TGF-β$_1$. Collagen I deposition was assessed by high-content imaging. Half-maximal inhibitory concentration (IC50) value was calculated using four-parameter nonlinear regression. Each data point shown is the mean +/- SEM of the fold change to baseline of three technical replicates per condition. Data are representative of three independent experiments. (**B**) Immunofluorescence staining showing collagen I deposition in pHLFs treated as in (A). Scale bar, 100μm. DAPI, 4′,6-diamidino-2-phenylindole.

I next investigated whether mTOR inhibition affected TGF-β$_1$–induced myofibroblast differentiation, based on the assessment of αSMA by high-content imaging. TGF-β$_1$–increased fibroblast αSMA expression, but AZD8055 did not inhibit this response (Figure 3.14, panel A and B).

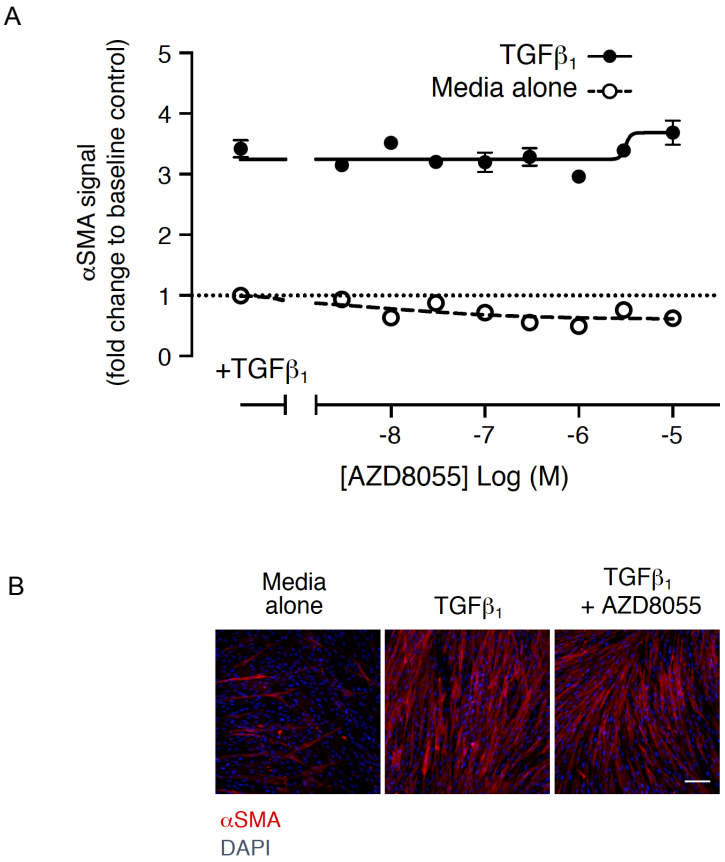

Figure 3.14 mTOR does not regulate αSMA protein expression in pHLFs. (**A**) Confluent pHLFs were pre-incubated with increasing concentrations of AZD8055 or vehicle (DMSO), then stimulated for 48 hours with TGF-β$_1$. αSMA stress fibre formation was assessed by high-content imaging and quantified. Each data point shown is the mean +/- SEM of the fold change to baseline of three technical replicates per condition. Data are representative of three independent experiments. (**B**) Immunofluorescence staining showing αSMA stress fibre formation in pHLFs treated as in (A). Scale bar, 100μm, DAPI, 4′,6-diamidino-2-phenylindole.

I next investigated the impact of mTOR inhibition (AZD8055, 1μM) on TGF-β$_1$-induced *COL1A1* gene expression in normal human lung fibroblasts. Inhibition of mTOR resulted in a 59.1% reduction in collagen gene expression levels at 24 hours ($p<0.0001$)(Figure 3.15).

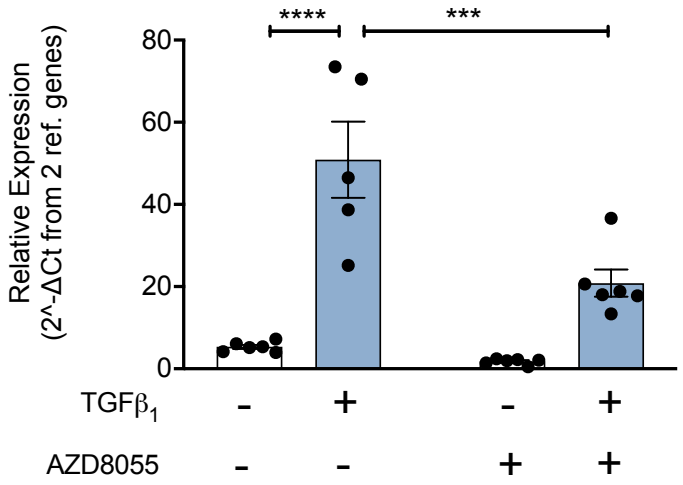

Figure 3.15 mTOR inhibition abrogates TGF-β_1-induced *COL1A1* gene expression in pHLFs. Confluent pHLFs were incubated in media alone or media plus TGF-β_1 with AZD8055 or vehicle control (DMSO) for 24 hours. Quantification of the relative abundance of *COL1A1* mRNA by real-time quantitative polymerase chain reaction (RT-qPCR). Data are presented as means +/- SEM from six technical replicates per condition and representative of three independent experiments. Differences between groups were evaluated by two-way ANOVA test with Tukey post hoc test. ****P <0.0001, ***P < 0.001.

Rapamycin is a partial inhibitor of mTORC1, preferentially inhibiting mTORC1 sites that are weakly phosphorylated by mTORC1 [p70S6K (Thr389) and 4E-BP1 (Ser65)]. Previous studies from our laboratory revealed that TGF-β_1-induced collagen synthesis was insensitive to rapamycin. In physiological media conditions, rapamycin had no effect on TGF-β_1-induced collagen synthesis as assessed in the macromolecular crowding assay (Figure 3.16).

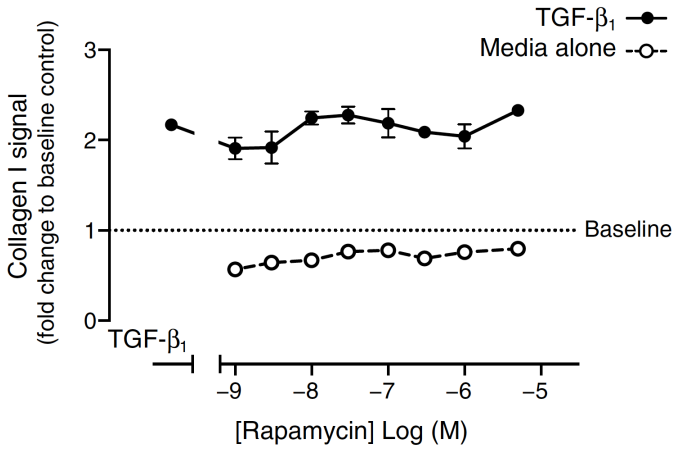

Figure 3.16 TGF-β$_1$ induced collagen synthesis is insensitive to rapamycin treatment. Confluent pHLFs were pre-incubated with media plus vehicle or rapamycin and stimulated for 48 hours with or without TGF-β$_1$. Collagen I deposition was assessed by high-content imaging. Each data point shown is the mean +/- SEM of the fold change relative to baseline of three technical replicates per condition. Data are representative of three independent experiments.

Summary

The results described in this section, examining the role of mTOR signalling during TGF-β$_1$-induced αSMA expression and collagen deposition in physiological media conditions, show that

- TGF-β$_1$ promotes mTORC1 signalling in HLFs under physiological conditions of glucose and glutamine.

- TGF-β$_1$-induced collagen I mRNA and protein production are significantly inhibited by ATP-competitive dual mTOR inhibition.

- ATP-competitive dual mTOR inhibition has no effect on αSMA protein levels.

- TGF-β_1–induced collagen deposition is insensitive to rapamycin treatment.

Taken together, these data support the recent observation that rapamycin-insensitive mTOR signalling is critical for mediating TGF-β_1-induced collagen deposition but is dispensable for αSMA protein synthesis.

3.3 The role of mTOR in regulating glycine biosynthesis during TGF-β_1 stimulated collagen synthesis

3.3.1 Introduction

mTOR acts as a key metabolic rheostat that integrates intracellular and environmental cues to regulate several downstream cellular effects, including metabolism. To identify potentially altered metabolic pathways that are regulated by rapamycin insensitive-mTOR signalling in HLFs, an unbiased bioinformatics approach was used to identify key transcriptional modules that are induced by TGF-β_1 and modulated by mTOR inhibition.

3.3.2. Identification of a rapamycin-insensitive, mTOR-dependent serine-glycine biosynthetic signature during TGF-β_1 –induced collagen deposition.

Having shown that rapamycin-insensitive mTOR signalling was critical for TGF-β_1–induced collagen deposition, I endeavoured to

define the underlying mechanism, by applying weighted gene co-expression network analysis (WGCNA) using MetaCore to interrogate an existing RNA sequencing (RNA-seq) dataset (GSE102674) from our laboratory, kindly provided by Dr Hannah Woodcock and Dr Manuela Plate (CITR), which compares the global transcriptomic effect of the highly selective ATP-competitive dual mTORC1 and mTORC2 inhibitor, AZD8055, to the partial mTORC1 inhibitor, rapamycin, in human lung fibroblasts exposed to TGF-β_1. WGCNA was performed by Dr Adam Taylor (GSK) and revealed 65 independent sets of highly correlated genes (also referred to as co-expression modules). For each of these modules, the measure of central tendency (the eigengene) correlated to a requisite profile showing complete reversal of the TGF-β_1 response by AZD8055 and no reversal by rapamycin. This led to the identification of a single module with the highest correlation (r = 0.99) (Figure. 3.17, panel A). Pathway analysis revealed that this module was enriched for genes encoding components of three amino acid synthesis pathways (serine-glycine, alanine-cysteine, and cysteine-glutamine), with the serine-glycine biosynthesis pathway representing the most enriched pathway (Figure. 3.18, panel B and Appendix table 3.1).

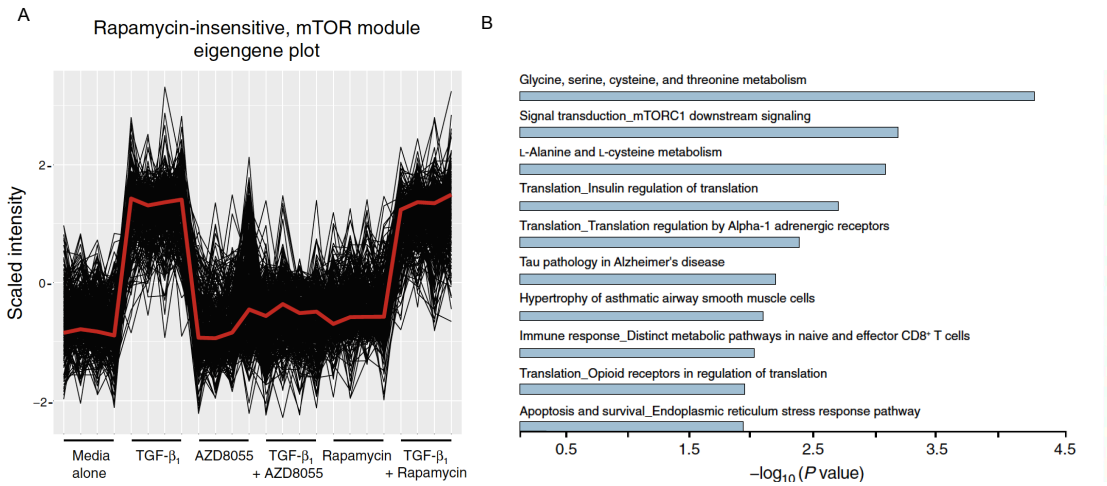

Figure 3.17 Identification of a rapamycin-insensitive, mTOR dependent serine-glycine biosynthetic signature during TGF-β$_1$- induced collagen deposition. (**A**) Plot showing scaled gene expression intensities from the rapamycin-insensitive mTOR module eigengene as calculated by WGCNA. The module eigengene is defined as the first principal component of the genes contained within the module and is representative of the gene expression profiles in the module. All expression values have been z-transformed, and signals that are negatively correlated to the module eigengene have been inverted for plotting (n = 4 independent experiments). (**B**) Bar plot showing the top 10 most significantly enriched pathways for the genes in the rapamycin-insensitive mTOR module. The serine-glycine biosynthesis pathway was most enriched ($P = 5.45 \times 10^{-5}$).

Expression of the serine-glycine biosynthetic pathway genes *phosphoglycerate dehydrogenase* (*PHGDH*), *phosphoserine aminotransferase 1* (*PSAT1*), *phosphoserine phosphatase* (*PSPH*), and *serine hydroxymethyltransferase 2* (*SHMT2*) was increased after TGF-β$_1$ treatment. This increase was inhibited by AZD8055 treatment, whereas rapamycin had no effect (Figure 3.18), indicating that rapamycin-insensitive mTOR signalling may play a critical role in enhancing the expression of genes involved in serine and glycine biosynthesis in response to TGF-β$_1$ stimulation. Of note GLUT1 (*SLC2A1*)(arrowed) was also present in this module, which I will examine later.

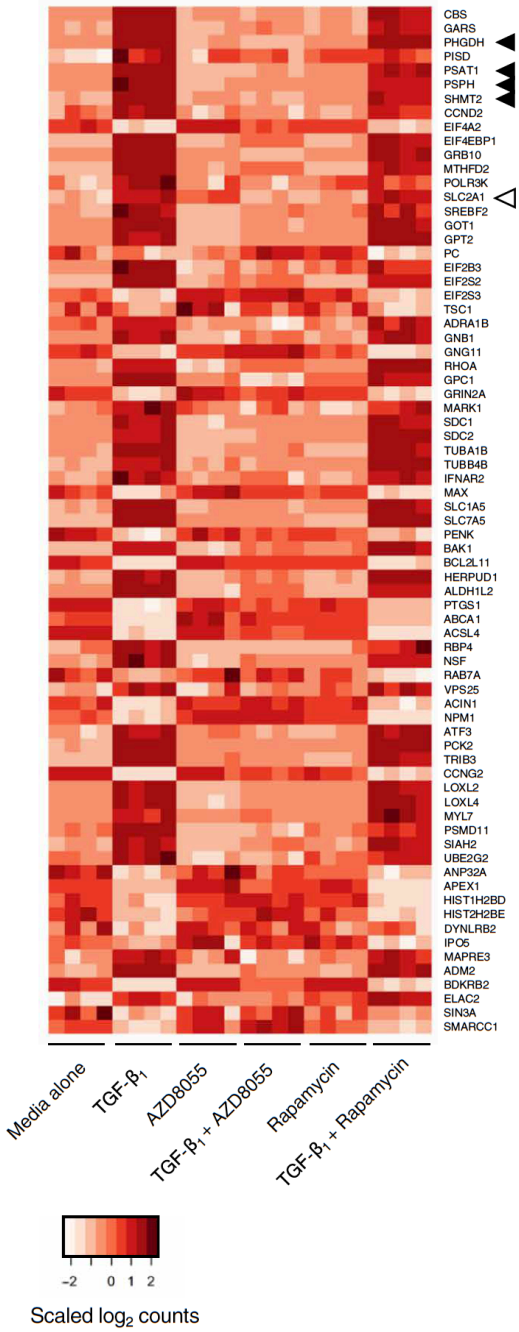

Figure 3.18 Heat map representing the genes from the top 20 most enriched pathways in the rapamycin-insensitive mTOR module. Genes are listed in order of the most to the least statistically significant. Genes that map to more than one pathway only appear for the pathway with the most significant P value. Scaled counts were used to generate the heat map, where darker red indicates higher number of counts. The black arrowheads indicate the genes belonging to the glycine metabolism pathway, and the clear arrowhead indicates *SLC2A1* (n = 4 independent experiments).

3.3.3 TGF-β_1 amplifies the serine-glycine biosynthesis pathway in an mTOR-dependent manner.

The original RNA-seq dataset and previous work in our laboratory demonstrating a key role for rapamycin-insensitive mTORC1 signalling during TGF-β_1–stimulated collagen deposition were generated in pHLFs cultured in standard medium containing 25 mM glucose and 2 mM glutamine. I therefore next demonstrated under physiological glucose and glutamine concentrations, the abundances of transcripts encoding all the enzymes involved in serine-glycine biosynthesis, PHGDH, PSAT1, PSPH, and SHMT2, were significantly increased in response to TGF-β_1 stimulation at 24 hours (Figure 3.19, panel A to D). Evaluation of the effect of TGF-β_1 at the protein level confirmed that the rate-limiting enzymes, PHGDH and PSPH, were increased in response to TGF-β_1 stimulation at 24 hours and that these increases were inhibited by AZD8055 (Figure 3.20, panel E and F).

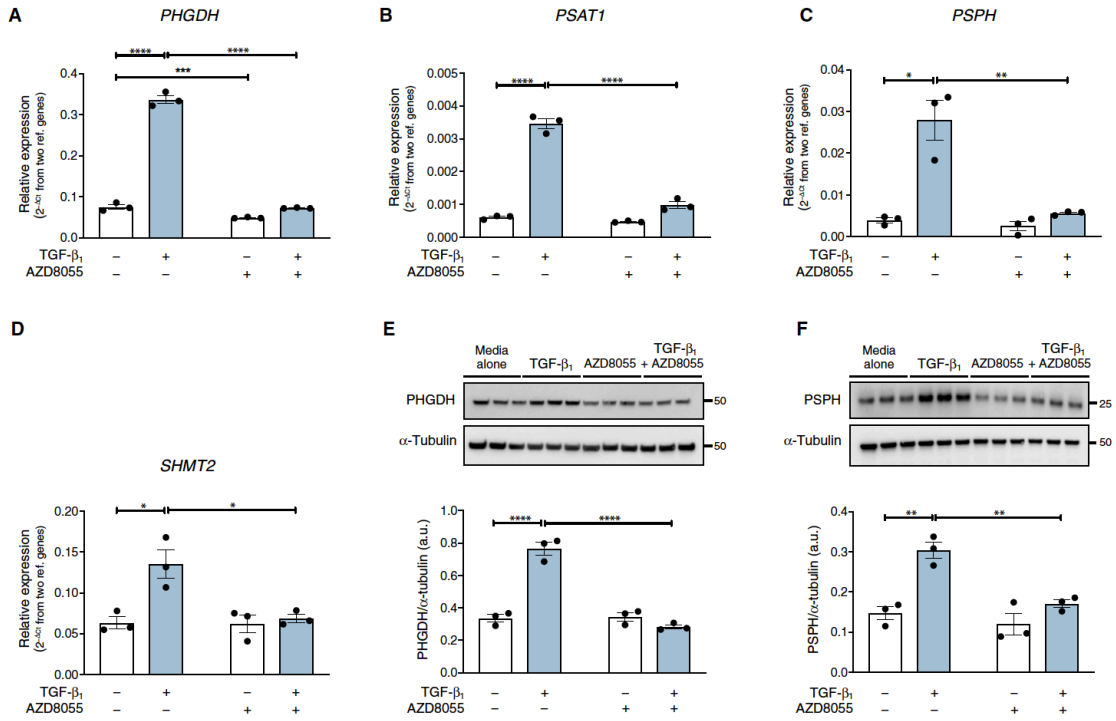

Figure 3.19. TGF-β_1 amplifies the serine-glycine biosynthesis pathway in an mTOR-dependent manner. Confluent pHLFs were incubated in media alone or media plus TGF-β_1 with AZD8055 or vehicle control (DMSO) for 24 hours. (**A** to **D**) Quantification of the relative abundance of *PHGDH* (**A**), *PSAT1* (**B**), *PSPH* (**C**), and *SHMT2* (**D**) mRNAs by real-time quantitative polymerase chain reaction (RT-qPCR). Data are presented as means +/-SEM from three technical replicates per condition and representative of three independent experiments. (**E** and **F**) Immunoblots of protein lysates and densitometric quantification of PHGDH (**E**) and PSPH (**F**). Data and images are representative of three independent experiments with three technical replicates per condition. Differences between groups were evaluated by two-way analysis of variance (ANOVA) test with Tukey post hoc test. *P < 0.05, **P < 0.01, ***P < 0.001, and ****P < 0.0001. a.u., arbitrary units.

In contrast, SHMT1, which preferentially converts glycine to serine (30), was not influenced by TGF-β_1 treatment (Figure. 3.20)

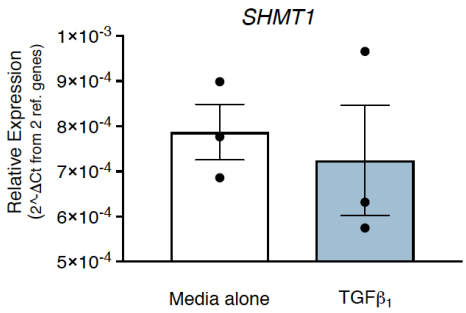

Figure 3.20. TGF-β_1 does not affect *SHMT1* gene expression. Confluent pHLFs were incubated in media alone or media plus TGF-β_1 for 24 hours. Quantification of the relative abundance of *SHMT1* mRNA by real-time quantitative polymerase chain reaction (RT-qPCR). Data are presented as means +/- SEM from three technical replicates per condition and representative of three independent experiments.

The TGF-β_1–induced increase in mRNA abundance of the serine-glycine pathway enzymes was also shown to be insensitive to rapamycin treatment (Figure 3.21) mirroring its effect on TGF-β_1 – induced collagen synthesis.

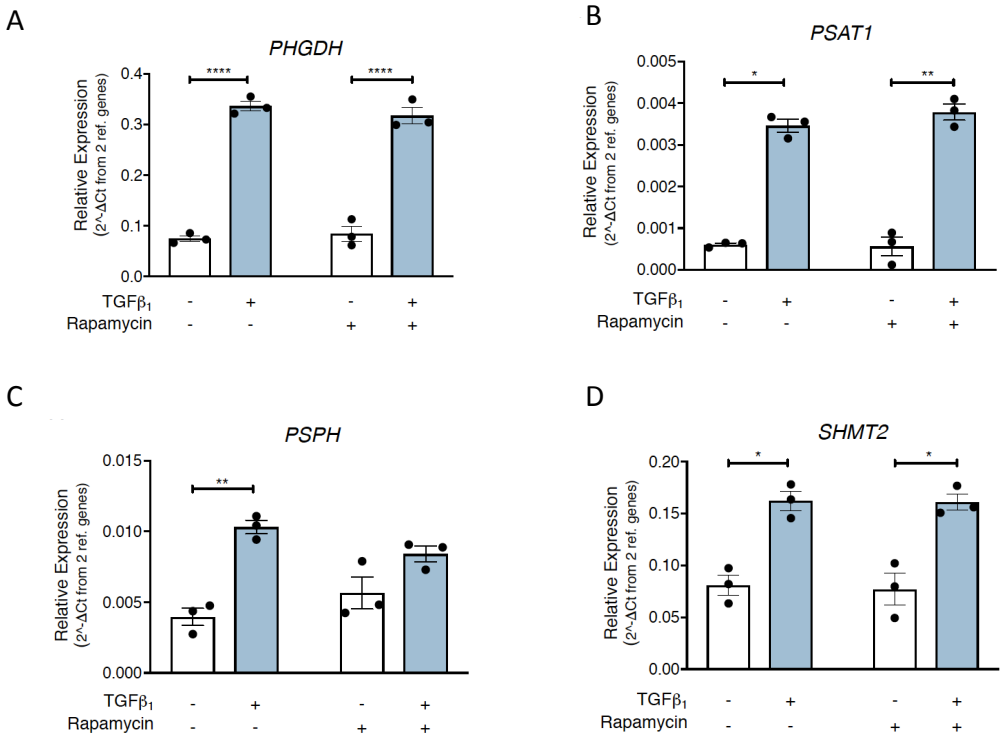

Figure 3.21 Rapamycin does not inhibit the TGF-β_1 induced increase in the gene expression of the glycine biosynthetic enzymes. Confluent pHLFs were pre-incubated with rapamycin or vehicle prior to TGF-β_1 incubation or media alone. After 24 hours, the relative abundances of *PHGDH* (**A**), *PSAT1*(**B**) , *PSPH*(**C**), and *SHMT2*(**D**) transcripts were measured by RT-qPCR. All data are representative of 3 independent experiments with 3 technical replicates per condition. Differences between groups were evaluated by two-way ANOVA (A-D) with Tukey post-hoc testing. *P<0.05, **P<0.01, ****P< 0.0001.

Summary

The results described in this section, investigating how rapamycin-insensitive mTOR signalling affects the global transcriptomic profile in HLFs, revealed that

- The serine-glycine synthetic pathway is the most enriched transcriptional module that is regulated by TGF-β_1-mTOR signalling yet insensitive to rapamycin treatment during collagen synthesis in HLFs.

- TGF-β_1 enhances the mRNA levels of all the enzymes of the glycine biosynthetic pathway in a rapamycin-insensitive, mTOR dependent manner.

- The key rate limiting enzymes, PHGDH and PSPH at the protein level are modulated by mTOR signalling in TGF-β_1 stimulated HLFs.

Taken together, the serine-glycine biosynthetic pathway is identified as a metabolic node that is modulated by mTOR in TGF-β_1 stimulated HLFs.

3.4 mTORC1-4E-BP1 enhances ATF4 production in TGF-β1 stimulated fibroblasts

3.4.1 Introduction

I next explored the potential mechanism by which rapamycin-insensitive mTOR signalling promotes the *de novo* serine-glycine synthesis pathway in response to TGF-β_1.

3.4.2 ATF4 is associated with the rapamycin-insensitive, mTOR-dependent glycine biosynthetic transcriptional signature during TGF-β_1–induced collagen deposition.

Overconnected node (OCN) analysis based on the MetaCore database of gene and protein interactions curated from the literature was used to identify potential master regulators of gene expression in our RNAseq data set. Using the principles of enrichment analysis (Fisher's exact test), a *P* value was calculated for each gene in the database by comparing the overlap of its known interactors with the gene list of interest. OCN analysis of the RNA-seq dataset revealed a cluster of transcription factors associated with the serine-glycine metabolism module of enriched mRNAs, including that encoding the transcription factor ATF4 (Figure. 3.22).

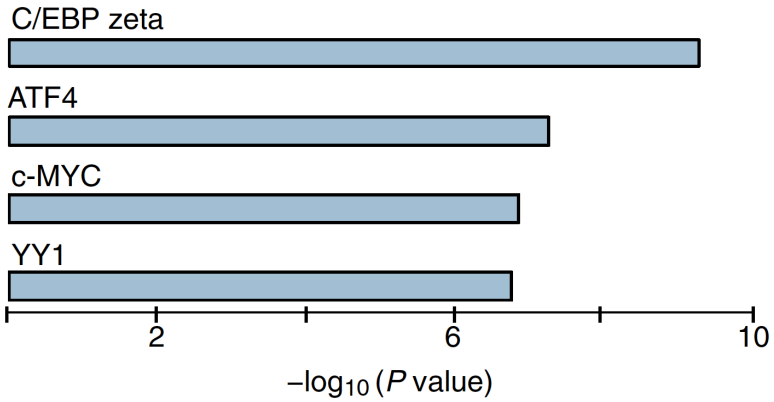

Figure 3.22 ATF4 is associated with the transcriptional regulation of serine-glycine biosynthesis. OCN analysis of the RNA-seq data revealed a cluster of transcription factors associated with the serine-glycine module of enriched mRNAs.

ATF4 is a known mTOR-responsive gene, and ATF4 is a key effector of the stress response that triggers increased gene transcription by binding to the CCAAT/enhancer binding protein

(C/EBP)–ATF response element in specific genes, including all enzymes of the *de novo* serine-glycine synthesis pathway *(159, 160)*. We therefore examined whether *ATF4* was the downstream target of mTOR involved in mediating the TGF-β_1–induced increase in *de novo* glycine biosynthesis and collagen deposition.

3.4.3 The effect of TGF-β_1 on ATF4 expression in human lung fibroblasts.

I first examined the relationship between *ATF4* and TGF-β_1 because *ATF4* is not known to be a TGF-β_1–responsive gene in fibroblasts. *ATF4* mRNA abundance was significantly increased by 2.60 ± 0.37–fold and by 2.02 ± 0.12–fold in cells stimulated with TGF-β_1 relative to cells treated with media alone at 12 and 24 hours, respectively (Figure. 3.23, panel A). At the protein level, ATF4 was barely detectable in untreated cells by immunoblotting. In contrast, ATF4 was abundant in TGF-β_1–stimulated cells at all time points examined from 8 hours onward (Figure. 3.23, panel B).

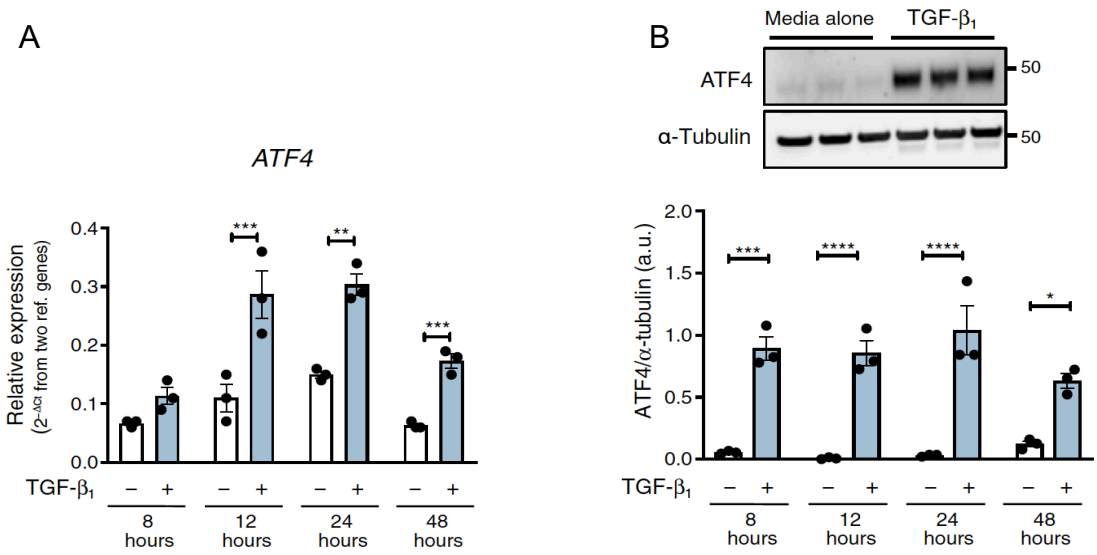

Figure 3.23 TGF-β$_1$ induces ATF4 expression in pHLFs. (**A**) Confluent pHLFs were incubated with or without TGF-β$_1$, and the relative abundance of *ATF4* mRNA over time was measured by RT-qPCR. (**B**) Immunoblot and densitometric quantification of ATF4 protein abundance in pHLF lysates over time after TGF-β$_1$ stimulation. The immunoblot shows ATF4 at 8 hours after TGF-β$_1$ addition. All data are expressed as means +/- SEM from three technical replicates per condition and representative of three independent experiments. Differences between groups were evaluated by two-way ANOVA test with Tukey post hoc test. *P < 0.05, **P < 0.01, ***P < 0.001, and ****P < 0.0001.

3.4.4 The effect of mTOR inhibition on ATF4 expression in TGF-β$_1$ stimulated fibroblasts.

I next determined whether TGF-β$_1$–induced ATF4 expression was sensitive to ATP-competitive mTOR inhibition. AZD8055 had no effect on TGF-β$_1$ -induced *ATF4* mRNA abundance (Figure 3.24, panel A) but completely blocked ATF4 protein production at all time points examined (Figure 3.24, panels B and C).

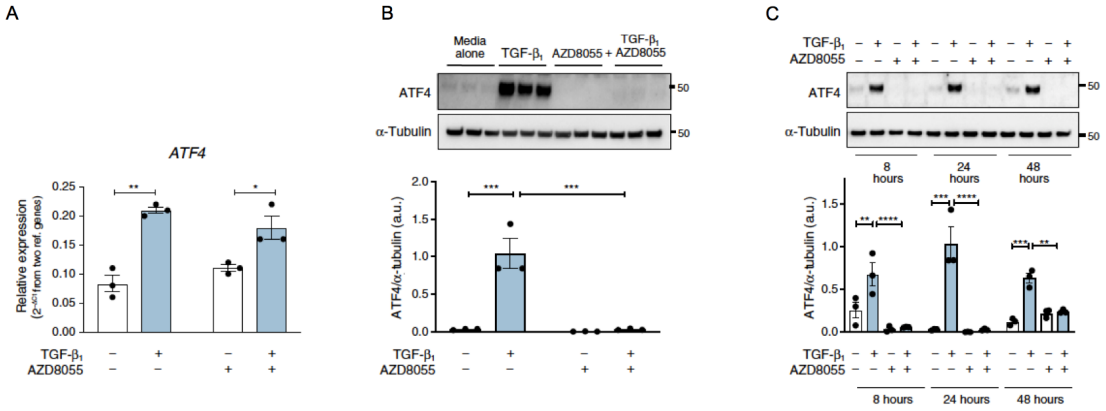

Figure 3.24 mTOR regulates TGF-β$_1$ induced ATF4 expression. Confluent pHLFs were incubated in media alone or media plus TGF-β$_1$ with AZ8055 or vehicle control (DMSO). (**A**) Relative abundance of *ATF4* mRNA measured 24 hours after TGF-β$_1$ addition. (**B**) Immunoblot and densitometric quantification of ATF4 abundance at 24 hours after TGF-β$_1$ addition. (**C**) Immunoblot and densitometric quantification of ATF4 abundance at the indicated times after TGF-β$_1$ addition. All data are expressed as means +/- SEM from three technical replicates per condition and representative of three independent experiments. Differences between groups were evaluated by two-way ANOVA test with Tukey post hoc test. *P < 0.05, **P < 0.01, ***P < 0.001, and ****P < 0.0001.

3.4.5 TGF-β$_1$-induced ATF4 expression is downstream of canonical Smad signalling.

I also examined the contribution of canonical TGF-β$_1$ signalling through the Smad pathway. Silencing *Smad3* using siRNA, I first demonstrated efficient knockdown of Smad3 protein expression (Figure 3.25, panel A). I next showed that silencing Smad3 completely inhibited the increase in *ATF4* mRNA abundance at 24 hours (Figure 3.25, panel B) and protein production assessed at 8 and 24 hours (Figure 3.25, panel C and D).

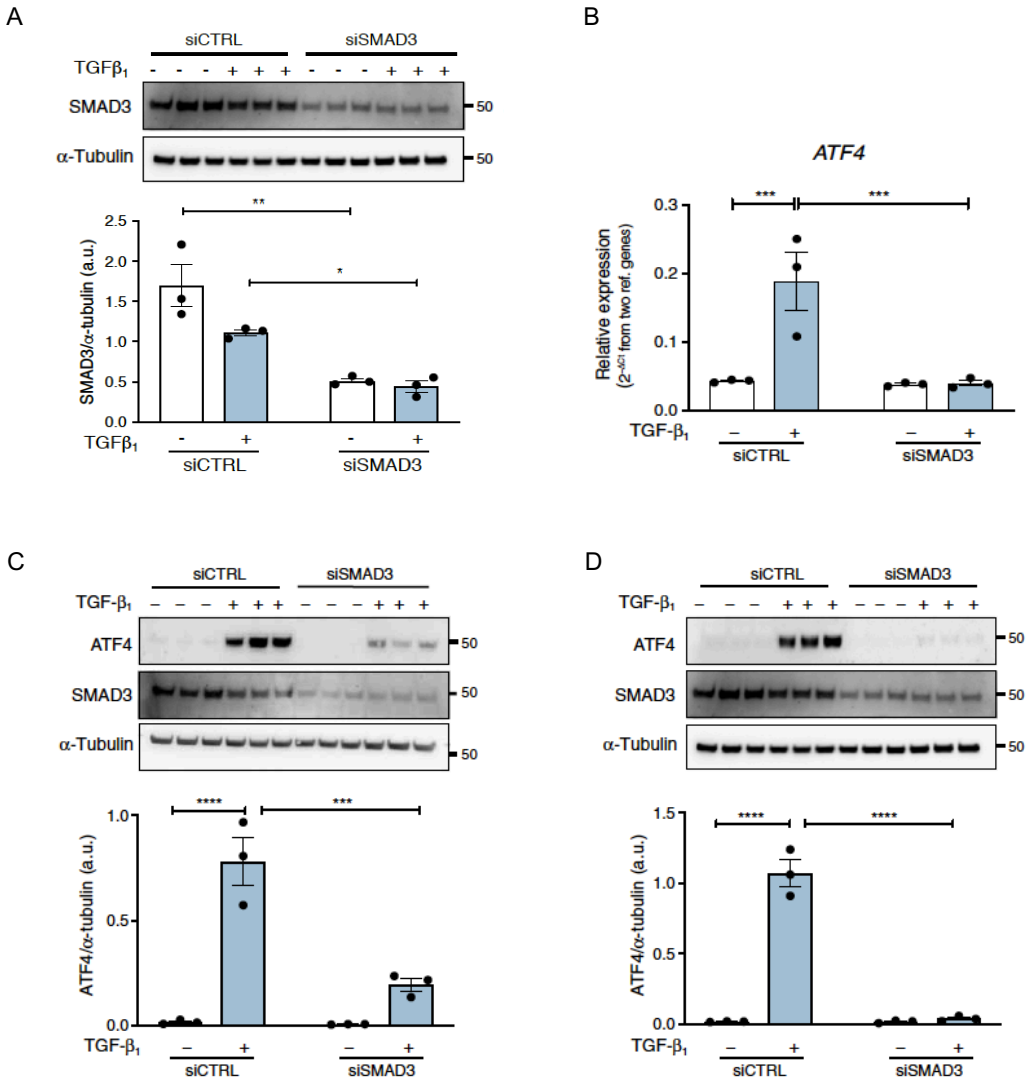

Figure 3.25 TGF-β$_1$ induced ATF4 expression is Smad3 dependent. (**A**) Confluent pHLFs were transfected with Smad3 siRNA (siSMAD3) or scrambled control (siCTRL) before incubation with or without TGF-β$_1$ for 24 hours. A representative immunoblot and densitometric quantification for Smad3 are shown. (**B**) Confluent pHLFs were transfected with scrambled control siRNA (small interfering RNA) (siCTRL) or Smad3 siRNA (siSMAD3) and incubated with or without TGF-β$_1$. Relative abundance of *ATF4* mRNA at 24 hours was measured by RT-qPCR. (**C** and **D**) ATF4 immunoblots and densitometric quantification for samples treated as in (B) analysed at 8 hours (**C**) and 24 hours (**D**). All data are expressed as means +/- SEM from three technical replicates per condition and representative of three independent experiments. Differences between groups were evaluated by two-way ANOVA test with Tukey post hoc test. *P < 0.05, **P < 0.01, ***P < 0.001, and ****P < 0.0001.

I next performed in silico analysis of the ATF4 promoter for Smad binding sequences using three different web-based platforms

identified putative binding sites for Smads 2, 3, and 4 in the *ATF4* promoter with a predicted Smad3 binding site located at base pairs −283 to −275 from the transcription start site (Figure 3.26). Together, these data led to the conclusion that TGF-β_1–induced ATF4 production is both Smad3- and mTOR-dependent and that TGF-β_1 acts at the transcriptional level, whereas mTOR acts post-transcriptionally.

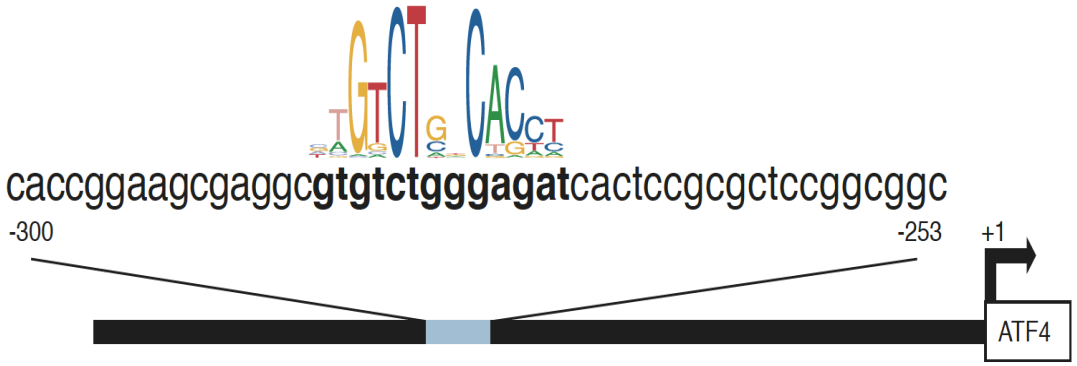

Figure 3.26. In silico analysis of SMAD2,3,4 binding sites in the promoter of ATF4. Location of the predicted binding site and its sequence in the ATF4 promoter are shown. The conserved core sequence is in bold and the consensus binding sequence obtained from the Jaspar database is indicated above it. The font size for each nucleotide reflects the likelihood of finding that nucleotide in that position in the consensus binding sequence (analysis done in collaboration with Dr. Manuela Plate [CITR]).

3.4.6 mTOR regulates TGF-β_1-induced ATF4 protein synthesis in a post-transcriptional manner.

I next explored whether mTOR regulated ATF4 protein abundance by influencing protein stability and/or by stimulating translation. To this end, the effect of AZD8055 on the rate of decline of ATF4 abundance was assessed in the presence of the translation inhibitor, lactimidomycin (LTM). Both compounds were added at 13

hours after the onset of TGF-β_1 stimulation to allow ATF4 protein to accumulate. ATF4 protein abundance was then monitored at different time points over an hour. These experiments revealed that AZD8055 did not influence the rate at which ATF4 protein abundance declined in the presence of LTM and therefore allowed us to conclude that mTOR did not promote ATF4 protein stability (Figure 3.27), implying that mTOR may instead promote the accumulation of ATF4 by stimulating ATF4 translation.

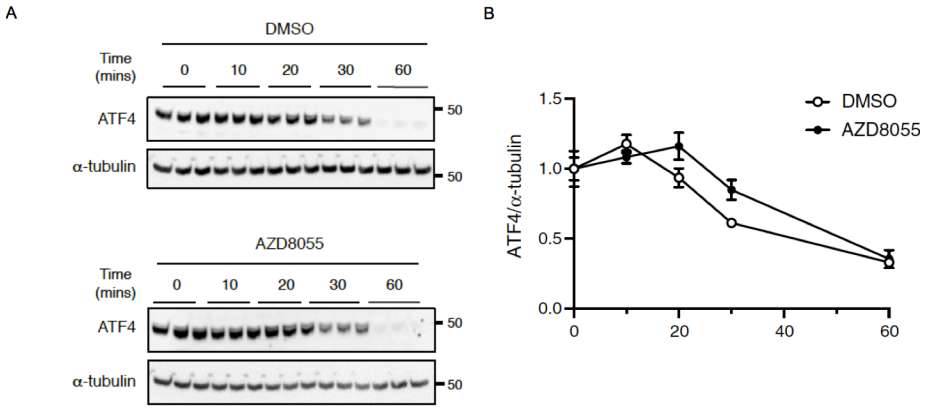

Figure 3.27 mTOR does not regulate ATF4 protein stability. Confluent pHLFs were treated with TGF-β_1 for 13 hours and the translation inhibitor lactimidomycin was added followed by AZD8055 or vehicle. (**A**) Immunoblotting for ATF4 and α-tubulin was performed at the indicated time points and (**B**) ATF4 abundance was measured by densitometric quantification. All data are expressed as means +/- SEM from three technical replicates per condition and representative of three independent experiments. Differences between groups were evaluated by repeated-measures two-way ANOVA (B).

3.4.7 mTORC1-4E-BP1 signalling is responsible for TGF-β_1 - induced ATF4 protein synthesis.

I next sought to identify the mTOR complex involved in mediating the TGF-β_1–induced ATF4 response. To this end, we generated pHLFs that lacked the mTOR accessory proteins RAPTOR or RICTOR by CRISPR-Cas9 gene editing to specifically disrupt either mTORC1 or mTORC2 signalling, respectively. Efficient *RPTOR* and *RICTOR* knockout was confirmed by western blotting (Figure 3.28, panel A and B). TGF-β_1–induced ATF4 protein accumulation was significantly reduced in *RPTOR* knockout fibroblasts but fully maintained in *RICTOR*-knockout fibroblasts, indicating that TGF-β_1 exerts its stimulatory effects on ATF4 production exclusively through an mTORC1-dependent mechanism (Figure 3.28, panel B).

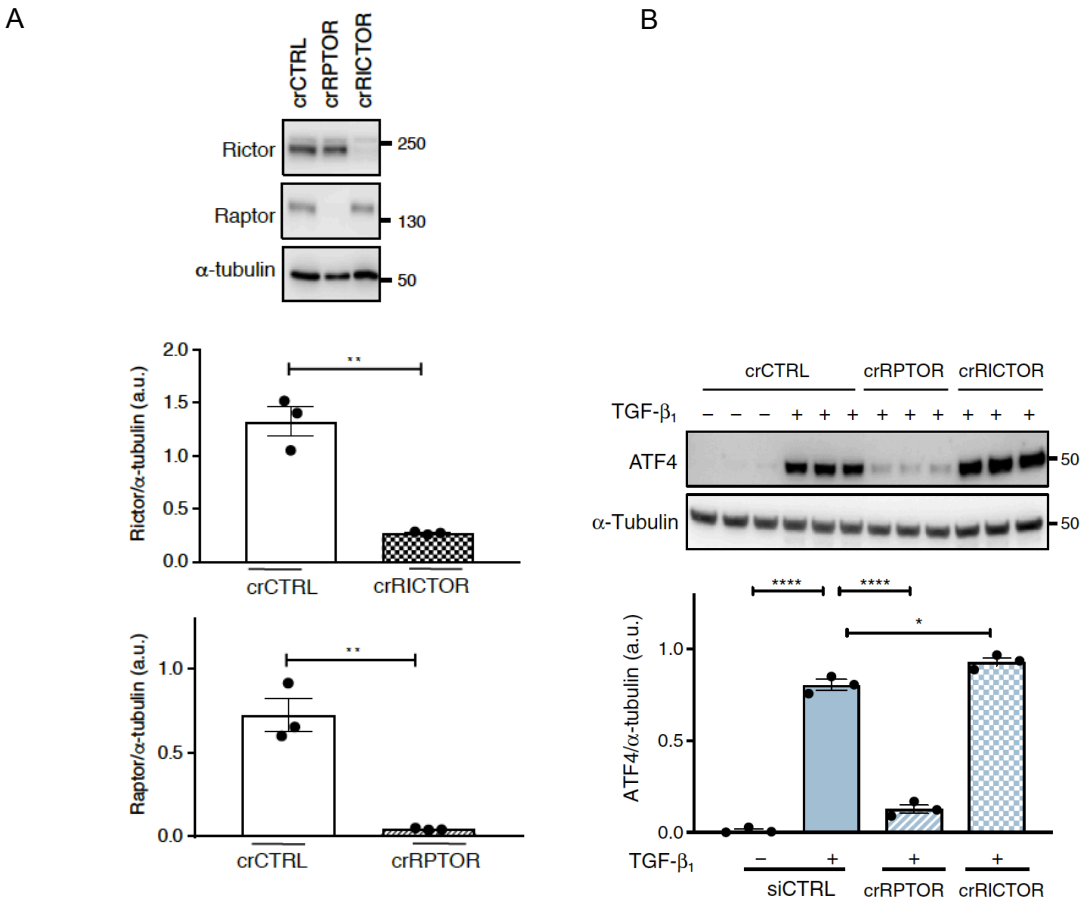

Figure 3.28 mTORC1 signalling promotes TGF-β$_1$ induced ATF4 production. pHLFs were modified by CRISPRCas9 gene editing of *RPTOR* (crRPTOR) or *RICTOR* (crRICTOR) before being incubated in media alone for 24 hours. (**A**)Immunoblotting and densitometric quantification of Raptor and Rictor are shown. (**B**) pHLFs were modified by CRISPR-Cas9 gene editing of RPTOR or RICTOR and stimulated with TGF-β$_1$. Immunoblot for ATF4 and densitometric quantification were performed at 24 hours. All data are expressed as means +/- SEM from three technical replicates per condition and representative of three independent experiments. Differences between groups were assessed by unpaired T-test (A) or one-way ANOVA with Tukey post hoc test (B). *P < 0.05, **P < 0.01,****P < 0.00.01. Data generated in collaboration with Dr Delphine Guillotine (CITR).

The role of 4E-BP1 downstream of mTORC1 in regulating ATF4 was interrogated next, by generating pHLFs expressing a doxycycline-inducible 4E-BP1 dominant-negative phospho-mutant in which the mTORC1 phosphorylation sites were replaced by alanine residues, abbreviated as 4E-BP1-4A *(78)*. pHLFs expressing a doxycycline-inducible 4E-BP1 dominant negative

phospho-mutant have mTORC1 phosphorylation sites Thr37, Thr46, Ser65, and Thr70 replaced by alanine (abbreviated as 4E-BP1-4A). In response to TGF-β_1, the phosphorylation sites on 4E-BP1-4A can not be phosphorylated by mTORC1, therefore the EIF4A complex can not dissociate from 4E-BP1-4A for cap dependent translation to occur. The wild type (WT) 4E-BP1 however can be phosphorylated and dissociates from the EIF4A complex and is replaced by the mutant, 4E-BP1-4A. The mutant 4E-BP1-4A will eventually bind to all the EIF4A complex preventing the WT from binding, therefore becoming the dominant variant and preventing translation occurring. The dominant negative 4E-BP1-4A mutant model therefore would mimic the effects of ATP-competitive mTOR inhibition on collagen deposition. Our laboratory previously confirmed that doxycycline treatment induces 4E-BP1-4A expression in transduced pHLFs and leads to inhibition of cap-dependent translation *(78)*. Here, we found that TGF-β_1–induced ATF4 protein production was completely abrogated in pHLFs expressing 4E-BP1-4A (Figure 3.29, panel A). These effects were not related to inhibition of ATF4 by doxycycline treatment because doxycycline treatment did not inhibit TGF-β_1–induced ATF4 protein production in non-transduced pHLFs (Figure 3.29, panel B). Together, these data demonstrate that the translation-regulating mTORC1–4E-BP1 axis is critical for TGF-β_1–induced ATF4 protein synthesis.

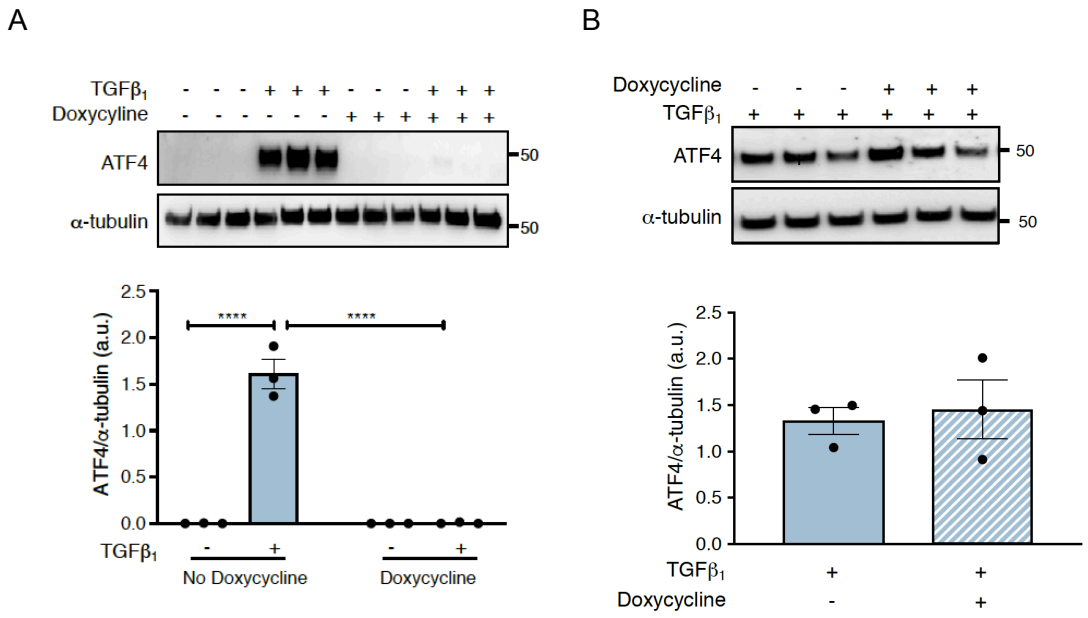

Figure 3.29 mTORC1-4EBP1 axis is critical for TGF-β$_1$–induced ATF4 protein synthesis. (**A**) pHLFs expressing a 4E-BP1-4A dominant-negative phospho-mutant were induced with doxycycline or media alone for 24 hours before TGF-β$_1$ stimulation. Immunoblotting for ATF4 and densitometric quantification were performed at 18 hours after TGF-β$_1$ addition. (**B**) Confluent pHLFs were treated with doxycycline or media alone for 24 hours prior to TGF-β$_1$ stimulation. Immunoblot for ATF4 and densitometric quantification were performed at 24 hours. All data are expressed as means +/- SEM from three technical replicates per condition and representative of three independent experiments. Differences between groups were evaluated by two-way ANOVA test with Tukey post hoc test (A) or unpaired T-test. ****P < 0.0001.

3.4.8 Increased ATF4 expression is independent of classical PERK-eIF2α signalling.

I also examined whether the ATF4 response to TGF-β$_1$ was downstream of the classical stress response involving the activation of protein kinase R–like endoplasmic reticulum kinase (PERK) and subsequent PERK-mediated phosphorylation of eukaryotic initiation factor 2α (eIF2α). However, this possibility was ruled out on the evidence that TGF-β$_1$ had no effect on eIF2α phosphorylation compared to unstimulated fibroblasts over 12

hours (Figure 3.30, panel A). Furthermore, the PERK inhibitor, GSK2656157, did not inhibit TGF-β$_1$–induced collagen deposition (Figure 3.30, panel B).

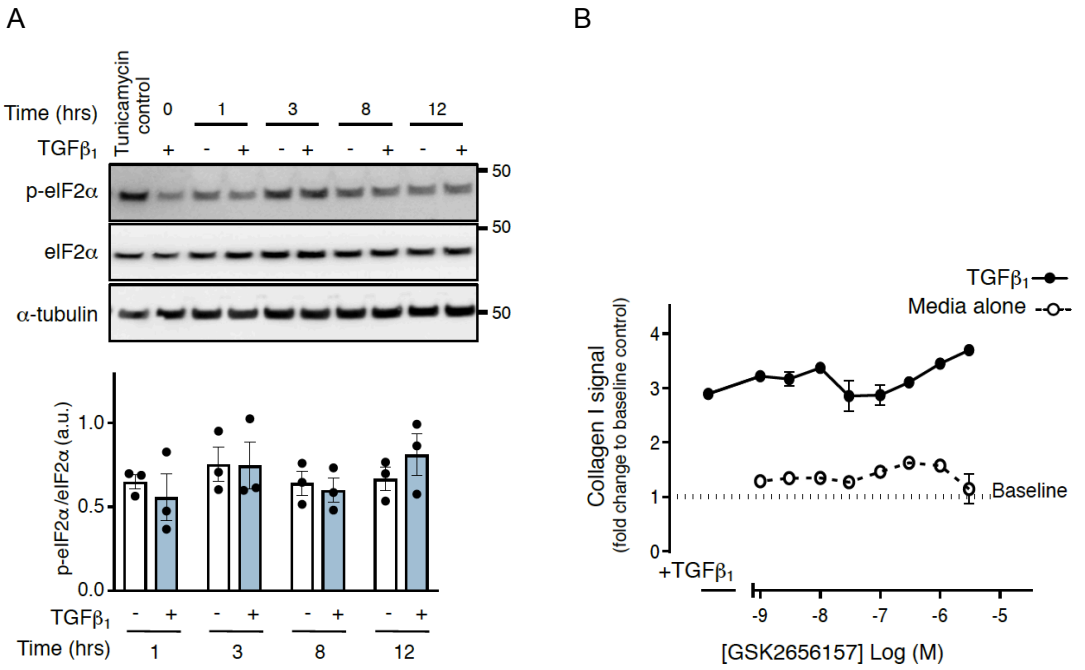

Figure 3.30 TGF-β$_1$ stimulation in human lung fibroblasts is not associated with PERK activation. (**A**) Confluent pHLFs were incubated with or without TGF-β$_1$ before immunoblotting and densitometric quantification of total and phosphorylated eIF2α (p-eIF2α) at the indicated time points. Tunicamycin was added as a positive control, and lysates collected at 12 hours after TGF-β$_1$ stimulation. (**B**) Confluent pHLFs were pre-incubated with the PERK inhibitor GSK2656157 or vehicle (DMSO) and stimulated for 48 hours with or without TGF-β$_1$ before collagen deposition was assessed by high-content imaging. All data are representative of 3 independent experiments with 3 technical replicates per condition. Differences between groups were assessed by two-way ANOVA with Tukey post-hoc test.

3.4.9 ATF4 co-localizes with αSMA–positive myofibroblasts within IPF fibrotic foci.

Having demonstrated that ATF4 production is enhanced in TGF-β$_1$–activated myofibroblasts *in vitro*, I questioned whether this observation held potential translational importance in the clinical

setting of fibrosis in humans. To this end, double immunofluorescence was used to determine whether ATF4 and the myofibroblast differentiation marker αSMA were co-expressed by the same cells in IPF fibrotic foci, the cardinal lesions and leading edge of the fibrotic response. These studies revealed that ATF4 immunofluorescence was consistently and widely present in the IPF lung and was associated with both αSMA–positive myofibroblasts within fibrotic foci and in the hyperplastic alveolar epithelial cells overlying fibrotic foci (Figure 3.31, panels A-C). In control lung parenchyma, ATF4 was mainly found in the alveolar epithelium (Figure 3.31, panel D). Myofibroblasts are generally not found in normal lung, but high-magnification images of myofibroblasts within IPF fibrotic foci demonstrate that ATF4 in myofibroblasts was localized to both the cytoplasm and the nucleus (Figure 3.31, panels E to H).

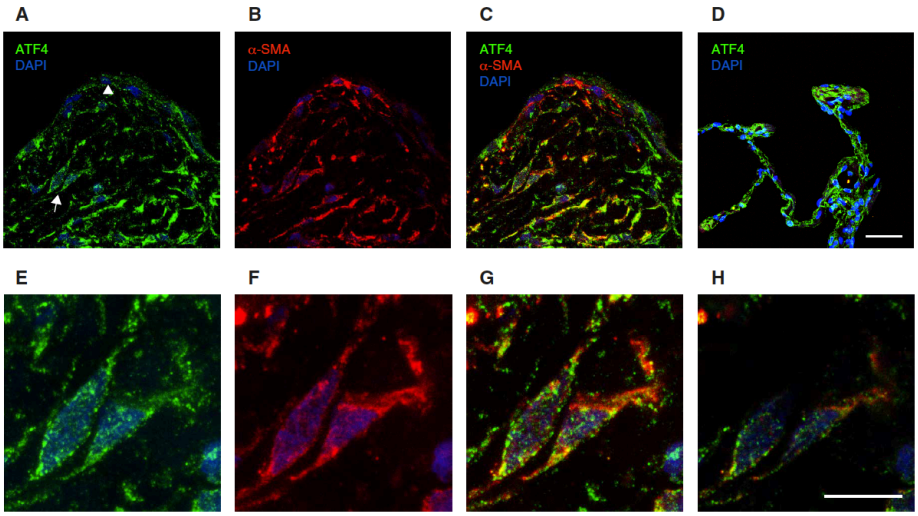

Figure 3.31 ATF4 colocalizes with αSMA–positive myofibroblasts within IPF fibrotic foci. (**A** to **C**) Immunofluoresence showing ATF4 (**A**, green), αSMA (**B**, red), and the overlay of ATF4 and αSMA (**C**, yellow) in a representative IPF fibrotic focus. The arrow indicates myofibroblasts within the fibrotic focus, and the arrowhead points to the hyperplastic epithelium. (**D**) Overlay of ATF4 and αSMA in non-IPF lung tissue. (**E** to **G**) Corresponding high-magnification images of ATF4 (**E**), αSMA (**F**), and the overlay (**G**) in

myofibroblasts within the fibrotic focus indicated by the arrow in (A). (**H**) Mid-level noncomposite confocal overlay image, of the same capture region in (G), showing nuclear localization of ATF4 (green) in an αSMA–positive myofibroblast cell. All images were counterstained with DAPI (blue). Scale bars, 50 μm (A to D) and 25 μm (E to H). n = 3 patients with IPF; n = 2 control subjects. Representative images are shown and were obtained in collaboration with Dr Pascal Durrenberger (CITR).

Summary

The results described in this section, investigating the potential mechanism by which rapamycin-insensitive mTOR signalling promotes the *de novo* serine-glycine synthesis pathway in TGF-β_1 stimulated HLFs, revealed that

- TGF-β_1 induces ATF4, a key transcriptional master regulator of amino acid metabolism, in a transcriptional and translational manner.

- Enhanced ATF4 transcription is modulated in a Smad3 dependent and mTOR independent manner.

- Enhanced ATF4 translation depends on the activation of mTORC1 and its downstream target, 4E-BP1.

Collectively, this section identifies a key role for the mTORC1-4E-BP1 axis in mediating the stimulatory effects of TGF-β_1 on the translation of ATF4, a key transcriptional regulator of glycine biosynthesis.

3.5 ATF4 regulates the expression of the glycine biosynthetic enzymes which is critical for TGF-β_1-induced collagen synthesis

3.5.1 Introduction

The results in the last section revealed that the transcription factor, ATF4 was a TGF-β_1 responsive gene and its translation was downstream of mTORC1-4E-BP1 activation. Overconnected node analysis of the RNAseq data set, identified that ATF4 was associated with the highly enriched transcriptional module encoding for genes associated with glycine biosynthesis in fibroblasts. ATF4 is a known transcriptional regulator of amino acid biosynthesis in other cell contexts and not known previously to be downstream of TGF-β_1 signalling. The next section aimed to interrogate whether the mTOR dependent increase in the expression of the glycine biosynthetic enzymes was permitted through ATF4 during TGF-β_1 induced collagen synthesis.

3.5.2 Enhanced mRNA and protein levels of glycine biosynthetic enzymes are ATF4 dependent in TGF-β_1 stimulated HLFs.

As ATF4 is a master transcriptional regulator, I next investigated whether enhanced ATF4 expression was required to increase the transcription of the key glycine biosynthetic enzymes. Silencing *ATF4* using siRNA, suppressed the TGF-β_1–induced increase in PHGDH, PSAT1, PSPH, and SHMT2 at the mRNA and protein levels (Figure 3.32)

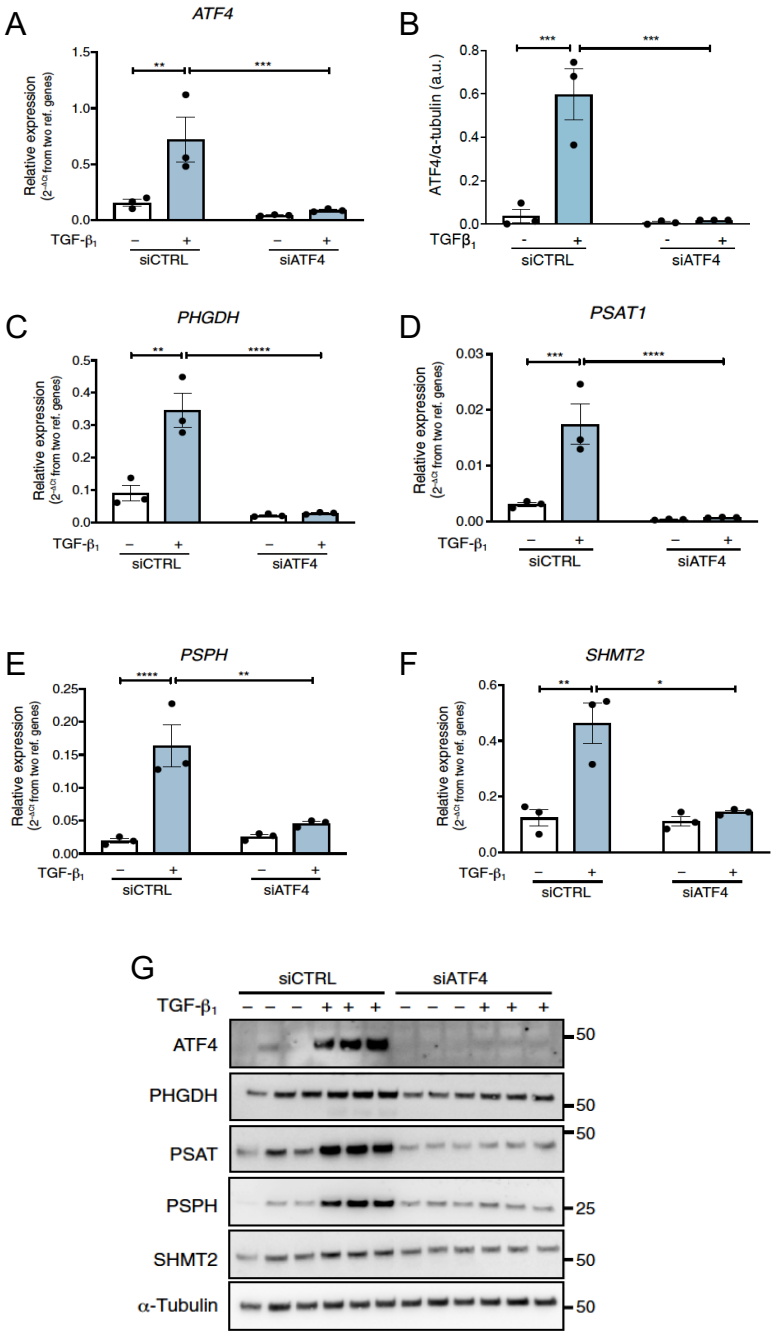

Figure 3.32 ATF4 modulates the expression of glycine biosynthetic enzymes in TGF-β$_1$ stimulated HLFs. (**A** to **E**) Confluent pHLFs were transfected with ATF4 siRNA (siATF4) or scrambled control (siCTRL) before exposure to media plus TGF-β$_1$ or media alone. (**A**) Relative abundance of *ATF4* was measured after 24 hours by RT-qPCR and (**B**) representative immunoblot and densitometry of protein lysates treated as indicated by (A), (**C**-**E**) Relative abundances of (**C**) *PHGDH*, (**D**) *PSAT1*, (**E**) *PSPH*, and (**F**) *SHMT2* mRNAs were measured after 24 hours by RT-qPCR. (**G**) Representative immunoblots of protein lysates treated as indicated in (A) to (E). Data are representative of three independent experiments with three technical replicates per condition. Differences between groups were

evaluated by two-way ANOVA test with Tukey post hoc test (A to E). *P < 0.05, **P < 0.01, ***P < 0.001, and ****P < 0.0001.

3.5.3 ATF4 is critical for TGF-β_1-induced collagen synthesis in pHLFs.

I next investigated the role of ATF4 in mediating the effects of TGF-β_1 on collagen production. Together with enhancing the transcription of all the enzymes involved in serine-glycine biosynthesis, siRNA silencing of ATF4 also inhibited TGF-β_1–induced collagen deposition (Figure 3.33, panel A and B). To control for potential off-target effects of the siRNA, CRISPR-Cas9 gene editing was used to knockout *ATF4*, with efficient knockout presented at the protein level (Figure 3.33, panel C). This approach similarly demonstrated that *ATF4*-deficient cells were unable to increase collagen production in response to TGF-β_1 (Figure 3.33, panel D).

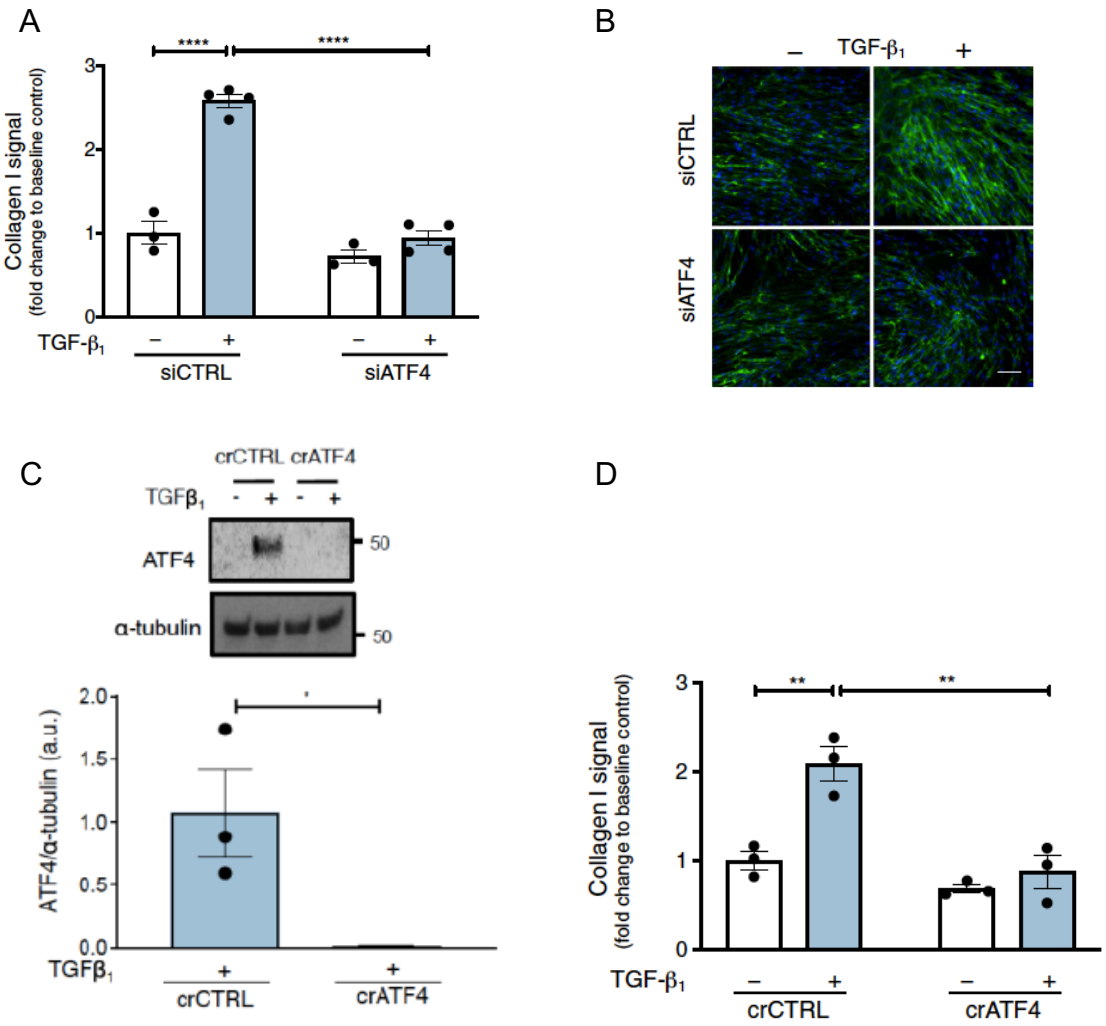

Figure 3.33 ATF4 is critical for TGF-β1–induced collagen deposition in HLFs. (**A**) Confluent pHLFs were transfected with ATF4 siRNA (siATF4) or scrambled control (siCTRL) before exposure to media plus TGF-β1 or media alone. Collagen deposition was assayed by high-content imaging after 48 hours. Each data point shown is the mean +/- SEM of the fold change relative to baseline of three to four technical replicates per condition, and data are representative of three independent experiments. (**B**) Representative immunofluorescence images showing collagen production by cells in (A). Scale bar, 100 μm. (**C**) Confluent wildtype and ATF4-/- CRISPR-mediated knockout pHLFs were incubated with or without TGF-β1. Representative immunoblotting and densitometric quantification for ATF4 are shown at 24 hours. (**D**) Confluent wild-type and ATF4−/− pHLFs were exposed to media plus TGF-β1 or media alone. Collagen deposition was assayed by high-content imaging after 48 hours. Each data point shown is the mean +/- SEM of the fold change relative to baseline of three technical replicates per condition, and data are representative of three independent experiments. Differences between groups were evaluated by two-way (A and D) ANOVA test with Tukey post hoc test and unpaired T-test (C). *P < 0.05, **P < 0.01, ****P < 0.0001.

Summary

The results described in this section, identifying whether ATF4 promotes the transcription of glycine biosynthetic enzymes during TGF-β_1-induced collagen synthesis, showed that

- Enhanced expression of glycine biosynthetic enzymes is dependent on ATF4 in TGF-β_1 stimulated HLFs.

- ATF4 is critical for promoting TGF-β_1-induced collagen synthesis in HLFs.

Together, these data suggest that ATF4 mediates the fibrogenic effects of TGF-β_1 by enhancing the *de novo* serine-glycine pathway.

3.6 mTOR amplifies glucose metabolism during TGF-β_1–induced fibroblast collagen synthesis through an ATF4-dependent mechanism

3.6.1 Introduction

In addition to increased expression of genes encoding serine-glycine biosynthetic enzymes, increased substrate availability is also necessary for increased metabolic pathway activity. Glycine can be synthesized *de novo* from glucose *(161)*, and *SLC2A1*, which encodes the facilitative glucose transporter GLUT1, was

present in the same WGCNA module as the serine-glycine pathway genes and followed the same pattern of induction with TGF-β_1, inhibition of induction in the presence of AZD8055, and insensitivity to rapamycin in our RNA-seq dataset (Figure 3.19). I therefore next considered whether rapamycin-insensitive mTOR signalling downstream of TGF-β_1 increased glucose uptake to support increased glycine biosynthesis during TGF-β_1–induced collagen deposition.

3.6.2. Pharmacological inhibition of mTOR prevents the TGF-β_1-induced increase in glycolytic flux.

ATP-competitive mTOR inhibition with AZD8055 significantly inhibited the TGF-β_1–induced increase in glycolytic flux, represented by the ratio of lactate to glucose measured in cell-conditioned media by 1H-NMR spectroscopy (Figure 3.34, panel A), with individual measurements of glucose and lactate shown (Figure 3.34, panel B and C respectively), as well as inhibition of the TGF-β_1–induced increase in ECAR (Figure 3.34, panel D).

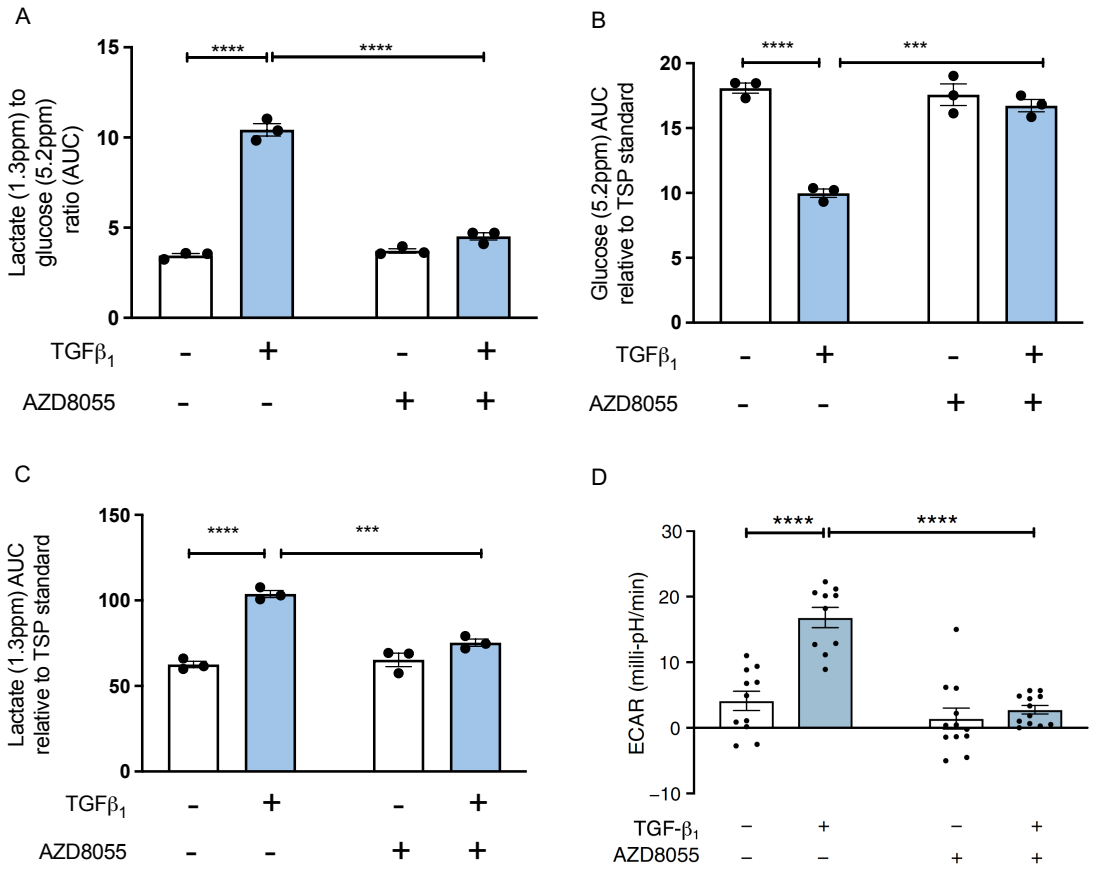

Figure 3.34 Pharmacological inhibition of mTOR prevents the TGF-β$_1$ induced increase in glycolytic flux. Confluent pHLFs were preincubated with AZD8055 or vehicle control (DMSO) before exposure to media plus TGF-β$_1$ or media alone. **(A)** The AUC of the lactate peak relative to the AUC of the glucose peak in cell supernatant was measured by NMR spectroscopy after 24 hours. Data are representative of three independent experiments with three technical replicates per condition. (**B**) The AUC of the glucose peak in the supernatant was measured by NMR spectroscopy after 24 hours. Data are representative of three independent experiments with three technical replicates per condition. (**C**) The AUC of the lactate peak in the supernatant was measured by NMR spectroscopy after 24 hours. Data are representative of three independent experiments with three technical replicates per condition. (**D**)The ECAR was assayed by Seahorse^{TM} XF96e after 24 hours with or without TGF-β$_1$ stimulation Data are representative of three independent experiments with at least three technical replicates per condition. Differences between groups were evaluated by two-way ANOVA test with Tukey post hoc test (A and B). ****P < 0.0001. Data generated in collaboration with Dr Ilan Azuelos (CITR).

Although enhanced glycolytic flux was mTOR dependent, the TGF-β$_1$ induced increase in the expression of the key glycolytic genes

LDHA and *PFKFB3* were insensitive to AZD8055 treatment (Figure 3.35).

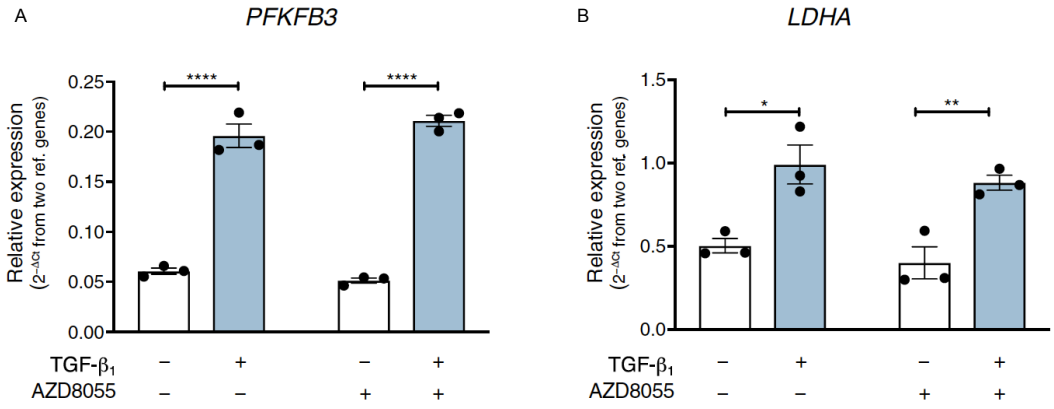

Figure 3.35 TGF-β$_1$–induced increase in PFKFB3 and LDHA gene expression is not regulated by mTOR. (**A** and **B**) Confluent pHLFs were preincubated with AZD8055 or vehicle control before stimulation with TGF-β$_1$ or media alone. Relative mRNA abundances of **(A)** *PFKFB3* at 3 hours after TGF-β$_1$ and **(B)** *LDHA* at 24 hours after TGF-β$_1$ measured by RT-qPCR. Data are representative of three independent experiments with three technical replicates per condition. Differences between groups were evaluated by two-way ANOVA test with Tukey post hoc test (A and B). *P < 0.05, **P < 0.01 and ****P < 0.0001.

In agreement with our RNA-seq dataset, AZD8055 significantly inhibited the TGF-β$_1$–induced increase in *SLC2A1* mRNA abundance and GLUT1 protein abundance (Fig. 3.38, panels A and B). The increase in *SLC2A1* mRNA abundance was Smad3 dependent but rapamycin insensitive (Fig. 3.36, panels C and D). Finally, silencing *ATF4* using siRNA inhibited the TGF-β$_1$–induced increase in *SLC2A1* mRNA levels and GLUT1 protein abundance (Fig. 3.36, panels E and F).

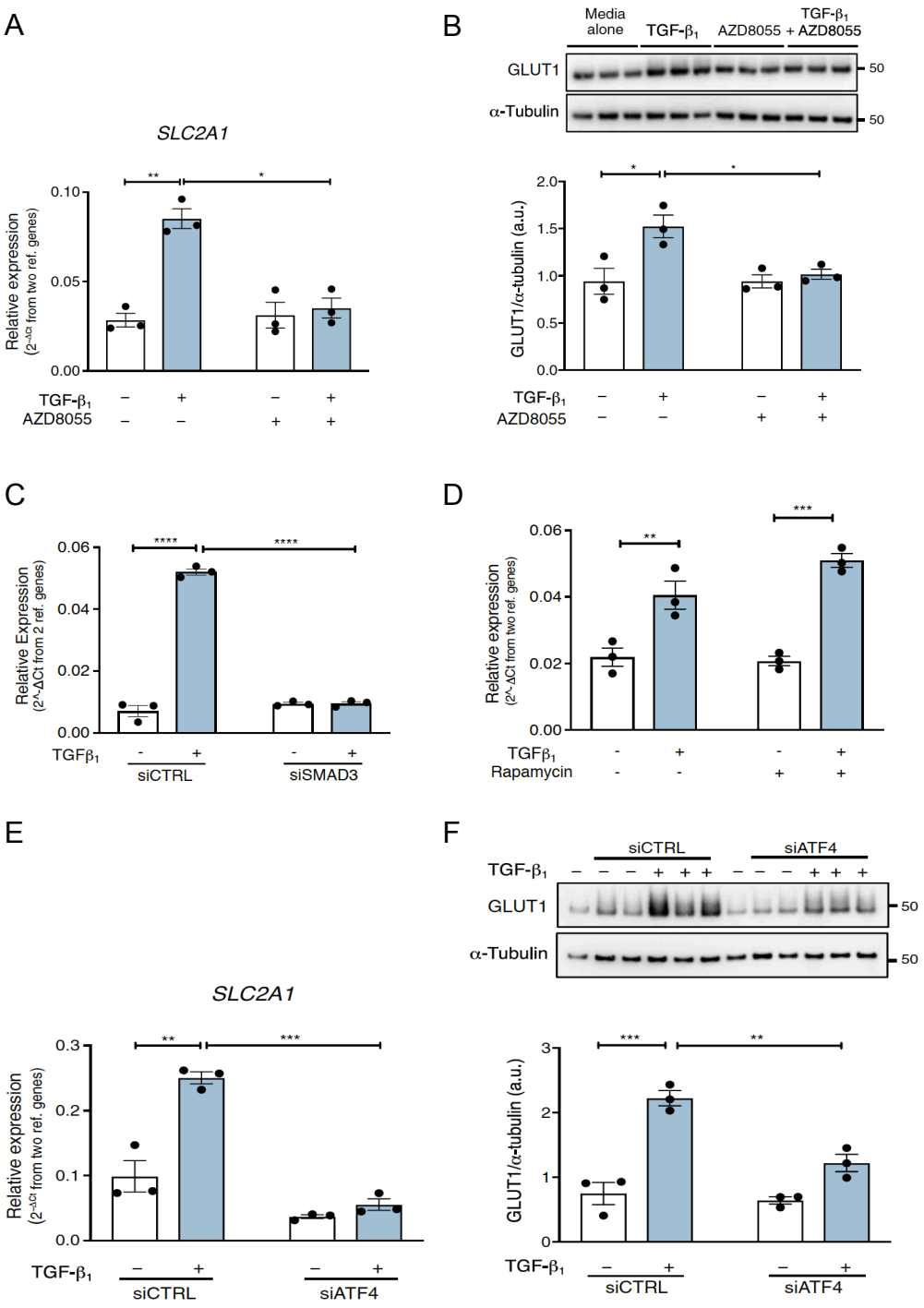

Figure 3.36 The mTOR-ATF4 axis regulates enhanced GLUT1 expression in TGF-β$_1$-stimulated pHLFs. Confluent pHLFs were preincubated with AZD8055 or vehicle control before stimulation with TGF-β$_1$ or media alone. (**A**) Relative mRNA abundance of *SLC2A1* at 24 hours after TGF-β$_1$ was measured by RT-qPCR. (**B**) Cell extracts were subjected to immunoblotting and densitometric quantification for GLUT1 (n = 3 independent experiments). (**C**) Confluent pHLFs were transfected with Smad3 siRNA (siSMAD3) or scrambled control (siCTRL) before incubation with or without TGF-β$_1$. Relative abundance of *SLC2A1* mRNA was measured at 24 hours. (**D**) Confluent

pHLFs were pre-incubated with rapamycin (or vehicle control) and exposed to media plus TGF-β_1 or media alone. Relative abundance of *SLC2A1* mRNA was measured at 24 hours. (**E**) Confluent pHLFs were transfected with ATF4 siRNA (siATF4) or scrambled control (siCTRL) and then exposed to media plus TGF-β_1 or media only. Relative abundance of *SLC2A1* mRNA at 24 hours was measured by RT-qPCR. Data are representative of three independent experiments with three technical replicates per condition. (**F**) Representative immunoblot and densitometric quantification of GLUT1 in lysates from pHLFs treated as in (E), and data are representative of three independent experiments with three technical replicates per condition. Differences between groups were evaluated by two-way ANOVA test with Tukey post hoc test. *P < 0.05, **P < 0.01, ***P < 0.001, and ****P < 0.0001.

Summary

The results described in this section, examining the role of the mTOR-ATF4 axis in promoting enhanced glucose metabolism during TGF-β_1-induced collagen synthesis, showed that

- mTOR enhances glycolytic flux during TGF-β_1-induced collagen synthesis in HLFs.

- Enhanced GLUT1 expression at the protein and mRNA levels is dependent on the mTOR-ATF4 axis during TGF-β_1-induced collagen synthesis.

Together, these data shows that enhanced glycolysis and GLUT1 expression is mTOR-ATF4 dependent, mirroring the role of the mTOR-ATF4 axis during glycine and collagen biosynthesis in TGF-β_1 stimulated fibroblasts.

3.7 mTOR promotes the synthesis of glucose derived glycine to support TGF-β_1-induced–induced collagen synthesis

3.7.1 Introduction

The observation that AZD8055 attenuated TGF-β_1–induced collagen deposition, *de novo* serine-glycine pathway gene expression, and glucose metabolism led me to speculate that mTOR signalling augments TGF-β_1–induced collagen deposition by providing the glycolytic intermediates required for enhanced glycine production and therefore directly contribute to the collagen structure.

3.7.2 Enhanced PHGDH expression promotes TGF-β_1-induced collagen deposition

PHGDH is the first rate-limiting enzyme in the glycine biosynthetic pathway, converting 3-phosphoglycerate (3-PG) from glycolysis into 3-phosphohydroxypyruvate (3-PHP). Therefore I next investigated the effects of inhibiting PHGDH on TGF-β_1- induced collagen deposition. Silencing *PHGDH* with siRNA, I first demonstrated efficient knockdown of PHGDH at the protein level (Figure 3.37, panel A). I next showed that disrupting *PHGDH* using siRNA or inhibition of PHGDH with a selective pharmacological inhibitor (NCT-503)*(162)* blocked TGF-β_1–induced collagen deposition (Figure. 3.39, panel B and C).

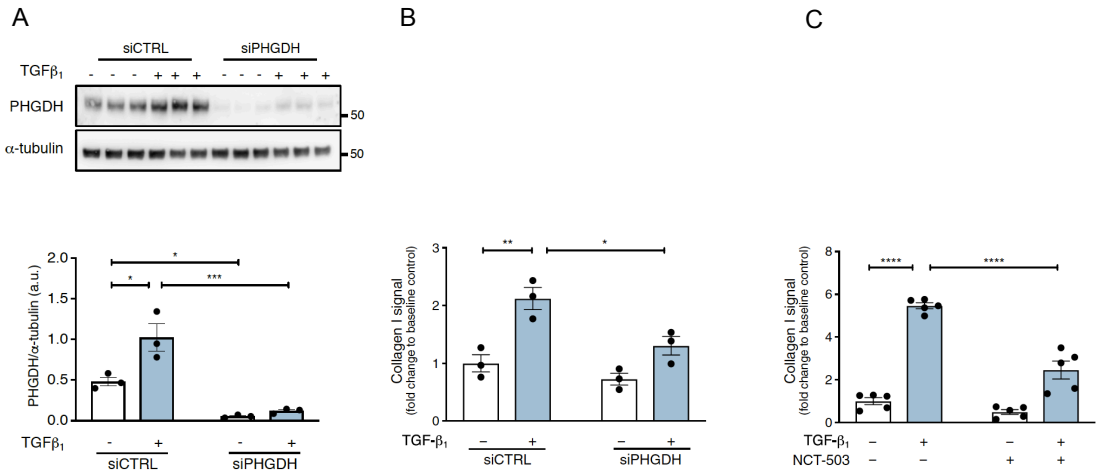

Figure 3.37 Enhanced PHGDH expression promotes TGF-β$_1$-induced collagen deposition. (**A**) Confluent pHLFs were transfected with PHGDH siRNA (siPHGDH) or scrambled control (siCTRL) before incubation with or without TGF-β$_1$. Immunoblotting and densitometric quantification of PHGDH were performed at 24 hours. (**B**) Confluent pHLFs were transfected with PHGDH siRNA (siPHGDH) or scrambled control (siCTRL) and exposed to media plus TGF-β$_1$ or media only for 48 hours. Collagen deposition was assessed by high-content imaging. Each data point shown is the mean +/- SEM of the fold change relative to baseline of three technical replicates per condition and is representative of three independent experiments. (**C**) pHLFs were treated with the PHGDH inhibitor NCT-503 or vehicle control and stimulated with or without TGF-β$_1$ for 48 hours. Collagen deposition was assessed by high-content imaging. Each data point represents the mean +/- SEM of the fold change relative to baseline of five technical replicates per condition and is representative of three independent experiments. Differences between groups were evaluated by two-way ANOVA test with Tukey post hoc test. *P < 0.05, **P < 0.01, ***P < 0.001, and ****P < 0.0001.

3.7.3 mTOR promotes glycine biosynthesis from glucose to support TGF-β$_1$-induced collagen synthesis

To evaluate the need for glucose-derived carbons for glycine biosynthesis and subsequent collagen synthesis, I next examined the impact of glycine supplementation. Glycine partially rescued the inhibitory effect of glucose deprivation on TGF-β$_1$–induced collagen deposition by 70 ± 12% (Figure 3.38, panel A).

Furthermore, glycine supplementation partially rescued the inhibitory effect of AZD8055 on the TGF-β_1–induced collagen response by 58 ± 5% (Figure 3.38, panel B). 450μM of glycine was required to rescue the phenotype with 400μM of glycine already existing in the media before addition of the rescue. In contrast, supplementation with a glycine precursor, serine, did not rescue this inhibitory effect (Figure 3.38, panel C). The conversion of serine to glycine by SHMT2 is an important source of 1-carbon units for the tetrahydrofolate (THF) cycle. Exogenous formate provides 1-carbon directly to the THF cycle and can rescue inhibited cellular growth caused by inhibition of serine homestasis. Addition of formate however failed to rescue the effects of AZD suggesting that mTOR enhances TGF-β_1–induced collagen deposition through the de novo glycine synthetic pathway rather than a need to make formate through 1-carbon metabolism (Figure 3.38, Panel D).

Glutaminolysis is the process through which glutamine is converted to α-ketoglutarate. Enhanced glutaminolysis has recently been implicated in TGF-β_1–induced collagen synthesis in fibroblasts *(163)*. Glutaminolysis involves the conversion of glutamine to glutamate which in turn is converted to α-ketoglutarate. Glutamine derived glutamate can support de novo proline synthesis which has been demonstrated to be essential for TGF-β_1–induced collagen protein production by lung fibroblasts *(163)*. As proline constitutes approximately 23% of the amino acids in collagen, I interrogated whether mTOR enhanced collagen deposition by increasing proline production to increase the supply

of proline for collagen production. Proline however failed to rescue the effects of mTOR inhibition on collagen deposition (Figure 3.38, Panel E), suggesting mTOR did not enhance TGF-β_1–induced collagen deposition through regulating glutamate driven proline synthesis.

Experiments with exogenous radiolabelled glucose and glycine were also performed to determine whether they are incorporated into collagen 1α1(I), which was isolated by immunoprecipitation (Appendix 1), in response to TGF-β_1 stimulation. After pHLFs were incubated with TGF-β_1 and either U-^{14}C-glucose or U-^{14}C-glycine, incorporation of the radiolabel was assessed by scintillation counting of immunoprecipitated collagen. The expected pattern of increased collagen α1(I) production in fibroblasts exposed to TGF-β_1 and the inhibitory impact of AZD8055 were observed by immunoprecipitation and western blotting (Figure 3.38, panel F).

Analysis of U-^{14}C-glucose incorporation into collagen α1(I) mirrored this pattern, with a five-fold increase in U-^{14}C-glucose incorporation into isolated collagen α1(I) in TGF-β_1–stimulated fibroblasts compared to unstimulated fibroblasts. U-^{14}C-glucose incorporation into collagen α1(I) was reduced to baseline values in TGF-β_1 stimulated fibroblasts treated with AZD8055 (Figure 3.38, panel G). We also examined whether exogenous U-^{14}C-glycine was incorporated into collagen α1(I) under conditions where the TGF-β_1–induced serine-glycine biosynthesis pathway was inhibited by AZD8055. Exogenous U-^{14}C-glycine incorporation into collagen α1(I) was low in TGF-β_1–stimulated cells in the absence of AZD8055 but increased six-fold in the presence of AZD8055,

indicating that TGF-β_1–stimulated fibroblasts used exogenous glycine to mount a collagen response when the *de novo* serine-glycine pathway was inhibited by AZD8055 (Figure 3.38, panel H).

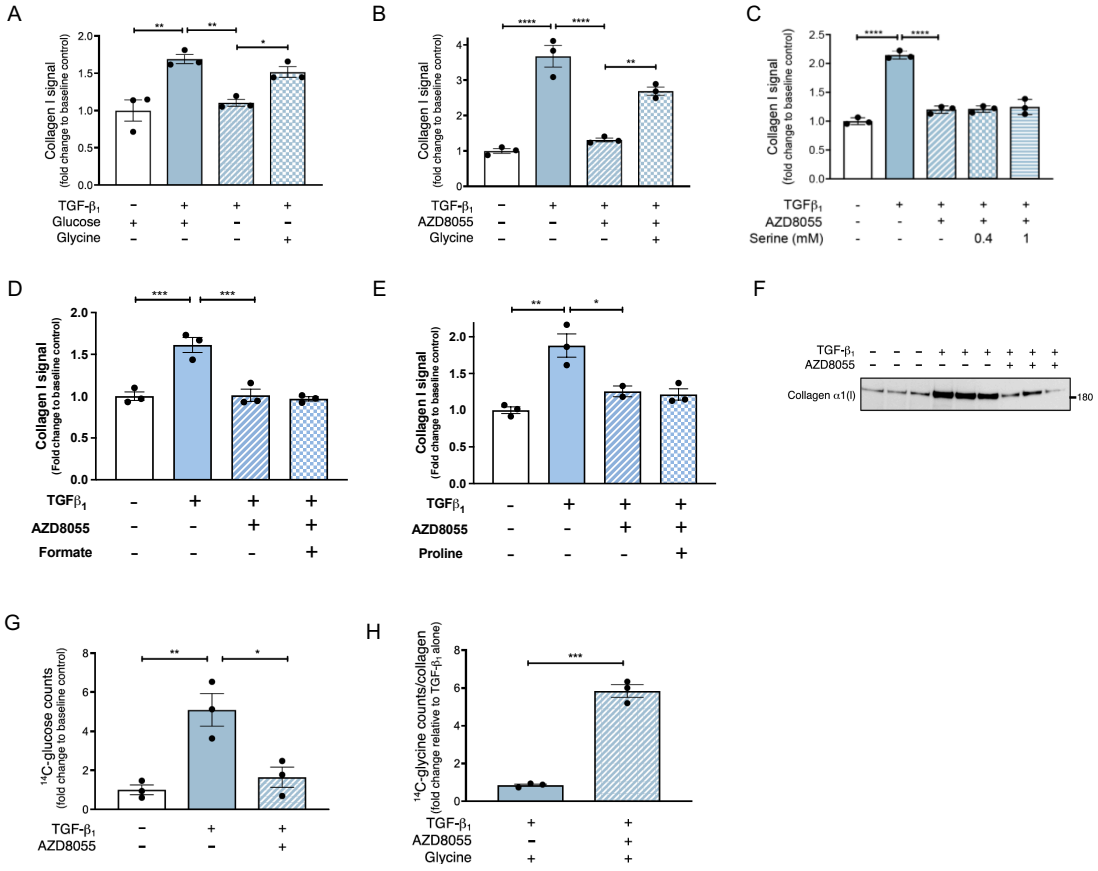

Figure 3.38 mTOR promotes glycine biosynthesis from glucose to support TGF-β_1–induced collagen synthesis. (**A**) Confluent pHLFs were deprived of glucose for 24 hours in the presence or absence of glycine (450μM), followed by TGF-β_1 stimulation for 48 hours before assessment of collagen deposition by high-content imaging. (**B**) Confluent pHLFs were incubated with AZD8055, supplemented 30 min later with or without glycine(450μM), and then incubated with or without TGF-β_1 for 48 hours before assessment of collagen deposition by high-content imaging. (**C**) Confluent pHLFs were incubated with AZD8055 and supplemented with or without increasing concentrations of serine as indicated, then incubated with or without TGF-β_1. Collagen deposition was assessed by high-content imaging at 48 hours. (**D**) Confluent pHLFs were incubated with AZD8055, supplemented 30 min later with or without formate (0.5mM), and then incubated with or without TGF-β_1 for 48 hours before assessment of collagen deposition by high-content imaging. (**E**) Confluent pHLFs were incubated with AZD8055, supplemented 30 min later with or without proline (1mM), and then

incubated with or without TGF-β_1 for 48 hours before assessment of collagen deposition by high-content imaging. (**F**) Confluent pHLFs were incubated with AZD8055 or vehicle (DMSO) and exposed to media plus TGF-β_1 or media alone in the presence of glucose for 48 hours. Collagen α1(I) was isolated by immunoprecipitation and immunoblotted. (**G**) Confluent pHLFs were incubated with AZD8055 or vehicle and then exposed to media plus TGF-β_1 or media alone in the presence of U-^{14}C-glucose for 48 hours. U-^{14}C-glucose incorporation into immunoprecipitated collagen α1(I) was assessed by scintillation counting. (**H**) Confluent pHLFs were incubated with AZD8055 or vehicle and then stimulated with TGF-β_1 in the presence of U-^{14}C-glycine (1mM) for 48 hours. U-^{14}C-glycine incorporation into immunoprecipitated collagen α1(I) was assessed by scintillation counting and expressed relative to immunoprecipitated collagen α1(I) abundance quantified in a parallel immunoblot. Data are presented as means +/- SEM from three technical replicates per condition and are representative of three independent experiments. Differences between groups were evaluated by unpaired t test (F) or one-way (A-C,E) ANOVA test with Tukey post hoc test. *P < 0.05, **P < 0.01, ***P < 0.001, and ****P < 0.0001.

Summary

The results obtained in studies examining the contribution of glucose derived glycine synthesis in permitting the pro-fibrogenic effects of TGF-β_1, show that

- PHGDH is critical for TGF-β_1-induced collagen deposition.

- mTOR drives TGF-β_1-induced collagen deposition by enhancing glucose-derived glycine synthesis to meet the requirements of collagen biosynthesis.

CHAPTER 4: DISCUSSION

Overview

Idiopathic pulmonary fibrosis (IPF) represents the most rapidly progressive and lethal of all fibrotic diseases and is associated with a dismal median survival of 3.5 years from diagnosis. Although the approval of pirfenidone and nintedanib for the treatment of IPF represented a seminal moment for the development of anti-fibrotic therapeutic strategies, these agents do not halt disease progression or significantly improve survival *(6, 164)*. Therefore, there remains a pressing need to develop novel anti-fibrotic therapeutic approaches *(165)*.

The myofibroblast is the key effector cell responsible for the synthesis and deposition of the dense collagen-rich extracellular matrix in multiple fibrotic conditions. Profibrotic mediators, notably transforming growth factor (TGF-β), released in the context of a highly aberrant wound healing response, promote the differentiation of fibroblasts into highly synthetic myofibroblasts *(166)*. Excessive ECM deposition by myofibroblasts is a key feature of multiple fibrotic conditions and has also been implicated in promoting cancer progression *(167)*. Targeting the mechanisms that promote myofibroblast differentiation and collagen deposition are strategies at the core of developing novel anti-fibrotics.

Metabolic reprogramming, a phenomenon describing the process by which cells rewire their metabolic networks to support cell

function and phenotype, is recognised as a hallmark feature of cancer. Common adaptions include enhanced glycolysis, and glutaminolysis as well as changes in mitochondrial function and redox homeostasis to support the requirements of exponential growth and proliferation. Outside the cancer setting, the reconfiguration of metabolic networks may contribute to the pathogenesis of non-oncological diseases, including Alzheimer's disease, obesity, cardiovascular disease, ageing and diabetes. There is also increasing recognition that metabolic reprogramming is critical for shaping inflammatory and immune responses by influencing innate and adaptive immune cell differentiation and function *(108, 120, 168–170)*. There is considerable mechanistic overlap observed in cancer and IPF, including some shared metabolic signatures. There is growing optimism for the implementation of targeting metabolic reprogramming as a therapeutic strategy with a number of recent trials reporting good tolerability and efficacy of metabolic inhibitors in the setting of cancer. This therefore represents repurposing opportunities in the context of fibrosis. However, the mechanisms through which metabolic reprogramming promotes fibrogenesis remain unclear.

The PI3K-Akt-mTOR pathway regulates a diverse range of key physiological processes, including metabolism *(171, 172)*. Aberrant activation of this pathway has been implicated in several disease processes, including cancer, diabetes and inflammation. There is also emerging evidence for dysregulated mTOR signalling in the context of fibrosis *(78, 173–178)*, including recent evidence from our laboratory demonstrating a key role of the mTORC1- 4E-BP1 axis in driving (myo)fibroblast collagen deposition in the

context of IPF *(78)*. However, the downstream mechanism(s) by which mTOR regulates collagen synthesis still remains poorly understood.

As well as furthering our understanding of the signalling and transcriptional events by which key fibrogenic mediators, including TGF-β, reprograms fibroblast metabolism to promote collagen biosynthesis, this new knowledge could have important implications for the development of future therapeutic strategies. Therefore understanding the interplay between metabolic reprogramming and the mTOR axis in potentially driving fibrosis may identify novel selective therapeutic opportunities in IPF.

This thesis therefore examined the hypothesis that **mTOR plays a key role in promoting TGF-β_1 induced myofibroblast differentiation and extracellular matrix deposition in the setting of IPF by influencing glucose metabolism.**

There is growing momentum for studying metabolic responses in more physiological environments *in vitro*. Historically, fibroblasts are cultured in high glucose containing DMEM (25mM) despite these levels being more reflective of diabetic conditions *in vivo.* The post-translational effects of hyperglycaemia on cellular proteins and downstream function are well characterised *(179)*. Furthermore, mTOR is a central metabolic hub responding to nutrient availability and is activated in hyperglycaemic conditions via the PI3K/Akt and AMPK pathway *(180)*. The use of high glucose containing DMEM *in vitro* may subsequently not faithfully recapitulate the role of mTOR *in vivo (181)*. To define the role of

mTOR's role in regulating fibroblast metabolism and collagen deposition, all experiments were performed in DMEM containing physiological levels of glucose (5mM) and glutamine (0.4mM) to more closely mimic *in vivo* conditions. To the best of our knowledge, we are the first group to study metabolic reprogramming in primary human lung fibroblasts (pHLFs) under physiological concentrations of glucose and glutamine.

To address my hypothesis, the initial experiments aimed to investigate:

- The effect of TGF-β_1 on glucose metabolism in primary lung fibroblasts.
- Determine the role of mTOR in regulating TGF-β_1-induced differentiation and collagen synthesis.
- Evaluate the role of mTOR in regulating glucose metabolism during TGF-β_1-induced collagen synthesis.

The data presented in this thesis demonstrate for the first time that:

- TGF-β_1 induces an mTOR-dependent increase in glucose uptake and glycolysis, which is critical for TGF-β_1, induced collagen deposition in human lung fibroblasts.

- In physiological media conditions, mTOR regulates collagen synthesis but not differentiation in TGF-β_1 stimulated human lung fibroblasts.

- TGF-β_1 increases the gene and protein expression of all the enzymes of the *de novo* glycine biosynthetic pathway in an mTOR-dependent and rapamycin-insensitive manner in human lung fibroblasts.

- TGF-β_1 induces ATF4 gene and protein expression through the cooperation of Smad3 signalling and the mTORC1-4E-BP1 axis in human lung fibroblasts.

- ATF4 is required for the mTOR-dependent enhancement of the serine-glycine biosynthetic pathway in TGF-β_1 stimulated fibroblasts.

- ATF4 is critical for TGF-β_1-induced collagen deposition in human lung fibroblasts.

- mTOR enhances glucose-derived glycine synthesis to meet the biosynthetic requirements of collagen production in TGF-β_1 stimulated fibroblasts.

The following sections will discuss these findings and their implications in further detail.

4.1 TGF-β_1 enhances glucose metabolism for myofibroblast differentiation and collagen synthesis.

Enhanced glucose uptake is a well-established feature of cellular proliferation and malignant transformation. All cells require energy to maintain homeostasis but proliferating cells have a further energetic requirement for growth and division, as well as an increased carbon need for biosynthesis *(153)*. A recent study highlighted that in non-small lung cancer cells, glucose represented an important source of ribose for nucleic acid replication and non-carbon material, such as reducing equivalents and energy while amino acids accounted for the majority of carbon cell mass in proliferating cells *(121)*.

The increased 18F-FDG PET signal observed in the fibrotic regions of the IPF lung was the first indication that increased glucose uptake was occurring in this region *(104)*. This observation potentially reflects a need for the hyperproliferative and hypersynthetic myofibroblasts in the fibrotic foci to meet an increased energy and carbon demand. This thesis first addressed whether enhanced glucose metabolism including glucose uptake is observed in primary human lung fibroblasts in response to TGF-β_1.

4.1.1 Increased glucose uptake is essential for TGF-β_1-induced myofibroblast differentiation and collagen synthesis

TGF-β_1 is a potent pro-fibrotic growth factor that promotes

fibroblast to myofibroblast differentiation, which is marked by the *de novo* expression of αSMA incorporation into stress fibres *(182)*. Once differentiated, the myofibroblast synthesizes extracellular matrix proteins, notably the fibrillary collagens I and III.

To understand the functional effects of TGF-β_1 on pHLFs, the temporal regulation of collagen I and αSMA gene expression following stimulation were considered. Levels of *COL1A1 and ACTA2* mRNAs were not significantly potentiated at early time intervals; however there was peak expression of αSMA at 24 hours and collagen I at 36 hours. This would temporally correspond with an increase in insoluble fibrillar collagen I deposition into an extracellular matrix and *de novo* induction and assimilation of αSMA into stress fibres using the macromolecular assay at 48 hours.

This thesis next demonstrates that glucose uptake is significantly enhanced during TGF-β_1 induced myofibroblast differentiation and collagen synthesis. Interestingly, enhanced glucose uptake from 8 hours following TGF-β_1 stimulation preceded the increase in αSMA and collagen gene expression. Glucose uptake continued to increase throughout TGF-β_1 induced differentiation with a maximal 3-fold increase once the fibroblast had acquired a myofibroblast phenotype and actively depositing collagen compared to media only treated fibroblasts.

Glucose is a basic requirement for many cellular processes, especially those that require high amounts of ATP and carbons for biosynthesis *(153)*, including differentiation and collagen

biosynthesis. Differentiation is an anabolic process, which requires an increased supply of ATP and precursors such as nucleotides and amino acids for *de novo* αSMA expression, while collagen biosynthesis involves a complex multistage process as described previously (Section 1.2.4). The data herein demonstrates that TGF-β_1 induced increase in glucose uptake precedes the increase in αSMA and collagen I gene expression. This suggests that TGF-β_1 signalling potentially triggers an early increase in glucose uptake for a process that precedes differentiation and peak collagen synthesis. Glucose uptake then continues to increase to potentially meet the needs of differentiation and collagen synthesis. Interestingly, the FDG signal observed in IPF has recently found to be higher in non-fibrotic areas of IPF lungs compared to control lungs, suggesting a global metabolic change may occur in IPF before radiological and pathological features of fibrosis are apparent *(124)*.

During the course of this work, recently published studies using monolayer cultures of murine or fetal human lung fibroblasts suggest that 24 hours of TGF-β_1 treatment induces ATP production and this is linked to an increase in mitochondrial biogenesis *(183, 184)*. Hence, an increase in glucose uptake may occur to facilitate ATP production in the mitochondria as well as glycolysis. However a recent paper examining the global metabolic profile in IPF lung tissue revealed increased amounts of ATP degradation products and decreased intracellular ATP. The authors suggested that oxidative stress and hypoxia could lead to mitochondrial damage, resulting in ATP depletion in IPF *(140)*. Further work is required to fully characterize the energy

requirements during TGF-β_1 induced myofibroblast differentiation and collagen synthesis in fibroblasts and IPF myofibroblasts. Performing detailed kinetic studies of ATP production during TGF-β_1 induced differentiation and collagen synthesis will help characterise the energy requirements of these processes.

The observed increase in glucose uptake during peak differentiation and collagen synthesis may mark the need for hypersynthetic and hyperproliferative myofibroblasts to feed carbons into macromolecular biosynthetic pathways to support fibrogenesis. Two profiling studies using GCMS to analyse the metabolite distributions in IPF lung tissue have revealed alterations in a number of metabolic synthetic pathways including glutathione biosynthesis and ornithinine amino transferase pathway for proline production*(135, 140)*. Furthermore, carbon-labelling studies presented in this thesis also demonstrate for the first time that glucose is required to provide carbons for *de novo* glycine synthesis, which is critical for collagen production, and will be discussed in detail later.

It is well established that glucose has other roles besides acting as a substrate for ATP production and providing carbons for biosynthesis. Notably, glucose is required for post-translational modifications, including glycosylation. Under normal conditions, around 1–3% of intracellular glucose is siphoned from the glycolytic pathway to the hexosamine biosynthesis pathway (HBP). HBP produces uridine diphosphate-N-acetyl-D-glucosamine (GlcNAc), an important donor molecule for post-translational modifications, such as N- and O-glycosylation. As previously

outlined, glycosylation is an essential modification during collagen synthesis but has recently been shown to influence TGF-β signalling. TGF-β normally interacts with two heterotetramic complexes of two related type I and II serine/threnone kinase receptors, TGF-β receptor I and II (TβRI/II). Binding of TGF-β to TβRII results in transphosphorylation of TβRI and then subsequent activation of SMAD and SMAD-independent pathways. A recent study demonstrated that N-linked glycosylation of TβRII influenced TGF-β signalling by regulating the transport of the TβRII to the surface and its interaction with TGF-β in cancer cell lines *(185)*. It is tempting to speculate that an early increase in glucose uptake may facilitate early N-linked glycosylation of the TGF-β receptor to increase the efficiency of TGF-β signalling. It would therefore be informative to assess the glycosylation patterns of the TGF-β receptors during TGF-β induced myofibroblast differentiation and collagen synthesis in human lung fibroblasts.

Enhanced glucose uptake during TGF-β_1 induced myofibroblast differentiation was accompanied by a significant increase in mRNA and protein levels of the glucose transporter type 1, GLUT1, at 24 hours. GLUT1 is the most commonly expressed facilitative glucose transporter in the lung and has been associated with increased 18F-FDG uptake in lung cancer (183). There are some reports documenting increases in GLUT1 expression secondary to TGF-β stimulation in murine fibroblasts however there is limited data on GLUT1 expression in human lung fibroblasts*(186, 187)*.

In terms of temporal responses, we observed a significant peak in GLUT1 gene expression at 24 hours of TGF-β_1 stimulation. The

finding that TGF-β promotes GLUT1 protein production is consistent with a previous study in the context of the autocrine activation of the receptor tyrosine kinases, platelet-derived growth factor and epidermal growth factor receptors, in murine embryonic ankyrin repeat domain-containing protein 2B (AKR-2B) fibroblasts stimulated with high concentrations of TGF-β_1*(186)*. This study also reported that the accumulation of GLUT1 mRNA was completely abolished by the transcriptional inhibitor, actinomycin D, with their preliminary results showing no change in mRNA stability, therefore suggesting that the regulation of GLUT1 gene expression by TGF-β occurs at the transcriptional level. As discussed earlier, raised GLUT1 expression has also been reported in lung tissue from IPF patients and in the bleomycin model *(188–190)*, suggesting that GLUT1 may play a role in promoting fibrosis.

It is noteworthy that increased glucose uptake precedes the increase in GLUT1 gene expression so it is likely that alternative mechanisms facilitate early glucose uptake during myofibroblast differentiation. These could include increased translocation of GLUT1 to the membrane or post-translational modifications of GLUT1 to increase its affinity for glucose. The translocation of GLUT1 has been examined in a number of cell types; including Ras transformed 3T3-L1 fibroblasts and IL7 activated T cells *(191, 192)*. Interestingly, the translocation of GLUT1 from an intracellular pool to the membrane in both instances has been associated with the activation of the PI3K/mTOR signalling axis *(193)*. Further work examining the effect of TGF-β_1 on GLUT1 translocation in our cell system would be interesting to

characterize the mechanism through which the early increase in glucose uptake occurs.

Increasing glucose uptake through the post-translational modification of the glucose transporters can also occur. A previous study has described TGF-β_1 induced changes in glycosylation patterns of GLUTs and the subsequent increase in their affinity to glucose in mouse fibroblasts *(194)*. This study showed that TGF-β modulated the branch structure of N-linked oligosaccharides on GLUT1 transporters in Swiss 3T3 mouse fibroblasts. This resulted in a greater affinity for glucose and increased glucose uptake. Together with characterizing the glycosylation patterns of the TGF-β receptor, it would be noteworthy to determine the effect of TGF-β on the glycosylation pattern of GLUT1 and its subsequent effect on glucose uptake and myofibroblast differentiation.

This thesis next investigated whether glucose availability was a functional pre-requisite for myofibroblast differentiation and collagen deposition. Incubating fibroblasts in medium deprived of glucose significantly inhibited TGF-β_1 induced myofibroblast differentiation and collagen production. Function blocking studies based on silencing GLUT1 (*SLC2A1*) with shRNA or by pharmacological inhibition using GLUT inhibitor II and phloretin, have also shown that TGF-β_1-induced αSMA expression was inhibited. During the course of this PhD work, phloretin was additionally found by other investigators to inhibit the production of collagen and fibronectin *in vitro* as well as attenuate lung fibrosis in the bleomycin model *(133, 188)*. This thesis also demonstrated

that glucose deprivation significantly inhibited the mRNA levels of αSMA but not of Collagen I, highlighting that differing mechanisms may control gene expression of the two main phenotypic markers of TGF-β_1- stimulated myofibroblasts.

It is worth commenting that in conditions of limited glucose availability, highly proliferative, glucose addicted cancer cells are thought to lose their enhanced growth ability due to a decreased pool of carbons, ATP depletion, accumulation of radical oxygen species (ROS) or general mitochondrial dysfunction (97). Glucose deprivation is also known to activate the unfolded protein response (UPR), especially in cancer cells *(195)*. UPR results in altered protein folding in response to different stimuli that may lead to either cell survival or cell death depending on the strength and duration of the stimulus. In the present study, there was no evidence of cell death in either control or TGF-β_1 treated fibroblasts up to the end of the experimental period (48 hours). It is tempting to speculate that myofibroblasts may use glutamine, and/or other substrates to overcome glucose starvation-induced cell death over 48 hours as has been reported for other cell types*(196)*.

As described previously, glucose is important for post-translational modifications, such as N-linked glycosylation which has been shown to affect TβRII function and is a modification required for collagen biosynthesis. It is therefore possible that glucose deprivation may exert a direct effect on TGF-β signalling during differentiation and collagen synthesis.

It is further possible that glucose deprivation may also exert its effect on collagen and myofibroblast differentiation through the central energy regulator, adenosine monophosphate-activated protein kinase (AMPK). AMPK is a member of the metabolite-sensing protein kinase family with serine/ threonine kinase activity and is expressed in all eukaryotic organisms. AMPK is activated under certain conditions, including glucose deprivation, which is associated with an increase in intracellular AMP levels. AMPK plays a fundamental role in conserving cellular energetic homeostasis by modifying the metabolic phenotype to manage nutritional stress *(197)*.

When ATP, oxygen or glucose levels are low, AMPK is activated via the tumour suppressor, LKB1 and directly phosphorylates the tuberous sclerosis complex (TSC), which negatively regulates mTORC1 and Raptor, an accessory subunit of the mTORC1 complex. Data published by other investigators during the course of this thesis, have demonstrated there is reduced AMPK activation in TGF-β_1 stimulated HLFs, IPF derived fibroblasts as well as associated with the fibrotic regions of IPF lung and the bleomycin model *(133, 198)*. Decreased AMPK phosphorylation is also associated with increased mTORC1 signalling and metabolic reprogramming including HIF1α stabilisation and downstream lactate production in IPF fibroblasts *(199)*. Therefore the effect of glucose deprivation on collagen deposition and αSMA protein expression might be explained by the activation of AMPK and its subsequent inhibition of mTORC1, which we know to be integral to TGF-β_1 collagen synthesis. However recent data has shown that in AMPK knockout cells, mTORC1 is still inactivated upon glucose

starvation, indicating other sensors of glucose levels regulate mTORC1 *(200)*. The AMPK activators, AICAR and metformin have also very recently been reported, to prevent αSMA and ECM protein production in TGF-β_1-stimulated fibroblasts and even reverse αSMA expression after 24 hours of TGF-β_1 stimulation *(198, 201)*. Furthermore, as well as preventing the development of experimental fibrosis, metformin promotes the resolution of fibrosis*(198)*.

4.1.2 Enhanced glycolysis is essential for TGF-β_1-induced myofibroblast differentiation and collagen synthesis

Glycolytic control is now emerging as a key event driving disease progression in a number of disease contexts. Lactate production is a product of increased glycolysis and this report demonstrates a significant increase in extracellular lactate production during TGF-β_1-induced myofibroblast differentiation and collagen synthesis compared to media treated fibroblasts.

The observation that lactate production is increased *in vivo* has been confirmed in IPF lung tissue *(103, 135, 136)* and in the murine model of bleomycin-induced fibrosis *(134, 137)*.

It is possible that lactate may simply represent a by-product of increased glycolysis, where increased glycolytic intermediates are siphoned off into biosynthetic and ATP producing pathways. On the other hand, lactate may play more essential roles. The conversion of pyruvate to lactate is important for regenerating

NAD+, which is essential for maintaining NAD+/NADH redox balance and for glycolysis to continue. Regeneration of NAD+ is key for the conversion of glyceraldehyde-3-phosphate to 1,3 bisphosphoglycerate and subsequent continued glycolytic flux. The lactate reaction also maintains the cellular redox state by providing the requisite NAD+ for nucleotide and amino acid biosynthesis thereby regulating gene expression *(202)*. Lactate production may therefore facilitate faster glycolytic flux to support increased production of biosynthetic intermediates, ATP production and maintain the redox balance for TGF-β_1 induced differentiation and collagen synthesis. It has also been postulated that lactic acid may activate latent TGF-β via a pH dependent mechanism that drives myofibroblast differentiation as discussed previously *(103)*.

Enhanced glycolysis is often facilitated by an increase in the expression of downstream glycolytic enzymes. This thesis also examined whether augmented glycolysis was accompanied by an increase in gene expression of key glycolytic enzymes. LDH was upregulated at around 8 hours while a significant increase in other rate-regulating enzymes were not demonstrated. In contrast, increased mRNA levels of the key rate-limiting glycolytic enzymes; hexokinase 2 (HK2), phosphofructokinase-1 (PFK1), and pyruvate kinase muscle isoenzyme M2 (PKM2) have recently been reported in TGF-β_1-stimulated control and IPF fibroblasts *(134, 189, 190)*. As mentioned previously, conflicting data obtained from different laboratories might be reflective of the fibroblasts used and potentially representing a temporally and spatially heterogeneous disease process present in the IPF lung.

LDH5 has been reported to be elevated in TGF-β_1-stimulated lung fibroblasts, IPF fibroblasts and in IPF lung tissue *(103, 137, 203)*. However selective inhibition of LDH5 failed to decrease fibronectin, collagen and αSMA expression despite inhibiting the TGF-β_1-induced increase in lactate production*(137)*. Lactate production may therefore be representative of enhanced glycolytic flux rather than specifically being required for TGF-β_1 collagen deposition.

In the present study, PFKFB3 mRNA levels were markedly increased at 3 hours. PFKFB3 is not a rate limiting glycolytic enzyme but catalyses the conversion of fructose-6-phosphate to fructose-2, 6-bisphosphate, an allosteric activator of PFK1 and a potent stimulator of glycolysis. These observations are further in agreement with very recent studies examining glycolytic enzyme gene and protein expression in IPF myofibroblasts which were published during the course of this thesis *(134)*. Moreover, PFKFB3 levels are elevated in pulmonary epithelial cells, macrophages and fibroblastic foci in IPF lungs, as well as in experimental models of pulmonary fibrosis*(134, 189, 190, 204, 205)*. Recent data has also shown that E2F1, a pro-oncogenic transcription factor, enhances the transcription of PFKFB3 which has been shown to promote mTORC1 translocation to the lysomes by enhancing mTORC1 interaction with RagB. Therefore one could speculate that the early increase in PFKFB3 expression in response to TGF-β_1 may arise to activate mTORC1 to promote collagen deposition *(200)*. Together, these data suggests that metabolic alterations such as increased PFKFB3 expression are displayed by a number of key cells involved in the fibrogenic

response and infers that enhanced glycolysis may play a pivotal role in promoting fibrosis, thereby revealing a potential therapeutic targeting strategy in IPF.

In the present study, the glucose analog, 2 deoxy-d-glucose (2-DG) also inhibited TGF-β_1-induced myofibroblast differentiation and collagen I synthesis at the mRNA and protein levels. It is worth noting that the effects of 2DG were achieved at concentrations that were subequimolar to glucose concentrations indicating that the effects may be mediated independently to its inhibitory effect on glycolysis. 2DG is widely recognized as a glycolytic inhibitor that leads to the depletion of cellular ATP and cell death *in vitro* (100) and has been shown to exert anti-tumour effects *in vitro* (101). However, there is some evidence to suggest that 2DG may exert its anti-tumour effects through alternative mechanisms.

One study revealed only a moderate decline in ATP levels with 2DG in eukaryotes (102) whilst another showed that 2FDG, a close analogue of 2DG as well as a more potent glycolytic inhibitor, did not have the equivalent toxicity on tumour cells as 2DG (103). Interestingly, metabolic profiling of 2DG in human fibroblasts did not reveal evidence of a decrease of downstream glycolytic intermediates (104).

2DG has been shown to interfere with N-linked glycosylation, which conveys an increased toxicity to tumour cells (106). A previous study has shown that manipulation of N-linked glycosylation of the TGF-β II receptor, TβRII, resulting in impaired

TGF-β signalling, therefore one may speculate that 2DG abrogates collagen and αSMA deposition through its effect on TGF-β_1 signalling.

2DG may also be affecting mTORC1 function directly. A study published very recently, has found that during glucose starvation, HK2 binds to mTORC1 to inhibit its downstream signalling and that 2DG blocks HK2's interaction with mTORC1 and its subsequent downstream signalling. Again, this identifies potential connections between glycolysis and the regulation of mTORC1, where key glycolytic enzymes are potentially enhanced to promote mTORC1 signalling for fibrogenesis *(200)*.

Regardless of the potential off-target effects of 2DG, subsequent *in vitro* fibroblast studies demonstrated the anti-fibrogenic effects of other glycolytic inhibitors by other investigators during the course of this work. Pharmacological inhibition of PFKFB3 (3PO) and HK2 (lonidamine) abrogated TGF-β_1-induced myofibroblast differentiation, collagen production and contractility *(134, 189, 190, 204)*. Pre-clinical models support the potential therapeutic utility of targeting glycolysis in fibrosis in that 3PO and lonidamine treatment also attenuated fibrosis in the bleomycin- and TGF-β_1-induced models of lung fibrosis in mice with the latter compound also improving lung function *(134)*.

4.1.3 Enhanced oxidative phosphorylation is dispensable for TGF- β_1 induced myofibroblast collagen synthesis

Very recent evidence suggests that IPF myofibroblasts and TGF-β_1-stimulated human lung fibroblasts, not only assume a glycolytic phenotype, but also increase mitochondrial respiration, albeit to a lesser degree *(204, 206)*. Increased mitochondrial respiration might therefore aim to provide ATP, TCA carbon intermediates and ROS to support a number of fibrogenic responses. However, in my experiments, in contrast to an absolute requirement for extracellular glucose and glycolysis, mitochondrial respiration was found to be dispensable for TGF-β_1–induced collagen deposition, suggesting that glycolytic flux in response to TGF-β_1 stimulation is sufficient to meet both the biosynthetic and energetic requirements of the complex multistage process of collagen biosynthesis in primary adult lung fibroblasts over the time course of these experiments (48 hours).

In addition, increased mitochondrial biogenesis has been reported to be important for the maintenance of the differentiated and contractile myofibroblast state in the fetal lung fibroblast line IMR-90 *(204)*. However my data demonstrated that inhibiting the ETC complex I and III with rotenone and antimycin A did not affect TGF-β_1-induced αSMA or collagen production and therefore suggests that enhanced oxidative phosphorylation may be required for maintaining the contractile phenotype of the differentiated myofibroblast as described in the literature, rather than for αSMA or collagen synthesis *(190)*.

4.2 mTOR promotes TGF-β_1 induced collagen deposition but not myofibroblast differentiation

The present work demonstrates that myofibroblasts adopt a glycolytic phenotype during TGF-β_1-induced differentiation and collagen synthesis. This chapter focused on delineating the role of mTOR in reconfiguring metabolic networks to meet the biosynthetic needs of fibroblast differentiation and collagen production in response to TGF-β_1 stimulation.

Previous work in our laboratory had demonstrated that the mTORC1/4E-BP1 axis was critical for TGF-β_1- induced collagen deposition *(78)* but these experiments were performed in standard DMEM, which contains supra-physiological concentrations of glucose and glutamine. The first series of experiments were therefore performed to address the effect of TGF-β_1 on mTORC1 activation and in driving myofibroblast differentiation and collagen production in physiological media conditions.

I was able to demonstrate that under physiological concentrations of glucose and glutamine, TGF-β_1 caused a marked increase in mTORC1 signalling in pHLFs as evidenced by p70S6K (Thr389) and 4E-BP1 (Ser65) phosphorylation peaking at 1 hour compared to three hours in supra-physiological levels of glucose and glutamine containing media *(78)*. The slightly earlier activation of mTORC1 in an environment that is less replete with substrate was somewhat unexpected, as increased availability of substrates enhances mTOR activation via AMPK inhibition. There may be multiple explanations but one possibility is that under conditions of

physiological levels of glucose and glutamine there may be a more pressing need to increase intracellular glucose availability in response to TGF-β_1 to promote earlier activation of mTORC1 signalling in order to increase GLUT1 expression and intracellular glucose to fuel downstream processes activated by TGF-β_1.

Recent work from our laboratory had shown that collagen deposition in activated fibroblasts and mesenchymal cells is strongly inhibited by dual pharmacological manipulation of mTORC1/2 but resistant to the partial mTORC1 inhibitor, rapamycin and further that mTORC1 signalling is critical for myofibroblasts to mount a collagen response downstream of TGF-β_1 stimulation.

I was now able to show that the TGF-β_1-induced increase in collagen I protein abundance and gene expression were similarly significantly attenuated in the presence of the highly selective mTOR inhibitor AZD8055 but was insensitive to rapamycin treatment in physiological DMEM.

Rapamycin is an allosteric mTORC1 inhibitor, and interacts with its obligate receptor FKFB3 and thought to block access of upstream substrates to the catalytic site*(207)*. Rapamycin has been shown to abolish the phosphorylation of p70S6K in response to TGF-β_1, however it does not block mTORC1 substrates equally. Whilst AZD8055 as been shown to suppress phosphorylation of all downstream mTORC1 and mTORC2 substrates, rapamycin preferentially inhibits mTORC1 sites that are weakly phosphorylated by mTORC1 (p70S6K [Thr389]), while its effects

on mTORC1–mediated 4E-BP1 phosphorylation are modest. Everolimus, a rapalog, failed to slow disease progression in an IPF clinical trial, and this may potentially be explained by the fact that TGF-β_1- induced collagen deposition is insensitive to rapamcyin treatment and modulated by the mTORC1-4E-BP1 axis *(208)*.

It is noteworthy that AZD8055 significantly attenuated the TGF-β_1-induced collagen mRNA response by 50% but in contrast, inhibited collagen protein production down to near baseline levels. This suggests that mTOR to a certain extent, drives the transcriptional but also the post-transcriptional machinery of collagen synthesis. Data from our laboratory has reported, that utilizing fibroblasts expressing the dominant negative 4E-BP1-4A phosphomutant, thereby mimicking the effect of mTORC1 inhibition, resulted in marked attenuation of TGF-β_1-induced collagen I mRNA abundance, indicating that mTORC1/4E-BP1 axis acts at least in part at the level of regulating collagen I mRNA levels to mediate the fibrogenic response in HLFs *(78)*.

Rapamycin-insensitive mTOR signalling may also regulate collagen protein abundance by indirectly regulating *COL1A1* mRNA translation. It is well established that mTORC1 controls protein synthesis by increasing ribsome biosynthesis and promoting mRNA translation. Active site mTOR inhibition has more marked effects on global protein synthesis over rapamycin, holding up the concept that mTORC1/4E-BP1 signalling is central for mTORC1 to promote its translational effects. Ribosomal profiling studies have identified that a particular subset of mRNAs with terminal oligopyrimidine (TOP) or pyrimidine – rich translation

element (PRTE) motif in the 5'UTR are preferentially translated by cap-dependent translation, downstream of the mTORC1/4E-BP1 axis *(209)*. However in the context of collagen expression, the predicted 5'UTR of *COL1A1* does not contain a typical TOP sequence, so *COL1A1* expression is unlikely to be mediated by cap-dependent translation.

The data presented in this section also demonstrated that mTOR inhibition failed to interfere with TGF-β_1–induced myofibroblast differentiation at the protein level which is in agreement with a very recent report showing that Torin, a less selective mTOR inhibitor, was also unable to block αSMA protein expression in TGF-β_1 stimulated HLFs.

Taken together, the data leads to the conclusion that rapamycin-insensitive mTOR signalling is critical for TGF-β_1-induced collagen synthesis yet is dispensable for *de novo* αSMA protein induction. This indicates that TGF-β_1-induced fibroblast differentiation and matrix synthesis, two cardinal features of the myofibroblast phenotype, are differentially regulated downstream of TGF-β_1.

4.3 mTOR amplifies the glycine biosynthetic pathway for TGF-β_1-induced collagen synthesis.

mTOR signalling is strongly implicated in metabolic reprogramming of a number of pathological and non-pathological cell types, including proliferative cancer cells and activated T cells *(109, 193)*, where modulation of mTOR alters metabolic networks with a significant impact on the fate of these cells. Therefore the next

section of this thesis investigated whether mTOR promotes extracellular matrix production in response to TGF-β_1 by reconfiguring metabolism.

WGCNA analysis of our existing RNA-seq dataset comparing the effect of ATP-competitive mTOR inhibition versus rapamycin on TGF-β_1–induced human lung fibroblasts provided key insights into the potential mechanism by which mTOR influences collagen deposition. The initial motivation to exploit these pharmacological differences using RNA-sequencing was predicated on previous studies that demonstrated that collagen deposition in activated fibroblasts and mesenchymal cells is sensitive to ATP-competitive mTOR inhibition but not to rapamycin treatment *(78, 84, 158)*.

In the present study, the WGCNA module representing the profile of genes modulated by TGF-β_1 treatment and sensitive to AZD8055, but insensitive to rapamycin, comprised all four genes encoding the enzymes of the serine-glycine synthetic pathway (PHGDH, PSAT, PSPH, and SHMT2), which were present in the top 20 most correlated genes overall. This finding merited further investigation, given that glycine is present in every third amino acid position of the triple helical region of collagen molecule and is integral to the composition and stability of its oligomerized triple helical structure *(210)*.

The glycolytic intermediate, 3 phosphoglycerate, produced after the 7th enzymatic step in glycolysis, is the initial substrate that feeds from glycolysis into the *de novo* glycine biosynthetic pathway, where it is oxidised to 3 phosphohydroxypyruvate.

PSAT1 transaminates 3 phosphohydroxypyruvate to phosphoserine and uses glutamate as a nitrogen donor. PSPH then dephosphophorylates phosphoserine to produce serine irreversibly. The mitochondrially located SHMT2 then coverts serine to glycine which then fuels glycine dependent pathways, such as glutathione biosynthesis and purine and DNA/histone methylation.

PCR validation of the results extracted from the RNAseq data was performed in physiological glucose and glutamine media conditions, which again mirrored a rapamycin-insenstive, mTOR-dependent increase in the abundance of transcripts encoding the glycine synthetic enzymes in response to TGF-β_1. PHGDH and PSPH are considered to be the first and second rate-limiting steps in glycine biosynthesis and protein abundance of both these enzymes are also increased in response to TGF-β_1. The conversion of serine to glycine by the SHMTs is an important source of one carbon units for the tetrahydrofolate (THF) cycle. My data shows that there was no change in the mRNA level of SHMT1 which is a cytosolic enzyme and considered to favour the conversion of glycine to serine whilst SHMT2 which facilitates the reverse reaction, of serine to glycine, was increased at the mRNA level.

4.4 mTORC1-4E-BP1 axis is critical for TGF-β_1-induced ATF4 production

Having identified that mTOR regulates the *de novo* glycine

biosynthesis during TGF-β_1-induced collagen synthesis, the next experiments aimed to dissect the mechanism through which mTOR permits these metabolic changes.

In cancer cells, it is well established that mTORC1 and its downstream substrate 4E-BP1 play critical roles in regulating metabolic pathways through the eukaryotic initiation factor 4F (eIF4F) complex–dependent translation of key transcription factors, including hypoxia-inducible factor 1α (HIF1α) and c-MYC *(211)*. In the present study, overconnected node analysis of the RNAseq data set identified several potential transcriptional regulators of interest, including ATF4. ATF4, a basic leucine zipper transcription factor, is a transcriptional master regulator of amino acid metabolism and is classically enhanced as part of the integrated stress response as a result of the activation of kinases, such as PERK and eukaryotic translation initiation factor 2 alpha kinase 4 (GCN2). These kinases phosphorylate the translation factor eIF2α, leading to global reduction in mRNA translation except for select mRNAs, including ATF4 *(212, 213)*. ATF4, in turn, increases gene transcription by binding to the C/EBP-ATF response element in the promoters of specific target genes, including ASNS, the glycine biosynthetic enzymes, PYCR1, SLC1A4, SLC7A1, SLC7A5, which were all present in the top 20 correlated genes in the highly enriched module identified in the RNA seq data set *(214–216)*. In the context of fibrosis, ATF4 expression has been reported to be increased in alveolar epithelial cells derived from IPF donors but in the context of injury and the stress response*(217)*. ATF4 has not previously been linked to TGF-β_1–induced collagen deposition in human lung fibroblasts

Experiments performed to address the mechanism by which TGF-β_1 increases ATF4 expression revealed that TGF-β_1 increases ATF4 production through the cooperation of both canonical Smad3 and mTOR signalling pathways. Combining the evidence obtained from kinetic studies of the signalling response with the data obtained in function-blocking studies based on pharmacological inhibition (AZD8055) and genetic inhibition with siRNA for Smad3, a model is now emerging where Smad3 plays a critical role in regulating ATF4 mRNA abundance, whereas the Smad dependent-mTOR axis is critical for ATF4 expression, post–transcriptionally. Data obtained with the translation inhibitor, lactimidomycin, further revealed that mTOR did not promote protein stability but may instead act by promoting ATF4 translation.

The Smad3 dependent increase in ATF4 mRNA levels at 12 hours post TGF-β_1 stimulation is also consistent with subsequent in silico analysis of the ATF4 promoter, revealing putative binding sites for Smad-2, -3 and -4 with a predicted Smad3 binding site close to the transcription start site.

It is also worth commenting that the earlier increase in ATF4 protein abundance at 8 hours compared to the increase in mRNA levels is potentially explained by increased Smad3-dependent, mTOR-mediated translation of existing ATF4 transcripts and is consistent with previous data that Smad3 is critical for TGF-β_1–mediated mTORC1 activation *(78)*.

The translation of ATF4 is well established to be triggered by the

integrated stress response (ISR), which in response to insults such as hypoxia and amino acid deprivation, leads to autophosphorylation of PERK and subsequent phosphorylation of eukaryotic initiation factor 2α (eIF2α) on Ser51 through a complex mechanism that requires several upstream open reading frames located in the 5' untranslated region of the ATF4 open reading frame *(212, 213)*. The data herein reveals, that the enhanced translation of ATF4 downstream of TGF-β_1 occurs in the absence of the PERK-eIF2α kinase–mediated integrated stress response. Increased expression of ATF4, that is independent from the classical stress response has also been reported for mouse embryonic fibroblasts stimulated by insulin *(218)* and in a study which did not detect eIF2α phosphorylation in response to TGF-β_1 in lung fibroblasts *(219)*.

I next considered the complex, through which mTOR regulates ATF4 translation in response to TGF-β_1. It is well established that the mTORC1/4E-BP1 axis controls protein synthesis by increasing ribosome biosynthesis and promoting mRNA translation. Function blocking studies, using CRISPR-Cas9 gene editing of Rictor and Raptor and 4E-BP1 phospho-mutants, revealed a key role for the mTORC1/4E-BP1 axis in mediating the stimulatory effects of TGF-β_1 on ATF4 translation. This finding has not been previously reported in lung fibroblasts but is in agreement with reports demonstrating a role for mTORC1 *(218)* or both mTORC1 and 4E-BP1 *(149)* in regulating the translation of ATF4 in other cell contexts.

As mentioned previously, mTORC1-4E-BP1 preferentially translates mRNAs which contain a TOP or pyrimidine-rich translational element (PRTE) motif in the 5'UTR by cap-dependent translation. 4EG1-I is a small molecule that disrupts the interaction between eIF4E and eIF4G to form a complex and thereby enhances the binding of eIF4E to 4E-BP1 to prevent cap dependent translation. In pHLFs, prolonged exposure to 4EG1-I resulted in significant cell toxicity (data not shown). Consistent with this, 4EG1-I has been reported to induce apoptosis in multiple cancer cell lines by promoting the down-regulation of oncogenic protein expression (such as c-MYC and Bcl-2) after 8 hours of treatment *(220–222)*. Examining the 5'UTR of ATF4, a typical TOP sequence (a cytidine at the transcriptional start site (TSS) followed by a stretch of 5-15 pyrimidines) was also not observed, again suggesting that enhanced translation of ATF4 mRNAs is likely not to be cap-dependent.

4.5 ATF4 promotes the expression of the glycine biosynthetic enzymes for TGF-β_1-induced collagen deposition.

ATF4 is a master transcriptional regulator that binds to the C/EBP-ATF response element in the promoter of specific target genes including those coding for the glycine biosynthetic enzymes, so the present study next evaluated whether TGF-β_1-induced ATF4 production was critical for *de novo* glycine biosynthesis and collagen deposition.

Inhibition of ATF4 with siRNA suppressed the TGF-β_1-induced increase in all the glycine biosynthetic enzymes at the gene and

protein levels. This data demonstrates that ATF4 is critical for TGF-β_1 induced glycine biosynthesis and this is consistent with the role of ATF4 in regulating glycine metabolism in other cell contexts *(214–216)*.

I next investigated whether mTORC1-4E-BP1 dependent ATF4 production was required for mediating the fibrogenic effects of TGF-β_1. ATF4 gene disruption using both CRISPR-Cas 9 gene editing and siRNA silencing were used. Pooled siRNAs were used, which consisted of a mixture of 4 siRNAs. The advantages of using pooled siRNA include increased potency and specificity to generate the true loss of phenotype of a particular gene as well as increased numbers of siRNAs targeting a particular gene should decrease the impact of off-target effects. CRISPR-Cas editing of low passage fibroblasts is difficult due to the inability to proliferate from a single cell following gene editing. Therefore our protocol was based on a published protocol, utilising bulk culture of a pool of edited fibroblasts. Editing efficiency therefore had to be high which was confirmed by western blotting.

ATF4 gene silencing demonstrated that ATF4 was indispensable for TGF-β_1-induced collagen deposition, mirroring the role of mTORC1/4E-BP1 axis during TGF-β_1-induced collagen deposition. Taken together, this thesis therefore provides strong evidence for a key role for ATF4 downstream of the mTORC1/4E-BP1 axis in mediating the pro-fibrogenic effects of TGF-β_1. These published findings were in agreement with a study published subsequently, that demonstrated that mTORC1 drives TGF-β_1-induced ATF4

activation and expression of the serine-glycine synthetic enzymes *(223)*.

In terms of potential relevance of these findings to the human disease setting, I further provide evidence that ATF4 is immunolocalized to αSMA–positive myofibroblasts within IPF fibrotic foci, as well as in the overlying epithelium. This latter observation is broadly in agreement with a previous report focusing on the role of ATF4 in the context of epithelial endoplasmic reticulum stress and apoptosis in IPF using a polyclonal antibody against ATF4 *(217)*. In contrast, ATF4 staining pattern in control lung is predominantly epithelial and is in agreement with the pattern reported for control lung in the Human Protein Atlas (https://www.proteinatlas.org/ENSG00000128272-ATF4/).

It is important to note that the primary human lung fibroblasts used in the cell-based experiments were extracted from a 'healthy' control patient and stimulated with TGF-β_1 to recapitulate a fibrotic model. However fibroblasts derived from IPF lung may behave differently. It is therefore reassuring that ATF4 does immunolocalise to αSMA–positive myofibroblasts within the IPF fibrotic foci, echoing the expression of ATF4 in TGF-β_1 stimulated normal human lung fibroblasts.

Taken together the data presented therefore extends our current understanding of the role of ATF4 in the transcriptional regulation of the serine-glycine pathway beyond the cancer setting, where this pathway has been strongly implicated in supporting cell growth

and proliferation, as well as clinical aggressiveness in non– small cell lung cancer *(160, 224)*.

4.6 The mTOR-ATF4 axis amplifies glucose metabolism during TGF-β_1-induced collagen synthesis

The experiments performed so far provided strong support that the mTORC1-4EBP1 axis modulates ATF4 dependent *de novo* glycine biosynthesis to promote TGF-β_1-induced collagen synthesis in myofibroblasts. *De novo* glycine biosynthesis initially requires the glycolytic intermediate 3-phosphoglycerate (3-PG) to be siphoned from glycolysis and converted by the first enzyme of the serine-glycine biosynthetic pathway, PHGDH, to 3-phosphohydroxypyruvate (3-PHP). The initial data presented in this thesis demonstrated that myofibroblasts adopt a glycolytic phenotype, including enhancing glucose uptake, which is critical for the TGF-β_1-induced fibrotic response. The final part of this thesis investigated whether the amplification of glucose uptake and glycolysis was modulated by the mTORC1-4E-BP1 axis to supply carbons for glycine biosynthesis for collagen synthesis.

In the present study, increased glucose uptake and GLUT1 expression at the protein and mRNA levels were all modulated by mTOR during TGF-β_1-induced collagen synthesis. In the context of cancer and immune cell responses, mTORC1 has been shown to enhance the intrinsic activity and translocation of GLUT1 via the transcription factor, hypoxic inducible factor(HIF) and increase the transcription of GLUT1 in a number of cell types (52).

Additionally mTORC1 is known to increase HIF1α protein levels by promoting cap–dependent translation through the 4E-BP1-e1F4 axis *(65)*. Furthermore in the context of fibrosis, activated HIF has been reported to be increased in IPF lung tissue *(206)*.

Interestingly the facilitative glucose transporter, GLUT, was present in the same WGCNA module as the serine–glycine pathway genes, again demonstrating a dependence on rapamycin-insensitive mTOR signalling in response to TGF-β_1. I confirmed that TGF-β_1-stimulated *SLC2A1* transcripts and GLUT1 protein production in a Smad3 dependent manner and was modulated by the mTOR-ATF4 axis but insensitive to rapamycin treatment, thereby mirroring the regulation of glycine and collagen biosynthesis. Interestingly, GLUT1 is not known to be a downstream transcriptional target of ATF4, however a previous study identified two enhancer binding elements in the regulatory elements of the *SLC2A1* gene that contain the same cyclic adenosine monophosphate response element consensus binding site shared by ATF4 *(225)*. It is however noteworthy, that high concentrations of TGF-β_1 was found to promote GLUT1 in murine embryonic AKR-2B fibroblasts, although in this context, the increase in GLUT1 was attributed to mTORC2 rather than to mTORC1 signalling *(188)*.

Over the last decade multiple studies have established that the PI3K-Akt-mTOR signalling pathway promotes glycolysis in cancer and activated T cells *(75, 76, 226)*. In this thesis, although the mTOR-ATF4 axis was found to stimulate the expression of *SLC2A1* transcripts and GLUT1 protein, I found no role for mTOR

in regulating the expression of the TGF-β_1–induced glycolytic genes PFKFB3 and LDHA. Although the TGF-β_1-induced increase in glycolytic flux was mTOR dependent, this was not facilitated by an increase in glycolytic enzyme expression and may in fact reflect increased glucose substrate entering glycolysis. As described earlier, the early increase in PFKFB3 in response to TGF-β_1 may potentially occur to stimulate the translocation of mTOR to the lysosome rather than be a downstream target of mTOR. Interestingly, ATF4 silencing has been demonstrated not to affect TGF-β_1 induced increase in ECAR and mitochondrial respiration in normal human lung fibroblasts, therefore future work is still required to determine the downstream targets of mTOR that affect these pathways *(223)*.

The mechanism by which mTOR influences glycolysis in myofibroblasts contrasts with its role in cancer cells, where mTOR has been reported to promote the expression of multiple glycolytic genes by enhancing the translation of HIF1α and c-MYC *(227–229)*. Although there is a degree of mechanistic overlap between cancer and fibrosis, the mutational landscapes are very different. mTOR is one of the most frequently mutated signalling hubs in cancer as a consequence of PI3K amplification or mutation; PTEN (phosphatase and tensin homolog) loss of function; AKT overexpression; or S6 kinase 1, 4E-BP1, or eIF4E overexpression *(230)*. In contrast, mTOR pathway activation is likely to be a consequence of the altered tissue microenvironment in pathological fibrosis and in the stromal response in cancer, because in both settings, fibrogenesis is generally considered a reactive rather than a malignant process *(231, 232)*. Although the

mechanism is not known, IPF myofibroblasts have been reported to display evidence of PTEN deficiency *(233)*.

4.7 mTOR promotes glucose derived glycine synthesis to supply the biosynthetic needs of TGF-β_1-induced collagen production.

The final part of the thesis addressed whether mTOR permitted its effects on TGF-β_1-induced collagen synthesis by enhancing glycolysis to provide glucose derived carbons for glycine synthesis, thereby contributing to the structure of collagen.

In terms of linking enhanced glycolysis to *de novo* glycine synthesis and subsequent TGF-β_1-induced collagen deposition, my experiments showed that pharmacological and genetic inhibition of PHGDH, which converts the glycolytic intermediate 3-phosphoglycerate (3-PG) to 3-phosphohydroxypyruvate (3-PHP), abrogates TGF-β_1-induced increase in collagen protein production in human lung fibroblasts. One should bear in mind, that the published IC50 of NCT-503 on PHGDH is 2.5 μM. However, previous work has shown that a concentration of 20-30 μM of NCT-503 is required to inhibit collagen deposition in TGF-β_1-induced fibroblasts *(234)*. This suggested that inhibition of collagen by NCT-503 may be an off-target effect which prompted the validation experiment with PHGDH siRNA. *In vivo* studies published during the course of this PhD further demonstrated that pharmacological inhibition of PHGDH with NCT-503 also attenuates bleomycin-induced lung fibrosis *(234)*. In the context of

IPF, these observations are also supported by a recent GCMS profiling study reporting an increase in glycine abundance in IPF lung tissue *(136)* and enhanced expression of PHGDH within the fibrotic foci of IPF lungs *(189)* .

In vivo studies published during the course of this PhD further demonstrated that pharmacological inhibition of PHGDH with NCT503 also attenuates bleomycin-induced lung fibrosis. In the context of IPF, these observations are also supported by a recent GCMS profiling study reporting an increase in glycine abundance in IPF lung tissue *(136)* and enhanced expression of PHGDH within the fibrotic foci of IPF lungs *(189)* .

Extracellular glycine supplementation was able to partially rescue the inhibitory effect of glucose deprivation, as well as mTOR inhibition, on TGF-β_1–induced collagen deposition. Interestingly, serine did not rescue the inhibitory effect of AZD on TGF-β_1–induced collagen desposition. SHMT1 which catalyses the reaction of glycine to serine was not regulated by TGF-β_1 or mTOR at the transcriptional level. TGF-β_1 however did enhance SHMT2 at the transcriptional and protein level which was dependent on mTOR. SHMT2 converts serine to glycine and therefore the lack of serine rescue suggests that it is the de novo production of glycine to serine that mTOR enhances to drive TGF-β_1–collagen deposition. However it has been shown that SHMT1 can catalyse the reverse reaction of serine to glycine if 1-carbon metabolism is inhibited*(235)*. One might therefore speculate that if SHMT2 is inhibited, SHMT1 may potentially catalyse the reverse reaction of serine conversion to glycine. However, the failure of exogenous

serine to rescue the effects of mTOR inhibition on collagen deposition does not support this notion. To further interrogate this failure of rescue, it would be interesting to trace radio-labelled exogenous serine to investigate whether exogenous serine is first transported into the cell and whether SHMT1 does indeed catalyse the reverse reaction of serine to glycine, when SHMT2 is inhibited by AZD8055. SLC1A5 is one of the main transporters for serine and was enhanced by TGF-β_1 in the RNAseq data set and interestingly downregulated by AZD8055. Therefore exogenous serine may not be able to rescue the phenotype if entry into the cell is inhibited. Exogenous glycine is transported by glycine transporters (Glyt) which was not modulated by TGF-β_1 or mTOR in the RNAseq data set.

1-carbon metabolism contributes to many biosynthetic pathways that fuel growth due to its contribution to core cellular building blocks (purine and pyrimidine nucleotides), epigenetics, post translation modifications (PTMs) and redox homeostasis. 1-carbon metabolism begins with the folate cycle and provides the 1C unit to the methionine cycle. The 1C unit is largely supplied by serine, either from the extracellular environment or de novo synthesis. SHMT2 donates a 1C unit from serine to tetrahydrofolate (THF). Glycine is another amino acid that can donate a 1C and this is facilitated by the glycine cleavage system (GCS). Both SHMT2 and the GCS generate 5,10-CH2-THF which is a substrate for the enzymes, methylenetetrahydrofolate dehydrogenase-cyclohydrolases (MTHFD2/2L). MTHFD2 and MTHFD2L catalyse the oxidation of 5,10-CH2-THF to 10-CHO-THF. MTHFD1L then regenerates THF and production of formate.

Exogenous formate can provide 1-carbon units directly to the THF cycle and can rescue cellular growth defects caused by loss of serine homeostasis. Addition of formate however failed to resuce the inhibitory effect of AZD8055 on TGF-β_1 induced collagen suggesting a loss of mitochondrial 1 carbon-units is not responsible for the reduction in collagen protein production. Interestingly, *MTHFD2* was also present in the same highly correlated module of genes in our WGCNA data set as the glycine synthetic genes and a previous study has revealed that fibroblasts established from embyros of MTHFD2 knockout render the fibroblasts dependent or auxotrophic for glycine, which may therefore impede collagen production further *(236)*.

Glutamine is the most abundant amino acid in plasma and tissue and its breakdown by glutaminolysis provides an essential carbon source for a number of fundamental cellular reactions. A number of studies have now demonstrated that glutaminolysis promotes a number of process that are critical for the pro-fibrotic phenotype of myofiboblasts in IPF *(163, 237, 238)*. Glutamate is an important precursor for proline, which makes up 23% of the collagen molecule *(239)*. Failure of proline to rescue the inhibition of AZD8055 inhibition on collagen production suggests that mTOR does not regulate collagen production via modulation of glutamine derived proline synthesis. It is also important to comment, that during the course of the experiment, there may be depletion of relevant amino acids including glutamine over the experimental time course, especially in physiological levels of glucose and glutamine in the media compared to standard DMEM. Depletion of amino acids during the course of the experiment may mask

alterations in response to TGF-β_1 and inhibitors. It would be pertinent to measure the concentrations of metabolites including glucose and glutamine in the media over 48 hours to see whether there is a significant depletion that may impact TGF-β_1-collagen deposition independently.

Finally, an enhanced demand for glucose to meet the biosynthetic demands of collagen production after TGF-β_1 stimulation was further demonstrated by experiments demonstrating that U-^{14}C-glucose incorporation into collagen I was increased in TGF-β_1–stimulated fibroblasts. U-^{14}C-glycine tracing experiments further demonstrated that exogenous glycine enabled fibroblasts to generate a TGF-β_1–induced collagen response when the *de novo* serine-glycine pathway was suppressed by mTOR inhibition with AZD8055. Interestingly, a previous study found that removal of serine and glycine from the media had no inhibitory effect on collagen synthesis *(189)* emphasizing the requirement for specifically *de novo* production of glycine but if absent, our data suggests extracellular glycine supply is sufficient to mount a collagen response.

Together, these data support the notion that mTOR promotes glycolysis to generate the necessary glycine to enable enhanced collagen production.

4.8 Therapeutic implications for the treatment of IPF

There is now compelling evidence presented in this thesis that supports the notion that mTOR may play a significant role in the pathogenesis of IPF through its regulation of glucose metabolism.

However there have been some reservations in the IPF community over the potential use of mTOR inhibitors in IPF patients. Everolimus is a rapalog that has shown tumour suppressive effects *in vivo* and is used to treat advanced renal cell carcinoma, advanced breast cancer and pancreatic neuroendocrine tumours. However, in a clinical trial investigating the efficacy of everolimus in IPF, the investigators found everolimus caused rapid disease progression, represented by deterioration in lung function when compared to placebo. There was also a high patient dropout rate due to the side effect profile *(240)*. In the context of cancer and transplantation, there have been concerns over the increased risk of pneumonitis, which can rarely be life threatening. Together with evidence, that the pro-fibrotic effects of TGF-β are insensitive to rapamycin *in vitro*, there is now a move to investigate the role of active site mTOR inhibitors in IPF.

Unlike, rapalogs, ATP-competitive mTOR inhibitors are able to induce apoptosis as well as arrest cell growth. There are now a number of phase I and II clinical trials testing ATP-competitive mTOR inhibitors, demonstrating good safety and pharmokinetic data. AZD2014 (Vistusertib) is used to treat estrogen receptor breast cancer, glioblastoma and unlike rapalogs, ATP -competitive mTOR inhibitors are not found to convey an increased risk of

pneumonitis *(241)*.

However, the tolerability of dual complex mTOR inhibitors for patients remain unclear and not fully investigated. Common side effects reported include fatigue, mucositis and metabolic complications like hyperglycemia. Therefore, further work is still required to understand the mechanisms through which mTOR inhibition causes these side effects to potentially improve tolerability and patient safety.

This thesis also revealed that TGF-β_1-induced ATF4 was pivotal for collagen synthesis in myofibroblasts and therefore could be a potential therapeutic target in IPF. However, targeting transcription factors has historically been challenging, as designing small molecule inhibitors to successfully target the protein-DNA or protein-protein interactions involved, is technically problematic compared to pharmacologically inhibiting active-site kinases or enzymes. However, ATF4 as demonstrated in this thesis, enhances the transcription of several metabolic enzymes which opens up more potential therapeutic targets in fibrosis that are easier to manipulate pharmacologically. Optimism is growing for the implementation of metabolism-targeting therapeutic strategies, including inhibiting glycolytic enzymes and kinase regulators of metabolism, with a number of recent trials reporting good tolerability and efficacy in the oncology setting (Table 4.1) *(242–244)*. Several of these agents may therefore represent repositioning opportunities for fibrosis either as potential standalone therapeutics or, as in cancer, as adjuvant therapies,

which could potentially sensitise fibroblasts to currently approved and emerging therapies.

Target	Metabolic pathway	Drug	Clinical trials
HK2	Glycolysis	2DG Lonidamine Ketoconazole Posaconazole	• Lonidamine: Phase III clinical trials in breast cancer and lung cancer (94) • 2DG: Phase I/II trials in advanced solid tumours and in combination with radiotherapy in cerebral gliomas (95,96) • Ketoconazole, posaconazole in advanced gliomas (NCT03763396)
PFKFB3	Glycolysis	3PO PFK158	• PFK158: Phase I trial in advanced solid malignancies (NCT02044861)
PKM2	Glycolysis	TLN-232	• TLN-232: Phase II studies in metastatic renal cancer and metastatic melanoma (NCT00422786, NCT00735332)
NOX4	Mitochondria	Cpd-88 GKT137831	• GKT137831: Not tested in cancer but phase II trials in diabetic nephropathy (NCT02010242) and primary biliary cholangitis (NCT03226067).
PDK1	Mitochondria	DCA	• DCA: Phase II trials in metastatic NSCLC and breast cancer (NCT01029925), head and neck cancer (NCT01163487), brain cancer (NCT00540176), in combination with cisplatin and radiotherapy in head and neck (NCT01386632).
AMPK		AICAR Metformin (ETC1 inhibitor)	• Metformin is licensed for the use in Type II DM Phase III trial in breast cancer
mTOR		AZD8055 AZD2014 MLN0128	• AZD8055: Phase I trials in recurrent gliomas (NCT01316809), liver cancer (NCT00999882),

Table 4.1 Metabolic inhibitors tested in cancer clinical trials.

Conclusion

This thesis examined the hypothesis that mTOR drives metabolic reprogramming to promote extracellular matrix deposition in TGF-β stimulated human lung fibroblasts and thus represents a potential therapeutic target for the treatment of IPF.

The work presented identified a novel mechanistic model whereby the mTORC1-ATF4 axis reconfigures the fibroblast biosynthetic and metabolic network to meet the collagen synthetic demands of TGF-β_1-induced myofibroblasts (Figure 4.1) . As well as providing insight into the signalling and transcriptional pathways by which the major pro-fibrotic mediator TGF-β_1 exerts its pro-fibrotic effects, the findings suggest that targeting the mTORC1-ATF4 axis and downstream metabolic networks might represent a novel approach for the future development of anti-fibrotic strategies.

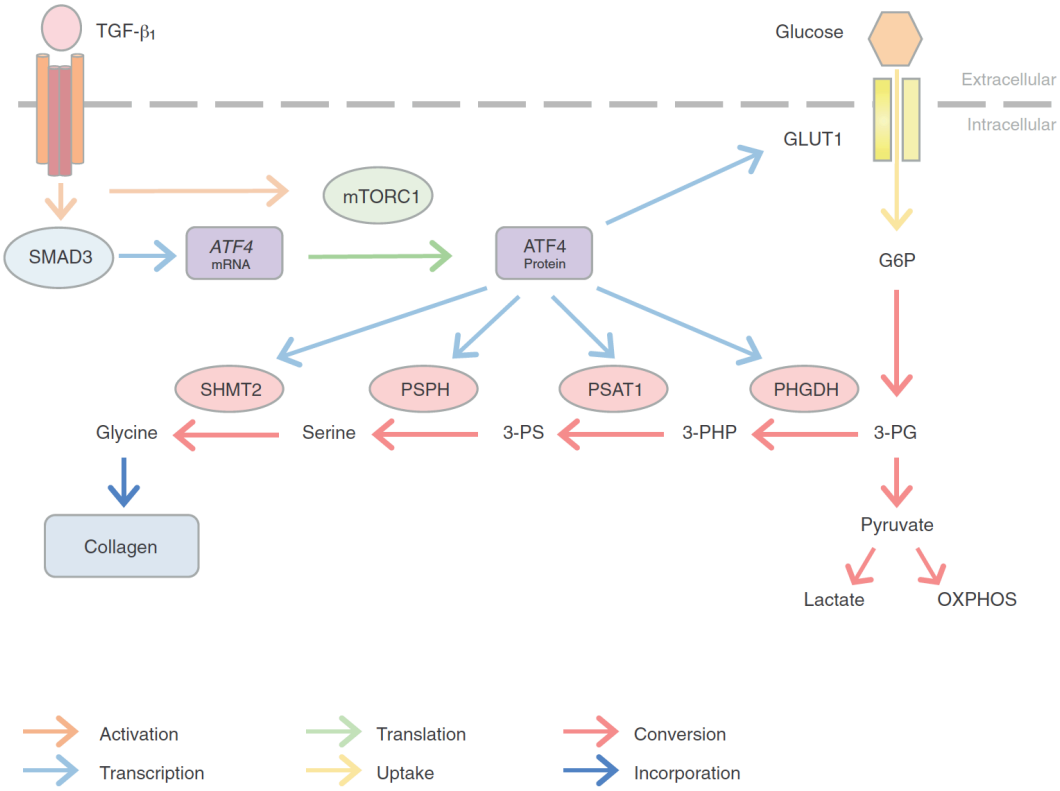

Figure 4.1 Model for ATF4-mediated metabolic and biosynthetic network reprogramming to support enhanced collagen biosynthesis in TGF-β_1–stimulated myofibroblasts. TGF-β_1–induced activation of the TGF-β_1 receptor complex leads to a Smad3-dependent increase in ATF4 mRNA abundance and mTOR activation. Activated mTORC1–4E-BP1 signalling, in turn, promotes ATF4 protein production through a translational mechanism. ATF4 subsequently promotes the transcription of key serine-glycine pathway genes and *SLC2A1* and, therefore, an increase in the abundance of the *SLC2A1* gene product, GLUT1. The serine-glycine biosynthesis enzymes and GLUT1 act together to promote glucose-derived glycine biosynthesis to support enhanced collagen synthesis rates in activated myofibroblasts. G6P, glucose 6-phosphate; 3-PG, 3-phosphoglycerate; 3-PHP, 3-phosphohydroxypyruvate; 3-PS, 3-phosphoserine; OXPHOS, oxidative phosphorylation.

Future directions

Fibrometabolism is an emerging and exciting avenue of research in that exploiting key metabolic vulnerabilities in multiple effector cells could potentially open up promising new therapeutic strategies to interfere with fibrogenesis in the context of multiple fibrotic conditions including IPF.

While the present study presents evidence that mTOR regulates TGF-β induced collagen synthesis in myofibroblasts, it is clear that this work has only just started to uncover the metabolic alterations occurring in IPF.

My future work would aim to build on these results and extend the evidence that targeting fibrometabolism could be a viable therapeutic strategy in IPF. Future studies would include:

- Profiling the metabolic changes that occur in IPF lung tissue.

- Profiling the dynamic metabolic changes, together with transcriptomic analysis using single cell sequencing of alveolar epithelial cells and myofibroblasts derived from IPF lung.

- Profiling the changes in metabolites from bronchoalveolar lavages and peripheral blood extracted from IPF patients to uncover potential novel biomarkers of disease severity and potential therapeutic efficacy.

Metabolomics, a field that has recently experienced major analytic advances, particularly in mass spectrometry, holds considerable potential to uncover specific metabolic 'fingerprints' of different pathologies including in IPF thereby offering possible applications for disease therapeutics and precision-based medical care.

Reports of the application of metabolomic techniques, including mass spectrometry and NMR as presented in this thesis, are only just beginning to emerge in the setting of fibrosis and have thus far only assessed the static metabolic changes associated with fibrogenesis.

To start to address the above aims, I would concentrate on gaining a more comprehensive understanding of the complex multi-directional metabolic networks underlying fibrogenesis in IPF, by adopting an equally dynamic and multi-layered metabolomic approach. In the cancer setting, *in vitro* and *in vivo* tracing of metabolic pathways using stable isotope-labelled metabolites (e.g. ^{13}C glucose) in combination with computational modelling, centred on network and pathway-based integrative methods (e.g. weighted gene co-expression network analysis (WGCNA), gene set analysis) to characterise the utilisation of different metabolites during tumorigenesis, have been transformational in terms of identifying novel metabolic vulnerabilities for therapeutic targeting. Bringing this approach to profile the metabolic changes and transcriptional changes in the IPF setting could potentially reveal new treatment strategies in IPF.

Matrix-assisted laser desorption ionisation (MALDI) imaging allows in situ simultaneous mapping and quantification of metabolites to anatomical structures without the loss of tissue integrity and has equally been informative in the cancer setting. This, or other MS-based imaging techniques, have not yet been widely applied in the context of fibrosis but a proof-of-mechanism study assessing the feasibility of using MALDI for the detection of metabolites in a mouse model of pulmonary fibrosis and treatment response to the approved anti-fibrotic agent, pirfenidone, has recently been reported. The investigators demonstrate a clear separation of metabolic profiles between treatment groups, warranting further investigation of this approach in more highly powered studies *(245)*.

Incorporating metabolomics into a systems biology approach, which will combine high-dimensional data from multiple omic platforms, including transcriptomics and metabolomics, will help identify the pathways underlying the development of pulmonary fibrosis in order to develop novel diagnostic and prognostic biomarkers and importantly to provide potential novel solutions to target these pathways therapeutically.

References

1. J. Gribbin, R. B. Hubbard, I. Le Jeune, C. J. P. Smith, J. West, L. J. Tata, Incidence and mortality of idiopathic pulmonary fibrosis and sarcoidosis in the UK., *Thorax* **61**, 980–5 (2006).

2. V. Navaratnam, K. M. Fleming, J. West, C. J. P. Smith, R. G. Jenkins, A. Fogarty, R. B. Hubbard, The rising incidence of idiopathic pulmonary fibrosis in the U.K., *Thorax* **66**, 462–7 (2011).

3. G. Raghu, H. R. Collard, J. J. Egan, F. J. Martinez, J. Behr, K. K. Brown, T. V Colby, J.-F. Cordier, K. R. Flaherty, J. A. Lasky, D. A. Lynch, J. H. Ryu, J. J. Swigris, A. U. Wells, J. Ancochea, D. Bouros, C. Carvalho, U. Costabel, M. Ebina, D. M. Hansell, T. Johkoh, D. S. Kim, T. E. King, Y. Kondoh, J. Myers, N. L. Müller, A. G. Nicholson, L. Richeldi, M. Selman, R. F. Dudden, B. S. Griss, S. L. Protzko, H. J. Schünemann, An official ATS/ERS/JRS/ALAT statement: idiopathic pulmonary fibrosis: evidence-based guidelines for diagnosis and management., *Am. J. Respir. Crit. Care Med.* **183**, 788–824 (2011).

4. A. Datta, C. J. Scotton, R. C. Chambers, Novel therapeutic approaches for pulmonary fibrosis, *Br. J. Pharmacol.* **163**, 141–172 (2011).

5. A. U. Wells, J. Behr, U. Costabel, V. Cottin, V. Poletti, Triple therapy in idiopathic pulmonary fibrosis: an alarming press release., *Eur. Respir. J.* **39**, 805–6 (2012).

6. T. E. King, W. Z. Bradford, S. Castro-Bernardini, E. A. Fagan, I. Glaspole, M. K. Glassberg, E. Gorina, P. M. Hopkins, D. Kardatzke, L. Lancaster, D. J. Lederer, S. D. Nathan, C. A. Pereira, S. A. Sahn, R. Sussman, J. J. Swigris, P. W. Noble, A phase 3 trial of pirfenidone in patients with idiopathic pulmonary

fibrosis., *N. Engl. J. Med.* **370**, 2083–92 (2014).
7. L. Richeldi, R. M. du Bois, G. Raghu, A. Azuma, K. K. Brown, U. Costabel, V. Cottin, K. R. Flaherty, D. M. Hansell, Y. Inoue, D. S. Kim, M. Kolb, A. G. Nicholson, P. W. Noble, M. Selman, H. Taniguchi, M. Brun, F. Le Maulf, M. Girard, S. Stowasser, R. Schlenker-Herceg, B. Disse, H. R. Collard, Efficacy and safety of nintedanib in idiopathic pulmonary fibrosis., *N. Engl. J. Med.* **370**, 2071–82 (2014).
8. P. W. Noble, C. Albera, W. Z. Bradford, U. Costabel, R. M. du Bois, E. A. Fagan, R. S. Fishman, I. Glaspole, M. K. Glassberg, L. Lancaster, D. J. Lederer, J. A. Leff, S. D. Nathan, C. A. Pereira, J. J. Swigris, D. Valeyre, T. E. King, Pirfenidone for idiopathic pulmonary fibrosis: analysis of pooled data from three multinational phase 3 trials., *Eur. Respir. J.* **47**, 243–53 (2016).
9. A. Di Sario, E. Bendia, G. Svegliati Baroni, F. Ridolfi, A. Casini, E. Ceni, S. Saccomanno, M. Marzioni, L. Trozzi, P. Sterpetti, S. Taffetani, A. Benedetti, Effect of pirfenidone on rat hepatic stellate cell proliferation and collagen production., *J. Hepatol.* **37**, 584–91 (2002).
10. H. Oku, T. Shimizu, T. Kawabata, M. Nagira, I. Hikita, A. Ueyama, S. Matsushima, M. Torii, A. Arimura, Antifibrotic action of pirfenidone and prednisolone: different effects on pulmonary cytokines and growth factors in bleomycin-induced murine pulmonary fibrosis., *Eur. J. Pharmacol.* **590**, 400–8 (2008).
11. K. B. Baumgartner, J. M. Samet, C. A. Stidley, T. V Colby, J. A. Waldron, Cigarette smoking: a risk factor for idiopathic pulmonary fibrosis., *Am. J. Respir. Crit. Care Med.* **155**, 242–8 (1997).
12. G. Raghu, T. D. Freudenberger, S. Yang, J. R. Curtis, C. Spada, J. Hayes, J. K. Sillery, C. E. Pope, C. A. Pellegrini, High

prevalence of abnormal acid gastro-oesophageal reflux in idiopathic pulmonary fibrosis., *Eur. Respir. J.* **27**, 136–42 (2006).
13. J. Gribbin, R. Hubbard, C. Smith, Role of diabetes mellitus and gastro-oesophageal reflux in the aetiology of idiopathic pulmonary fibrosis., *Respir. Med.* **103**, 927–31 (2009).
14. R. Hubbard, S. Lewis, K. Richards, I. Johnston, J. Britton, Occupational exposure to metal or wood dust and aetiology of cryptogenic fibrosing alveolitis., *Lancet (London, England)* **347**, 284–9 (1996).
15. K. B. Baumgartner, J. M. Samet, D. B. Coultas, C. A. Stidley, W. C. Hunt, T. V Colby, J. A. Waldron, Occupational and environmental risk factors for idiopathic pulmonary fibrosis: a multicenter case-control study. Collaborating Centers., *Am. J. Epidemiol.* **152**, 307–15 (2000).
16. J. P. Stewart, J. J. Egan, A. J. Ross, B. G. Kelly, S. S. Lok, P. S. Hasleton, A. A. Woodcock, The detection of Epstein-Barr virus DNA in lung tissue from patients with idiopathic pulmonary fibrosis., *Am. J. Respir. Crit. Care Med.* **159**, 1336–41 (1999).
17. M. A. Seibold, A. L. Wise, M. C. Speer, M. P. Steele, K. K. Brown, J. E. Loyd, T. E. Fingerlin, W. Zhang, G. Gudmundsson, S. D. Groshong, C. M. Evans, S. Garantziotis, K. B. Adler, B. F. Dickey, R. M. du Bois, I. V Yang, A. Herron, D. Kervitsky, J. L. Talbert, C. Markin, J. Park, A. L. Crews, S. H. Slifer, S. Auerbach, M. G. Roy, J. Lin, C. E. Hennessy, M. I. Schwarz, D. A. Schwartz, A common MUC5B promoter polymorphism and pulmonary fibrosis., *N. Engl. J. Med.* **364**, 1503–12 (2011).
18. A. L. Peljto, Y. Zhang, T. E. Fingerlin, S.-F. Ma, J. G. N. Garcia, T. J. Richards, L. J. Silveira, K. O. Lindell, M. P. Steele, J. E. Loyd, K. F. Gibson, M. A. Seibold, K. K. Brown, J. L. Talbert, C.

Markin, K. Kossen, S. D. Seiwert, E. Murphy, I. Noth, M. I. Schwarz, N. Kaminski, D. A. Schwartz, Association between the MUC5B promoter polymorphism and survival in patients with idiopathic pulmonary fibrosis., *JAMA* **309**, 2232–9 (2013).
19. P. L. Molyneaux, M. J. Cox, S. A. G. Willis-Owen, P. Mallia, K. E. Russell, A.-M. Russell, E. Murphy, S. L. Johnston, D. A. Schwartz, A. U. Wells, W. O. C. Cookson, T. M. Maher, M. F. Moffatt, The Role of Bacteria in the Pathogenesis and Progression of IdiopathicPulmonary Fibrosis, *Am. J. Respir. Crit. Care Med.* **190**, 906 (2014).
20. I. V Yang, T. E. Fingerlin, C. M. Evans, M. I. Schwarz, D. A. Schwartz, MUC5B and Idiopathic Pulmonary Fibrosis., *Ann. Am. Thorac. Soc.* **12 Suppl 2**, S193-9 (2015).
21. L. M. Nogee, A. E. Dunbar, S. E. Wert, F. Askin, A. Hamvas, J. A. Whitsett, A mutation in the surfactant protein C gene associated with familial interstitial lung disease., *N. Engl. J. Med.* **344**, 573–9 (2001).
22. B. Driscoll, S. Buckley, K. C. Bui, K. D. Anderson, D. Warburton, Telomerase in alveolar epithelial development and repair, *Am. J. Physiol. Cell. Mol. Physiol.* **279**, L1191–L1198 (2000).
23. M. Y. Armanios, J. J.-L. Chen, J. D. Cogan, J. K. Alder, R. G. Ingersoll, C. Markin, W. E. Lawson, M. Xie, I. Vulto, J. A. Phillips, P. M. Lansdorp, C. W. Greider, J. E. Loyd, Telomerase mutations in families with idiopathic pulmonary fibrosis., *N. Engl. J. Med.* **356**, 1317–26 (2007).
24. T. E. Fingerlin, E. Murphy, W. Zhang, A. L. Peljto, K. K. Brown, M. P. Steele, J. E. Loyd, G. P. Cosgrove, D. Lynch, S. Groshong, H. R. Collard, P. J. Wolters, W. Z. Bradford, K. Kossen, S. D.

Seiwert, R. M. du Bois, C. K. Garcia, M. S. Devine, G. Gudmundsson, H. J. Isaksson, N. Kaminski, Y. Zhang, K. F. Gibson, L. H. Lancaster, J. D. Cogan, W. R. Mason, T. M. Maher, P. L. Molyneaux, A. U. Wells, M. F. Moffatt, M. Selman, A. Pardo, D. S. Kim, J. D. Crapo, B. J. Make, E. A. Regan, D. S. Walek, J. J. Daniel, Y. Kamatani, D. Zelenika, K. Smith, D. McKean, B. S. Pedersen, J. Talbert, R. N. Kidd, C. R. Markin, K. B. Beckman, M. Lathrop, M. I. Schwarz, D. A. Schwartz, Genome-wide association study identifies multiple susceptibility loci for pulmonary fibrosis, *Nat. Genet.* **45**, 613–620 (2013).

25. I. Noth, Y. Zhang, S.-F. Ma, C. Flores, M. Barber, Y. Huang, S. M. Broderick, M. S. Wade, P. Hysi, J. Scuirba, T. J. Richards, B. M. Juan-Guardela, R. Vij, M. K. Han, F. J. Martinez, K. Kossen, S. D. Seiwert, J. D. Christie, D. Nicolae, N. Kaminski, J. G. N. Garcia, Genetic variants associated with idiopathic pulmonary fibrosis susceptibility and mortality: a genome-wide association study., *Lancet. Respir. Med.* **1**, 309–317 (2013).

26. C. J. Scotton, M. A. Krupiczojc, M. Königshoff, P. F. Mercer, Y. C. G. Lee, N. Kaminski, J. Morser, J. M. Post, T. M. Maher, A. G. Nicholson, J. D. Moffatt, G. J. Laurent, C. K. Derian, O. Eickelberg, R. C. Chambers, Increased local expression of coagulation factor X contributes to the fibrotic response in human and murine lung injury., *J. Clin. Invest.* **119**, 2550–63 (2009).

27. V. J. Thannickal, J. C. Horowitz, Evolving concepts of apoptosis in idiopathic pulmonary fibrosis., *Proc. Am. Thorac. Soc.* **3**, 350–6 (2006).

28. L. Hecker, R. Vittal, T. Jones, R. Jagirdar, T. R. Luckhardt, J. C. Horowitz, S. Pennathur, F. J. Martinez, V. J. Thannickal, NADPH oxidase-4 mediates myofibroblast activation and

fibrogenic responses to lung injury., *Nat. Med.* **15**, 1077–81 (2009).
29. V. J. Thannickal, G. B. Toews, E. S. White, J. P. Lynch, F. J. Martinez, Mechanisms of pulmonary fibrosis., *Annu. Rev. Med.* **55**, 395–417 (2004).
30. M. Plataki, A. V Koutsopoulos, K. Darivianaki, G. Delides, N. M. Siafakas, D. Bouros, Expression of apoptotic and antiapoptotic markers in epithelial cells in idiopathic pulmonary fibrosis., *Chest* **127**, 266–74 (2005).
31. C. G. Lee, S. J. Cho, M. J. Kang, S. P. Chapoval, P. J. Lee, P. W. Noble, T. Yehualaeshet, B. Lu, R. A. Flavell, J. Milbrandt, R. J. Homer, J. A. Elias, Early growth response gene 1-mediated apoptosis is essential for transforming growth factor beta1-induced pulmonary fibrosis., *J. Exp. Med.* **200**, 377–89 (2004).
32. K. Psathakis, D. Mermigkis, G. Papatheodorou, S. Loukides, P. Panagou, V. Polychronopoulos, N. M. Siafakas, D. Bouros, Exhaled markers of oxidative stress in idiopathic pulmonary fibrosis., *Eur. J. Clin. Invest.* **36**, 362–7 (2006).
33. T. M. Maher, I. C. Evans, S. E. Bottoms, P. F. Mercer, A. J. Thorley, A. G. Nicholson, G. J. Laurent, T. D. Tetley, R. C. Chambers, R. J. McAnulty, Diminished prostaglandin E2 contributes to the apoptosis paradox in idiopathic pulmonary fibrosis., *Am. J. Respir. Crit. Care Med.* **182**, 73–82 (2010).
34. R. Wang, A. Zagariya, O. Ibarra-Sunga, C. Gidea, E. Ang, S. Deshmukh, G. Chaudhary, J. Baraboutis, G. Filippatos, B. D. Uhal, Angiotensin II induces apoptosis in human and rat alveolar epithelial cells., *Am. J. Physiol.* **276**, L885-9 (1999).
35. R. Wang, A. Zagariya, O. Ibarra-Sunga, C. Gidea, E. Ang, S. Deshmukh, G. Chaudhary, J. Baraboutis, G. Filippatos, B. D. Uhal, Angiotensin II induces apoptosis in human and rat alveolar

epithelial cells., *Am. J. Physiol.* **276**, L885-9 (1999).
36. R. Wang, C. Ramos, I. Joshi, A. Zagariya, A. Pardo, M. Selman, B. D. Uhal, Human lung myofibroblast-derived inducers of alveolar epithelial apoptosis identified as angiotensin peptides, *Am. J. Physiol. Cell. Mol. Physiol.* **277**, L1158–L1164 (1999).
37. J. R. Rock, C. E. Barkauskas, M. J. Cronce, Y. Xue, J. R. Harris, J. Liang, P. W. Noble, B. L. M. Hogan, Multiple stromal populations contribute to pulmonary fibrosis without evidence for epithelial to mesenchymal transition., *Proc. Natl. Acad. Sci. U. S. A.* **108**, E1475-83 (2011).
38. J. J. Tomasek, G. Gabbiani, B. Hinz, C. Chaponnier, R. a Brown, Myofibroblasts and mechano-regulation of connective tissue remodelling., *Nat. Rev. Mol. Cell Biol.* **3**, 349–63 (2002).
39. B. Hinz, The myofibroblast: paradigm for a mechanically active cell., *J. Biomech.* **43**, 146–55 (2010).
40. P.-J. Wipff, D. B. Rifkin, J.-J. Meister, B. Hinz, Myofibroblast contraction activates latent TGF-beta1 from the extracellular matrix., *J. Cell Biol.* **179**, 1311–23 (2007).
41. Y. Fukuda, M. Ishizaki, S. Kudoh, M. Kitaichi, N. Yamanaka, Localization of matrix metalloproteinases-1, -2, and -9 and tissue inhibitor of metalloproteinase-2 in interstitial lung diseases., *Lab. Invest.* **78**, 687–98 (1998).
42. R. G. Jenkins, J. K. Simpson, G. Saini, J. H. Bentley, A.-M. Russell, R. Braybrooke, P. L. Molyneaux, T. M. McKeever, A. U. Wells, A. Flynn, R. B. Hubbard, D. J. Leeming, R. P. Marshall, M. A. Karsdal, P. T. Lukey, T. M. Maher, Longitudinal change in collagen degradation biomarkers in idiopathic pulmonary fibrosis: an analysis from the prospective, multicentre PROFILE study., *Lancet. Respir. Med.* **3**, 462–72 (2015).

43. M. W. Parker, D. Rossi, M. Peterson, K. Smith, K. Sikström, E. S. White, J. E. Connett, C. A. Henke, O. Larsson, P. B. Bitterman, Fibrotic extracellular matrix activates a profibrotic positive feedback loop., *J. Clin. Invest.* **124**, 1622–35 (2014).
44. J. A. Madri, H. Furthmayr, Collagen polymorphism in the lung. An immunochemical study of pulmonary fibrosis., *Hum. Pathol.* **11**, 353–66 (1980).
45. S. Gay, G. R. Martin, P. K. Muller, R. Timpl, K. Kuhn, Simultaneous synthesis of types I and III collagen by fibroblasts in culture., *Proc. Natl. Acad. Sci. U. S. A.* **73**, 4037–40 (1976).
46. A. J. Booth, R. Hadley, A. M. Cornett, A. A. Dreffs, S. A. Matthes, J. L. Tsui, K. Weiss, J. C. Horowitz, V. F. Fiore, T. H. Barker, B. B. Moore, F. J. Martinez, L. E. Niklason, E. S. White, Acellular normal and fibrotic human lung matrices as a culture system for in vitro investigation., *Am. J. Respir. Crit. Care Med.* **186**, 866–76 (2012).
47. M. D. Shoulders, R. T. Raines, Collagen structure and stability., *Annu. Rev. Biochem.* **78**, 929–58 (2009).
48. N. Khalil, R. N. O'Connor, K. C. Flanders, H. Unruh, TGF-beta 1, but not TGF-beta 2 or TGF-beta 3, is differentially present in epithelial cells of advanced pulmonary fibrosis: an immunohistochemical study., *Am. J. Respir. Cell Mol. Biol.* **14**, 131–8 (1996).
49. A. Leask, A. Holmes, C. M. Black, D. J. Abraham, Connective tissue growth factor gene regulation. Requirements for its induction by transforming growth factor-beta 2 in fibroblasts., *J. Biol. Chem.* **278**, 13008–15 (2003).
50. K. T. Goldsmith, R. B. Gammon, R. I. Garver, Modulation of bFGF in lung fibroblasts by TGF-beta and PDGF., *Am. J. Physiol.*

261, L378-85 (1991).
51. Y. Soma, G. R. Grotendorst, TGF-beta stimulates primary human skin fibroblast DNA synthesis via an autocrine production of PDGF-related peptides., *J. Cell. Physiol.* **140**, 246–53 (1989).
52. K. Ask, P. Bonniaud, K. Maass, O. Eickelberg, P. J. Margetts, D. Warburton, J. Groffen, J. Gauldie, M. Kolb, Progressive pulmonary fibrosis is mediated by TGF-beta isoform 1 but not TGF-beta3., *Int. J. Biochem. Cell Biol.* **40**, 484–95 (2008).
53. H. Higashiyama, D. Yoshimoto, T. Kaise, S. Matsubara, M. Fujiwara, H. Kikkawa, S. Asano, M. Kinoshita, Inhibition of activin receptor-like kinase 5 attenuates bleomycin-induced pulmonary fibrosis., *Exp. Mol. Pathol.* **83**, 39–46 (2007).
54. A. B. Kulkarni, C. G. Huh, D. Becker, A. Geiser, M. Lyght, K. C. Flanders, A. B. Roberts, M. B. Sporn, J. M. Ward, S. Karlsson, Transforming growth factor beta 1 null mutation in mice causes excessive inflammatory response and early death., *Proc. Natl. Acad. Sci. U. S. A.* **90**, 770–4 (1993).
55. Q. Yu, I. Stamenkovic, Cell surface-localized matrix metalloproteinase-9 proteolytically activates TGF-beta and promotes tumor invasion and angiogenesis., *Genes Dev.* **14**, 163–76 (2000).
56. R. M. Lyons, J. Keski-Oja, H. L. Moses, Proteolytic activation of latent transforming growth factor-beta from fibroblast-conditioned medium., *J. Cell Biol.* **106**, 1659–65 (1988).
57. M. H. Barcellos-Hoff, T. A. Dix, Redox-mediated activation of latent transforming growth factor-beta 1., *Mol. Endocrinol.* **10**, 1077–83 (1996).
58. J. S. Munger, X. Huang, H. Kawakatsu, M. J. . Griffiths, S. L. Dalton, J. Wu, J.-F. Pittet, N. Kaminski, C. Garat, M. A. Matthay, D.

B. Rifkin, D. Sheppard, A Mechanism for Regulating Pulmonary Inflammation and Fibrosis: The Integrin αvβ6 Binds and Activates Latent TGF β1, *Cell* **96**, 319–328 (1999).
59. H. GS, W. S, O. V, L. DJ, L. ME, W. PH, S. KJ, H. K, A. NE, R. NJ, G. J, F.-B. CA, M. EL, O. C, L. R, D. GS, H. X, S. D, V. SM, Partial inhibition of integrin alpha(v)beta6 prevents pulmonary fibrosis without exacerbating inflammation, *Am. J. Respir. Crit. Care Med.* **177** (2008), doi:10.1164/RCCM.200706-805OC.
60. R. Zoncu, A. Efeyan, D. M. Sabatini, mTOR: from growth signal integration to cancer, diabetes and ageing., *Nat. Rev. Mol. Cell Biol.* **12**, 21–35 (2011).
61. P. F. Mercer, H. V Woodcock, J. D. Eley, M. Platé, M. G. Sulikowski, P. F. Durrenberger, L. Franklin, C. B. Nanthakumar, Y. Man, F. Genovese, R. J. McAnulty, S. Yang, T. M. Maher, A. G. Nicholson, A. D. Blanchard, R. P. Marshall, P. T. Lukey, R. C. Chambers, Exploration of a potent PI3 kinase/mTOR inhibitor as a novel anti-fibrotic agent in IPF., *Thorax* , thoraxjnl-2015-207429-(2016).
62. L. C. Cantley, The phosphoinositide 3-kinase pathway., *Science* **296**, 1655–7 (2002).
63. P. T. Hawkins, K. E. Anderson, K. Davidson, L. R. Stephens, Signalling through Class I PI3Ks in mammalian cells., *Biochem. Soc. Trans.* **34**, 647–62 (2006).
64. M. Laplante, D. Sabatini, mTOR Signaling in Growth Control and Disease, *Cell* **149**, 274–293 (2012).
65. M. Laplante, D. M. Sabatini, MTOR signaling in growth control and disease, *Cell* **149**, 274–293 (2012).
66. H. J, D. CC, M. M, M. BD, The TSC1-TSC2 complex is required for proper activation of mTOR complex 2, *Mol. Cell. Biol.*

28 (2008), doi:10.1128/MCB.00289-08.
67. T. K, B. I, N. D, A. D, G. D, G. B, D. J, Z. S, Y. H, D. J. J, A. AN, Z. Y, D. CC, D. H, R. A, Y. WH, V. HV, G. JF, C. WK, C. TF, M. BD, B. AS, M. PS, Oncogenic EGFR signaling activates an mTORC2-NF-κB pathway that promotes chemotherapy resistance, *Cancer Discov.* **1** (2011), doi:10.1158/2159-8290.CD-11-0124.
68. B. Raught, F. Peiretti, A.-C. Gingras, M. Livingstone, D. Shahbazian, G. L. Mayeur, R. D. Polakiewicz, N. Sonenberg, J. W. B. Hershey, Phosphorylation of eucaryotic translation initiation factor 4B Ser422 is modulated by S6 kinases., *EMBO J.* **23**, 1761–9 (2004).
69. S. R. Datta, H. Dudek, X. Tao, S. Masters, H. Fu, Y. Gotoh, M. E. Greenberg, Akt phosphorylation of BAD couples survival signals to the cell-intrinsic death machinery., *Cell* **91**, 231–41 (1997).
70. A. Brunet, A. Bonni, M. J. Zigmond, M. Z. Lin, P. Juo, L. S. Hu, M. J. Anderson, K. C. Arden, J. Blenis, M. E. Greenberg, Akt promotes cell survival by phosphorylating and inhibiting a Forkhead transcription factor., *Cell* **96**, 857–68 (1999).
71. J. Liang, J. Zubovitz, T. Petrocelli, R. Kotchetkov, M. K. Connor, K. Han, J.-H. Lee, S. Ciarallo, C. Catzavelos, R. Beniston, E. Franssen, J. M. Slingerland, PKB/Akt phosphorylates p27, impairs nuclear import of p27 and opposes p27-mediated G1 arrest., *Nat. Med.* **8**, 1153–60 (2002).
72. J. A. Diehl, M. Cheng, M. F. Roussel, C. J. Sherr, Glycogen synthase kinase-3beta regulates cyclin D1 proteolysis and subcellular localization., *Genes Dev.* **12**, 3499–511 (1998).
73. H. Sano, S. Kane, E. Sano, C. P. Mîinea, J. M. Asara, W. S. Lane, C. W. Garner, G. E. Lienhard, Insulin-stimulated phosphorylation of a Rab GTPase-activating protein regulates

GLUT4 translocation., *J. Biol. Chem.* **278**, 14599–602 (2003).
74. A. Barthel, S. T. Okino, J. Liao, K. Nakatani, J. Li, J. P. Whitlock, R. A. Roth, Regulation of GLUT1 gene transcription by the serine/threonine kinase Akt1., *J. Biol. Chem.* **274**, 20281–6 (1999).
75. M. G. Vander Heiden, D. R. Plas, J. C. Rathmell, C. J. Fox, M. H. Harris, C. B. Thompson, Growth factors can influence cell growth and survival through effects on glucose metabolism., *Mol. Cell. Biol.* **21**, 5899–912 (2001).
76. J. Deprez, D. Vertommen, D. R. Alessi, L. Hue, M. H. Rider, Phosphorylation and activation of heart 6-phosphofructo-2-kinase by protein kinase B and other protein kinases of the insulin signaling cascades., *J. Biol. Chem.* **272**, 17269–75 (1997).
77. L. Zhang, F. Zhou, P. ten Dijke, Signaling interplay between transforming growth factor-β receptor and PI3K/AKT pathways in cancer., *Trends Biochem. Sci.* **38**, 612–20 (2013).
78. H. V. Woodcock, J. D. Eley, D. Guillotin, M. Platé, C. B. Nanthakumar, M. Martufi, S. Peace, G. Joberty, D. Poeckel, R. B. Good, A. R. Taylor, N. Zinn, M. Redding, E. J. Forty, R. E. Hynds, C. Swanton, M. Karsdal, T. M. Maher, G. Bergamini, R. P. Marshall, A. D. Blanchard, P. F. Mercer, R. C. Chambers, The mTORC1/4E-BP1 axis represents a critical signaling node during fibrogenesis, *Nat. Commun.* **10**, 6 (2019).
79. J. C. Horowitz, D. Y. Lee, M. Waghray, V. G. Keshamouni, P. E. Thomas, H. Zhang, Z. Cui, V. J. Thannickal, Activation of the pro-survival phosphatidylinositol 3-kinase/AKT pathway by transforming growth factor-beta1 in mesenchymal cells is mediated by p38 MAPK-dependent induction of an autocrine growth factor., *J. Biol. Chem.* **279**, 1359–67 (2004).

80. J. C. Horowitz, D. S. Rogers, V. Sharma, R. Vittal, E. S. White, Z. Cui, V. J. Thannickal, Combinatorial activation of FAK and AKT by transforming growth factor-beta1 confers an anoikis-resistant phenotype to myofibroblasts., *Cell. Signal.* **19**, 761–71 (2007).
81. E. Conte, E. Gili, M. Fruciano, M. Korfei, E. Fagone, M. Iemmolo, D. Lo Furno, R. Giuffrida, N. Crimi, A. Guenther, C. Vancheri, PI3K p110γ overexpression in idiopathic pulmonary fibrosis lung tissue and fibroblast cells: in vitro effects of its inhibition., *Lab. Invest.* **93**, 566–76 (2013).
82. L. C. Cantley, The phosphoinositide 3-kinase pathway., *Science* **296**, 1655–7 (2002).
83. H. Xia, D. Diebold, R. Nho, D. Perlman, J. Kleidon, J. Kahm, S. Avdulov, M. Peterson, J. Nerva, P. Bitterman, C. Henke, Pathological integrin signaling enhances proliferation of primary lung fibroblasts from patients with idiopathic pulmonary fibrosis., *J. Exp. Med.* **205**, 1659–72 (2008).
84. N. M. Walker, E. A. Belloli, L. Stuckey, K. M. Chan, J. Lin, W. Lynch, A. Chang, S. M. Mazzoni, D. C. Fingar, V. N. Lama, Mechanistic Target of Rapamycin Complex 1 (mTORC1) and mTORC2 as Key Signaling Intermediates in Mesenchymal Cell Activation., *J. Biol. Chem.* **1** (2016), doi:10.1074/jbc.M115.672170.
85. H. Xia, D. Diebold, R. Nho, D. Perlman, J. Kleidon, J. Kahm, S. Avdulov, M. Peterson, J. Nerva, P. Bitterman, C. Henke, Pathological integrin signaling enhances proliferation of primary lung fibroblasts from patients with idiopathic pulmonary fibrosis, *J. Exp. Med.* **205**, 1659 (2008).
86. W. X, H. J, C. ZZ, Q. BW, W. GC, M. YH, Z. H, L. YF, W. YQ, C. LJ, A phosphoinositide 3-kinase-gamma inhibitor, AS605240 prevents bleomycin-induced pulmonary fibrosis in rats, *Biochem.*

Biophys. Res. Commun. **397** (2010), doi:10.1016/J.BBRC.2010.05.109.
87. R. RC, G. CC, B. LS, R. MA, G. R, R. E, S. AL, S. LP, M. M, D. A, C. GD, P. V, L. M, T. MM, Phosphoinositide 3-kinase γ plays a critical role in bleomycin-induced pulmonary inflammation and fibrosis in mice, *J. Leukoc. Biol.* **89** (2011), doi:10.1189/JLB.0610346.
88. G. Kim, J.-B. Jun, K. B. Elkon, Necessary role of phosphatidylinositol 3-kinase in transforming growth factor ?-mediated activation of Akt in normal and rheumatoid arthritis synovial fibroblasts, *Arthritis Rheum.* **46**, 1504–1511 (2002).
89. J. C. Horowitz, D. S. Rogers, V. Sharma, R. Vittal, E. S. White, Z. Cui, V. J. Thannickal, Combinatorial activation of FAK and AKT by transforming growth factor-beta1 confers an anoikis-resistant phenotype to myofibroblasts., *Cell. Signal.* **19**, 761–71 (2007).
90. E. Conte, M. Fruciano, E. Fagone, E. Gili, F. Caraci, M. Iemmolo, N. Crimi, C. Vancheri, H. W. Chu, Ed. Inhibition of PI3K Prevents the Proliferation and Differentiation of Human Lung Fibroblasts into Myofibroblasts: The Role of Class I P110 Isoforms, *PLoS One* **6**, e24663 (2011).
91. A. A. Kulkarni, T. H. Thatcher, K. C. Olsen, S. B. Maggirwar, R. P. Phipps, P. J. Sime, R. K. Aziz, Ed. PPAR-γ Ligands Repress TGFβ-Induced Myofibroblast Differentiation by Targeting the PI3K/Akt Pathway: Implications for Therapy of Fibrosis, *PLoS One* **6**, e15909 (2011).
92. P. F. Mercer, H. V Woodcock, J. D. Eley, M. Platé, M. G. Sulikowski, P. F. Durrenberger, L. Franklin, C. B. Nanthakumar, Y. Man, F. Genovese, R. J. McAnulty, S. Yang, T. M. Maher, A. G. Nicholson, A. D. Blanchard, R. P. Marshall, P. T. Lukey, R. C.

Chambers, Exploration of a potent PI3 kinase/mTOR inhibitor as a novel anti-fibrotic agent in IPF, *Thorax* **71**, 701–711 (2016).
93. P. T. Lukey, S. A. Harrison, S. Yang, Y. Man, B. F. Holman, A. Rashidnasab, G. Azzopardi, M. Grayer, J. K. Simpson, P. Bareille, L. Paul, H. V. Woodcock, R. Toshner, P. Saunders, P. L. Molyneaux, K. Thielemans, F. J. Wilson, P. F. Mercer, R. C. Chambers, A. M. Groves, W. A. Fahy, R. P. Marshall, T. M. Maher, A Randomised, Placebo-Controlled Study of Omipalisib (PI3K/mTOR) in Idiopathic Pulmonary Fibrosis, *Eur. Respir. J.* , 1801992 (2019).
94. L. Shan, Y. Ding, Y. Fu, L. Zhou, X. Dong, S. Chen, H. Wu, W. Nai, H. Zheng, W. Xu, X. Bai, C. Jia, M. Dai, mTOR Overactivation in Mesenchymal cells Aggravates CCl4− Induced liver Fibrosis, *Sci. Rep.* **6**, 36037 (2016).
95. A. A. A. A. Yoshizaki, K. Yanaba, A. A. A. A. Yoshizaki, Y. Iwata, K. Komura, F. Ogawa, M. Takenaka, K. Shimizu, Y. Asano, M. Hasegawa, M. Fujimoto, S. Sato, Treatment with rapamycin prevents fibrosis in tight-skin and bleomycin-induced mouse models of systemic sclerosis., *Arthritis Rheum.* **62**, 2476–87 (2010).
96. G. Chen, H. Chen, C. Wang, Y. Peng, L. Sun, H. Liu, F. Liu, B. Ryffel, Ed. Rapamycin Ameliorates Kidney Fibrosis by Inhibiting the Activation of mTOR Signaling in Interstitial Macrophages and Myofibroblasts, *PLoS One* **7**, e33626 (2012).
97. J. S. Park, H. J. Park, Y. S. Park, S.-M. Lee, J.-J. Yim, C.-G. Yoo, S. K. Han, Y. W. Kim, Clinical significance of mTOR, ZEB1, ROCK1 expression in lung tissues of pulmonary fibrosis patients, *BMC Pulm. Med.* **14**, 168 (2014).
98. E. Conte, M. Fruciano, E. Fagone, E. Gili, F. Caraci, M.

Iemmolo, N. Crimi, C. Vancheri, Inhibition of PI3K Prevents the Proliferation and Differentiation of Human Lung Fibroblasts into Myofibroblasts : The Role of Class I P110 Isoforms, **6** (2011), doi:10.1371/journal.pone.0024663.
99. R. CE, S. HW, P. AC, The phosphatidylinositol 3-kinase/Akt pathway enhances Smad3-stimulated mesangial cell collagen I expression in response to transforming growth factor-beta1, *J. Biol. Chem.* **279** (2004), doi:10.1074/JBC.M310412200.
100. M. D. Buck, D. O'Sullivan, E. L. Pearce, T cell metabolism drives immunity, *J. Exp. Med.* **212**, 1345–1360 (2015).
101. J. M. Cleary, G. I. Shapiro, Development of phosphoinositide-3 kinase pathway inhibitors for advanced cancer., *Curr. Oncol. Rep.* **12**, 87–94 (2010).
102. S. A. Kang, M. E. Pacold, C. L. Cervantes, D. Lim, H. J. Lou, K. Ottina, N. S. Gray, B. E. Turk, M. B. Yaffe, D. M. Sabatini, mTORC1 Phosphorylation Sites Encode Their Sensitivity to Starvation and Rapamycin, *Science (80-.).* **341**, 1236566–1236566 (2013).
103. R. M. Kottmann, A. a. Kulkarni, K. a. Smolnycki, E. Lyda, T. Dahanayake, R. Salibi, S. Honnons, C. Jones, N. G. Isern, J. Z. Hu, S. D. Nathan, G. Grant, R. P. Phipps, P. J. Sime, Lactic acid is elevated in idiopathic pulmonary fibrosis and induces myofibroblast differentiation via pH-dependent activation of transforming growth factor-β, *Am. J. Respir. Crit. Care Med.* **186**, 740–751 (2012).
104. A. M. Groves, T. Win, N. J. Screaton, M. Berovic, R. Endozo, H. Booth, I. Kayani, L. J. Menezes, J. C. Dickson, P. J. Ell, Idiopathic pulmonary fibrosis and diffuse parenchymal lung disease: implications from initial experience with 18F-FDG PET/CT., *J. Nucl. Med.* **50**, 538–545 (2009).

105. C. M. Metallo, M. G. Vander Heiden, Metabolism strikes back: metabolic flux regulates cell signaling., *Genes Dev.* **24**, 2717–22 (2010).
106. W. G. Kaelin, S. L. McKnight, Influence of metabolism on epigenetics and disease., *Cell* **153**, 56–69 (2013).
107. O. Warburg, F. Wind, E. Negelein, THE METABOLISM OF TUMORS IN THE BODY., *J. Gen. Physiol.* **8**, 519–30 (1927).
108. R. a Cairns, I. S. Harris, T. W. Mak, Regulation of cancer cell metabolism., *Nat. Rev. Cancer* **11**, 85–95 (2011).
109. C. S. Palmer, M. Ostrowski, B. Balderson, N. Christian, S. M. Crowe, Glucose metabolism regulates T cell activation, differentiation, and functions, *Front. Immunol.* **6**, 5–7 (2015).
110. C.-H. Chang, J. D. Curtis, L. B. Maggi, B. Faubert, A. V. Villarino, D. O'Sullivan, S. C.-C. Huang, G. J. W. van der Windt, J. Blagih, J. Qiu, J. D. Weber, E. J. Pearce, R. G. Jones, E. L. Pearce, Posttranscriptional Control of T Cell Effector Function by Aerobic Glycolysis, *Cell* **153**, 1239–1251 (2013).
111. C.-H. Chang, J. D. Curtis, L. B. Maggi, B. Faubert, A. V. Villarino, D. O'Sullivan, S. C.-C. Huang, G. J. W. van der Windt, J. Blagih, J. Qiu, J. D. Weber, E. J. Pearce, R. G. Jones, E. L. Pearce, Posttranscriptional Control of T Cell Effector Function by Aerobic Glycolysis, *Cell* **153**, 1239–1251 (2013).
112. R. C. Chambers, P. F. Mercer, Mechanisms of Alveolar Epithelial Injury, Repair, and Fibrosis, *Ann. Am. Thorac. Soc.* **12**, S16–S20 (2015).
113. C. Vancheri, Common pathways in idiopathic pulmonary fibrosis and cancer., *Eur. Respir. Rev.* **22**, 265–72 (2013).
114. Y. P. Kang, S. B. Lee, J.-M. Lee, H. M. Kim, J. Y. Hong, W. J. Lee, C. W. Choi, H. K. Shin, D.-J. Kim, E. S. Koh, C.-S. Park, S.

W. Kwon, S.-W. Park, Metabolic Profiling Regarding Pathogenesis of Idiopathic Pulmonary Fibrosis., *J. Proteome Res.* **15**, 1717–24 (2016).
115. J. H. Fisher, M. Kolb, M. Algamdi, J. Morisset, K. A. Johannson, S. Shapera, P. Wilcox, T. To, M. Sadatsafavi, H. Manganas, N. Khalil, N. Hambly, A. J. Halayko, A. S. Gershon, C. D. Fell, G. Cox, C. J. Ryerson, Baseline characteristics and comorbidities in the CAnadian REgistry for Pulmonary Fibrosis, *BMC Pulm. Med.* **19**, 223 (2019).
116. R. G. Jenkins, J. K. Simpson, G. Saini, J. H. Bentley, A.-M. Russell, R. Braybrooke, P. L. Molyneaux, T. M. McKeever, A. U. Wells, A. Flynn, R. B. Hubbard, D. J. Leeming, R. P. Marshall, M. A. Karsdal, P. T. Lukey, T. M. Maher, Longitudinal change in collagen degradation biomarkers in idiopathic pulmonary fibrosis: an analysis from the prospective, multicentre PROFILE study., *Lancet. Respir. Med.* **3**, 462–72 (2015).
117. S. Guo, Insulin signaling, resistance, and the metabolic syndrome: insights from mouse models into disease mechanisms., *J. Endocrinol.* **220**, T1–T23 (2014).
118. N. B. Ruderman, D. Carling, M. Prentki, J. M. Cacicedo, AMPK, insulin resistance, and the metabolic syndrome, *J. Clin. Invest.* **123**, 2764 (2013).
119. R. J. DeBerardinis, N. S. Chandel, Fundamentals of cancer metabolism, *Sci. Adv.* **2**, e1600200 (2016).
120. M. Vander Heiden, L. Cantley, C. Thompson, Understanding the Warburg effect: The metabolic Requiremetns of cell proliferation, *Science (80-.).* **324**, 1029–1033 (2009).
121. A. M. Hosios, V. C. Hecht, L. V Danai, M. O. Johnson, J. C. Rathmell, M. L. Steinhauser, S. R. Manalis, M. G. Vander Heiden,

Amino Acids Rather than Glucose Account for the Majority of Cell Mass in Proliferating Mammalian Cells., *Dev. Cell* **36**, 540–9 (2016).
122. Y. Fu, S. Liu, S. Yin, W. Niu, W. Xiong, M. Tan, G. Li, M. Zhou, The reverse Warburg effect is likely to be an Achilles' heel of cancer that can be exploited for cancer therapy., *Oncotarget* **8**, 57813–57825 (2017).
123. R. A. Gatenby, R. J. Gillies, Why do cancers have high aerobic glycolysis?, *Nat. Rev. Cancer* **4**, 891–9 (2004).
124. T. Win, B. a. Thomas, T. Lambrou, B. F. Hutton, N. J. Screaton, J. C. Porter, T. M. Maher, R. Endozo, R. I. Shortman, A. Afaq, P. Lukey, P. J. Ell, A. M. Groves, Areas of normal pulmonary parenchyma on HRCT exhibit increased FDG PET signal in IPF patients, *Eur. J. Nucl. Med. Mol. Imaging* **41**, 337–342 (2014).
125. B. Bondue, A. Castiaux, G. Van Simaeys, C. Mathey, F. Sherer, D. Egrise, S. Lacroix, F. Huaux, G. Doumont, S. Goldman, Absence of early metabolic response assessed by 18F-FDG PET/CT after initiation of antifibrotic drugs in IPF patients, *Respir. Res.* **20**, 10 (2019).
126. A. Justet, A. Laurent-Bellue, G. Thabut, A. Dieudonné, M.-P. Debray, R. Borie, M. Aubier, R. Lebtahi, B. Crestani, [18F]FDG PET/CT predicts progression-free survival in patients with idiopathic pulmonary fibrosis, *Respir. Res.* **18**, 74 (2017).
127. T. Win, N. J. Screaton, J. C. Porter, B. Ganeshan, T. M. Maher, F. Fraioli, R. Endozo, R. I. Shortman, L. Hurrell, B. F. Holman, K. Thielemans, A. Rashidnasab, B. F. Hutton, P. T. Lukey, A. Flynn, P. J. Ell, A. M. Groves, Pulmonary 18F-FDG uptake helps refine current risk stratification in idiopathic pulmonary fibrosis (IPF)., *Eur. J. Nucl. Med. Mol. Imaging* **45**, 806–

815 (2018).
128. B. F. Holman, V. Cuplov, L. Millner, B. F. Hutton, T. M. Maher, A. M. Groves, K. Thielemans, Improved correction for the tissue fraction effect in lung PET/CT imaging, *Phys. Med. Biol.* **60**, 7387–7402 (2015).
129. D. L. Chen, J. Cheriyan, E. R. Chilvers, G. Choudhury, C. Coello, M. Connell, M. Fisk, A. M. Groves, R. N. Gunn, B. F. Holman, B. F. Hutton, S. Lee, W. MacNee, D. Mohan, D. Parr, D. Subramanian, R. Tal-Singer, K. Thielemans, E. J. R. van Beek, L. Vass, J. W. Wellen, I. Wilkinson, F. J. Wilson, Quantification of Lung PET Images: Challenges and Opportunities., *J. Nucl. Med.* **58**, 201–207 (2017).
130. Z. Tan, C. Yang, X. Zhang, P. Zheng, W. Shen, Expression of glucose transporter 1 and prognosis in non-small cell lung cancer: a pooled analysis of 1665 patients, *Oncotarget* **8**, 60954 (2017).
131. H. W. Stout-Delgado, S. J. Cho, S. G. Chu, D. N. Mitzel, J. Villalba, S. El-Chemaly, S. W. Ryter, A. M. K. Choi, I. O. Rosas, Age-Dependent Susceptibility to Pulmonary Fibrosis Is Associated with NLRP3 Inflammasome Activation., *Am. J. Respir. Cell Mol. Biol.* **55**, 252–63 (2016).
132. L. Hecker, N. J. Logsdon, D. Kurundkar, A. Kurundkar, K. Bernard, T. Hock, E. Meldrum, Y. Y. Sanders, V. J. Thannickal, Reversal of persistent fibrosis in aging by targeting Nox4-Nrf2 redox imbalance., *Sci. Transl. Med.* **6**, 231ra47 (2014).
133. S. J. Cho, J.-S. Moon, C.-M. Lee, A. M. K. Choi, H. W. Stout-Delgado, Glucose Transporter 1–Dependent Glycolysis Is Increased during Aging-Related Lung Fibrosis, and Phloretin Inhibits Lung Fibrosis, *Am. J. Respir. Cell Mol. Biol.* **56**, 521–531 (2017).

134. N. Xie, Z. Tan, S. Banerjee, H. Cui, J. Ge, Glycolytic reprogramming mediates myofibroblast differentiation and promotes lung fibrosis, *Am. J. Respir. Crit. Care Med.* , 1–40 (2015).
135. Y. D. Zhao, L. Yin, S. Archer, C. Lu, G. Zhao, Y. Yao, L. Wu, M. Hsin, T. K. Waddell, S. Keshavjee, J. Granton, M. de Perrot, Metabolic heterogeneity of idiopathic pulmonary fibrosis: a metabolomic study, *BMJ Open Respir. Res.* (2017), doi:10.1136/bmjresp-2017-000183.
136. Y. P. Kang, S. B. Lee, J. M. Lee, H. M. Kim, J. Y. Hong, W. J. Lee, C. W. Choi, H. K. Shin, D. J. Kim, E. S. Koh, C. S. Park, S. W. Kwon, S. W. Park, Metabolic profiling regarding pathogenesis of idiopathic pulmonary fibrosis, *J. Proteome Res.* **15**, 1717–1724 (2016).
137. J. L. Judge, D. J. Nagel, K. M. Owens, A. Rackow, R. P. Phipps, P. J. Sime, R. M. Kottmann, B. Ryffel, Ed. Prevention and treatment of bleomycin-induced pulmonary fibrosis with the lactate dehydrogenase inhibitor gossypol, *PLoS One* **13**, e0197936 (2018).
138. D. Álvarez, N. Cárdenes, J. Sellarés, M. Bueno, C. Corey, V. S. Hanumanthu, Y. Peng, H. D'Cunha, J. Sembrat, M. Nouraie, S. Shanker, C. Caufield, S. Shiva, M. Armanios, A. L. Mora, M. Rojas, IPF lung fibroblasts have a senescent phenotype, *Am. J. Physiol. Cell. Mol. Physiol.* **313**, L1164–L1173 (2017).
139. D. C. Zank, M. Bueno, A. L. Mora, M. Rojas, Idiopathic Pulmonary Fibrosis: Aging, Mitochondrial Dysfunction, and Cellular Bioenergetics., *Front. Med.* **5**, 10 (2018).
140. Y. P. Kang, S. B. Lee, J.-M. Lee, H. M. Kim, J. Y. Hong, W. J. Lee, C. W. Choi, H. K. Shin, D.-J. Kim, E. S. Koh, C.-S. Park, S.

W. Kwon, S.-W. Park, Metabolic Profiling Regarding Pathogenesis of Idiopathic Pulmonary Fibrosis., *J. Proteome Res.* **15**, 1717–24 (2016).
141. M. I. Koukourakis, A. Giatromanolaki, E. Sivridis, G. Bougioukas, V. Didilis, K. C. Gatter, A. L. Harris, Lactate dehydrogenase-5 (LDH-5) overexpression in non-small-cell lung cancer tissues is linked to tumour hypoxia, angiogenic factor production and poor prognosis, *Br. J. Cancer* **89**, 877–885 (2003).
142. R. M. Kottmann, E. Trawick, J. L. Judge, L. A. Wahl, A. Epa, K. M. Owens, T. H. Thatcher, R. P. Phipps, P. J. Sime, Pharmacologic inhibition of lactate production prevents myofibroblast differentiation, *Am. J. Physiol. - Lung Cell. Mol. Physiol.* , ajplung.00058.2015 (2015).
143. E. Schruf, V. Schroeder, C. A. Kuttruff, S. Weigle, M. Krell, M. Benz, T. Bretschneider, A. Holweg, M. Schuler, M. Frick, P. Nicklin, J. P. Garnett, M. C. Sobotta, Human lung fibroblast-to-myofibroblast transformation is not driven by an LDH5-dependent metabolic shift towards aerobic glycolysis, *Respir. Res.* **20**, 87 (2019).
144. C. B. Keerthisingam, R. G. Jenkins, N. K. Harrison, N. A. Hernandez-Rodriguez, H. Booth, G. J. Laurent, S. L. Hart, M. L. Foster, R. J. McAnulty, Cyclooxygenase-2 deficiency results in a loss of the anti-proliferative response to transforming growth factor-beta in human fibrotic lung fibroblasts and promotes bleomycin-induced pulmonary fibrosis in mice., *Am. J. Pathol.* **158**, 1411–22 (2001).
145. R. Dreos, G. Ambrosini, R. Cavin Périer, P. Bucher, EPD and EPDnew, high-quality promoter resources in the next-generation sequencing era., *Nucleic Acids Res.* **41**, D157-64 (2013).

146. X. Messeguer, R. Escudero, D. Farré, O. Núñez, J. Martínez, M. M. Albà, PROMO: detection of known transcription regulatory elements using species-tailored searches., *Bioinformatics* **18**, 333–4 (2002).
147. Ł. Kreft, A. Soete, P. Hulpiau, A. Botzki, Y. Saeys, P. De Bleser, ConTra v3: a tool to identify transcription factor binding sites across species, update 2017, *Nucleic Acids Res.* **45**, W490–W494 (2017).
148. M. Martufi, R. B. Good, R. Rapiteanu, T. Schmidt, E. Patili, K. Tvermosegaard, M. New, C. B. Nanthakumar, J. Betts, A. D. Blanchard, K. Maratou, Single-Step, High-Efficiency CRISPR-Cas9 Genome Editing in Primary Human Disease-Derived Fibroblasts., *Cris. J.* **2**, 31–40 (2019).
149. Y. Park, A. Reyna-Neyra, L. Philippe, C. C. Thoreen, mTORC1 Balances Cellular Amino Acid Supply with Demand for Protein Synthesis through Post-transcriptional Control of ATF4, *Cell Rep.* **19**, 1083–1090 (2017).
150. J. Vande Voorde, T. Ackermann, N. Pfetzer, D. Sumpton, G. Mackay, G. Kalna, C. Nixon, K. Blyth, E. Gottlieb, S. Tardito, Improving the metabolic fidelity of cancer models with a physiological cell culture medium, *Sci. Adv.* **5**, eaau7314 (2019).
151. M. Laplante, D. M. Sabatini, Regulation of mTORC1 and its impact on gene expression at a glance., *J. Cell Sci.* **126**, 1713–9 (2013).
152. S. Patching, Roles of facilitative glucose transporter GLUT1 in [18F]FDG positron emission tomography (PET) imaging of human diseases, *J. Diagnostic Imaging Ther.* **2**, 30–102 (2015).
153. S. Y. Lunt, M. G. Vander Heiden, Aerobic glycolysis: meeting the metabolic requirements of cell proliferation., *Annu. Rev. Cell*

Dev. Biol. **27**, 441–64 (2011).
154. C. Chen, Y. Peng, Z. Wang, P. Fish, J. Kaar, R. Koepsel, A. Russell, R. Lareu, M. Raghunath, The Scar-in-a-Jar: studying potential antifibrotic compounds from the epigenetic to extracellular level in a single well, *Br. J. Pharmacol.* **158**, 1196–1209 (2009).
155. T. Soga, Cancer metabolism: key players in metabolic reprogramming., *Cancer Sci.* **104**, 275–81 (2013).
156. E. M. Beauchamp, L. C. Platanias, The evolution of the TOR pathway and its role in cancer, *Oncogene* **32**, 3923–3932 (2013).
157. E. C. Lien, C. A. Lyssiotis, L. C. Cantley, in (2016), pp. 39–72.
158. W. Chang, K. Wei, L. Ho, G. J. Berry, S. S. Jacobs, C. H. Chang, G. D. Rosen, A critical role for the mTORC2 pathway in lung fibrosis, *PLoS One* **9** (2014), doi:10.1371/journal.pone.0106155.
159. C. M. Adams, Role of the transcription factor ATF4 in the anabolic actions of insulin and the anti-anabolic actions of glucocorticoids., *J. Biol. Chem.* **282**, 16744–53 (2007).
160. G. M. DeNicola, P.-H. Chen, E. Mullarky, J. A. Sudderth, Z. Hu, D. Wu, H. Tang, Y. Xie, J. M. Asara, K. E. Huffman, I. I. Wistuba, J. D. Minna, R. J. DeBerardinis, L. C. Cantley, NRF2 regulates serine biosynthesis in non–small cell lung cancer, *Nat. Genet.* **47**, 1475–1481 (2015).
161. J. W. Locasale, Serine, glycine and one-carbon units: cancer metabolism in full circle, *Nat. Rev. Cancer* **13**, 572–583 (2013).
162. M. E. Pacold, K. R. Brimacombe, S. H. Chan, J. M. Rohde, C. A. Lewis, L. J. Y. M. Swier, R. Possemato, W. W. Chen, L. B. Sullivan, B. P. Fiske, S. Cho, E. Freinkman, K. Birsoy, M. Abu-Remaileh, Y. D. Shaul, C. M. Liu, M. Zhou, M. J. Koh, H. Chung, S. M. Davidson, A. Luengo, A. Q. Wang, X. Xu, A. Yasgar, L. Liu,

G. Rai, K. D. Westover, M. G. Vander Heiden, M. Shen, N. S. Gray, M. B. Boxer, D. M. Sabatini, A PHGDH inhibitor reveals coordination of serine synthesis and one-carbon unit fate, *Nat. Chem. Biol.* **12**, 452–458 (2016).
163. R. B. Hamanaka, E. M. O'Leary, L. J. Witt, Y. Tian, G. A. Gökalp, A. Y. Meliton, N. O. Dulin, G. M. Mutlu, Glutamine Metabolism is Required for Collagen Protein Synthesis in Lung Fibroblasts, *Am. J. Respir. Cell Mol. Biol.* , rcmb.2019-0008OC (2019).
164. L. Richeldi, R. M. du Bois, G. Raghu, A. Azuma, K. K. Brown, U. Costabel, V. Cottin, K. R. Flaherty, D. M. Hansell, Y. Inoue, D. S. Kim, M. Kolb, A. G. Nicholson, P. W. Noble, M. Selman, H. Taniguchi, M. Brun, F. Le Maulf, M. Girard, S. Stowasser, R. Schlenker-Herceg, B. Disse, H. R. Collard, Efficacy and safety of nintedanib in idiopathic pulmonary fibrosis., *N. Engl. J. Med.* **370**, 2071–82 (2014).
165. A. S. Lee, I. Mira-Avendano, J. H. Ryu, C. E. Daniels, The burden of idiopathic pulmonary fibrosis: An unmet public health need, *Respir. Med.* **108**, 955–967 (2014).
166. R. C. Chambers, P. F. Mercer, in *Annals of the American Thoracic Society*, (2015), vol. 12, pp. S16–S20.
167. P. J. Wolters, H. R. Collard, K. D. Jones, Pathogenesis of idiopathic pulmonary fibrosis., *Annu. Rev. Pathol.* **9**, 157–79 (2014).
168. E. Gaude, C. Frezza, Defects in mitochondrial metabolism and cancer., *Cancer Metab.* **2**, 10 (2014).
169. C. S. Palmer, M. Ostrowski, B. Balderson, N. Christian, S. M. Crowe, Glucose metabolism regulates T cell activation, differentiation, and functions., *Front. Immunol.* **6**, 1 (2015).

170. L. A. J. O. Neill, E. J. Pearce, Immunometabolism governs dendritic cell and macrophage function, , 15–23 (2016).
171. R. A. Saxton, D. M. Sabatini, mTOR Signaling in Growth, Metabolism, and Disease, *Cell* **168**, 960–976 (2017).
172. M. Haissaguerre, N. Saucisse, D. Cota, Influence of mTOR in energy and metabolic homeostasis, *Mol. Cell. Endocrinol.* **397**, 67–77 (2014).
173. Y.-S. Gui, L. Wang, X. Tian, X. Li, A. Ma, W. Zhou, N. Zeng, J. Zhang, B. Cai, H. Zhang, J.-Y. Chen, K.-F. Xu, mTOR Overactivation and Compromised Autophagy in the Pathogenesis of Pulmonary Fibrosis., *PLoS One* **10**, e0138625 (2015).
174. S. K. Madala, V. Sontake, R. Edukulla, C. R. Davidson, S. Schmidt, W. D. Hardie, Unique and Redundant Functions of p70 Ribosomal S6 Kinase Isoforms Regulate Mesenchymal Cell Proliferation and Migration in Pulmonary Fibrosis, *Am. J. Respir. Cell Mol. Biol.* **55**, 792–803 (2016).
175. Y. Romero, M. Bueno, R. Ramirez, D. ??lvarez, J. C. Sembrat, E. A. Goncharova, M. Rojas, M. Selman, A. L. Mora, A. Pardo, mTORC1 activation decreases autophagy in aging and idiopathic pulmonary fibrosis and contributes to apoptosis resistance in IPF fibroblasts, *Aging Cell* **15**, 1103–1112 (2016).
176. N. R. Simler, D. C. J. Howell, R. P. Marshall, N. R. Goldsack, P. S. Hasleton, G. J. Laurent, R. C. Chambers, J. J. Egan, The rapamycin analogue SDZ RAD attenuates bleomycin-induced pulmonary fibrosis in rats., *Eur. Respir. J.* **19**, 1124–7 (2002).
177. B. Tulek, E. Kiyan, H. Toy, A. Kiyici, C. Narin, M. Suerdem, Anti-inflammatory and anti-fibrotic effects of sirolimus on bleomycin-induced pulmonary fibrosis in rats., *Clin. Invest. Med.* **34**, E341 (2011).

178. R. a Rahimi, M. Andrianifahanana, M. C. Wilkes, M. Edens, T. J. Kottom, J. Blenis, E. B. Leof, Distinct roles for mammalian target of rapamycin complexes in the fibroblast response to transforming growth factor-beta., *Cancer Res.* **69**, 84–93 (2009).
179. H. Zheng, J. Wu, Z. Jin, L.-J. Yan, Protein Modifications as Manifestations of Hyperglycemic Glucotoxicity in Diabetes and Its Complications., *Biochem. insights* **9**, 1–9 (2016).
180. R. Zoncu, A. Efeyan, D. M. Sabatini, mTOR: from growth signal integration to cancer, diabetes and ageing., *Nat. Rev. Mol. Cell Biol.* **12**, 21–35 (2011).
181. J. Vande Voorde, T. Ackermann, N. Pfetzer, D. Sumpton, G. Mackay, G. Kalna, C. Nixon, K. Blyth, E. Gottlieb, S. Tardito, Improving the metabolic fidelity of cancer models with a physiological cell culture medium, *Sci. Adv.* **5**, eaau7314 (2019).
182. B. Hinz, The myofibroblast: paradigm for a mechanically active cell., *J. Biomech.* **43**, 146–55 (2010).
183. U. Negmadjanov, Z. Godic, F. Rizvi, L. Emelyanova, G. Ross, J. Richards, E. L. Holmuhamedov, A. Jahangir, TGF-β1-mediated differentiation of fibroblasts is associated with increased mitochondrial content and cellular respiration., *PLoS One* **10**, e0123046 (2015).
184. K. Bernard, N. J. Logsdon, S. Ravi, N. Xie, B. P. Persons, S. Rangarajan, J. W. Zmijewski, K. Mitra, G. Liu, V. M. Darley-Usmar, V. J. Thannickal, Metabolic reprogramming is required for myofibroblast contractility and differentiation, *J. Biol. Chem.* **290**, 25427–25438 (2015).
185. Y.-W. Kim, J. Park, H.-J. Lee, S.-Y. Lee, S.-J. Kim, TGF-β sensitivity is determined by N-linked glycosylation of the type II TGF-β receptor., *Biochem. J.* **445**, 403–11 (2012).

186. T. Kitagawa, A. Masumi, Y. Akamatsu, Transforming growth factor-??1 stimulates glucose uptake and the expression of glucose transporter mRNA in quiescent Swiss mouse 3T3 cells, *J. Biol. Chem.* **266**, 18066–18071 (1991).
187. A. Masumi, Y. Akamatsu, T. Kitagawa, Modulation of the synthesis and glycosylation of the glucose transporter protein by transforming growth factor-beta 1 in Swiss 3T3 fibroblasts., *Biochim. Biophys. Acta* **1145**, 227–34 (1993).
188. M. Andrianifahanana, D. M. Hernandez, X. Yin, J.-H. Kang, M.-Y. Jung, Y. Wang, E. S. Yi, A. C. Roden, A. H. Limper, E. B. Leof, Profibrotic up-regulation of glucose transporter 1 by TGF-β involves activation of MEK and mammalian target of rapamycin complex 2 pathways, *FASEB J.* **30**, 3733–3744 (2016).
189. R. Nigdelioglu, R. B. Hamanaka, A. Y. Meliton, E. O'Leary, L. J. Witt, T. Cho, K. Sun, C. Bonham, D. Wu, P. S. Woods, A. N. Husain, D. Wolfgeher, N. O. Dulin, N. S. Chandel, G. M. Mutlu, Transforming Growth Factor (TGF)-β Promotes de Novo Serine Synthesis for Collagen Production., *J. Biol. Chem.* **291**, 27239–27251 (2016).
190. B. Selvarajah, I. Azuelos, M. Platé, D. Guillotin, E. J. Forty, G. Contento, H. V. Woodcock, M. Redding, A. Taylor, G. Brunori, P. F. Durrenberger, R. Ronzoni, A. D. Blanchard, P. F. Mercer, D. Anastasiou, R. C. Chambers, mTORC1 amplifies the ATF4-dependent de novo serine-glycine pathway to supply glycine during TGF-β_1–induced collagen biosynthesis, *Sci. Signal.* **12**, eaav3048 (2019).
191. L. Kozma, K. Baltensperger, J. Klarlund, A. Porras, E. Santos, M. P. Czech, The ras signaling pathway mimics insulin action on glucose transporter translocation., *Proc. Natl. Acad. Sci. U. S. A.*

90, 4460–4 (1993).
192. J. A. Wofford, H. L. Wieman, S. R. Jacobs, Y. Zhao, J. C. Rathmell, IL-7 promotes Glut1 trafficking and glucose uptake via STAT5-mediated activation of Akt to support T-cell survival., *Blood* **111**, 2101–11 (2008).
193. H. Makinoshima, M. Takita, K. Saruwatari, S. Umemura, Y. Obata, G. Ishii, S. Matsumoto, E. Sugiyama, A. Ochiai, R. Abe, K. Goto, H. Esumi, K. Tsuchihara, Signaling through the Phosphatidylinositol 3-Kinase (PI3K)/ Mammalian Target of Rapamycin (mTOR) Axis is Responsible for Aerobic Glycolysis mediated by Glucose Transporter in Epidermal Growth Factor Receptor (EGFR)-mutated Lung Adenocarcinoma, *J. Biol. Chem.* **290**, jbc.M115.660498 (2015).
194. A. Masumi, Y. Akamatsu, T. Kitagawa, Alteration by transforming growth factor-β1 of asparagine-linked sugar chains in glucose transporter protein in Swiss 3T3 cells, *Biochim. Biophys. Acta - Mol. Cell Res.* **1221**, 330–338 (1994).
195. R. Palorini, F. P. Cammarata, F. Cammarata, C. Balestrieri, A. Monestiroli, M. Vasso, C. Gelfi, L. Alberghina, F. Chiaradonna, Glucose starvation induces cell death in K-ras-transformed cells by interfering with the hexosamine biosynthesis pathway and activating the unfolded protein response., *Cell Death Dis.* **4**, e732 (2013).
196. H. Rubin, Deprivation of glutamine in cell culture reveals its potential for treating cancer., *Proc. Natl. Acad. Sci. U. S. A.* **116**, 6964–6968 (2019).
197. D. G. Hardie, AMP-activated protein kinase-an energy sensor that regulates all aspects of cell function, *Genes Dev.* **25**, 1895–1908 (2011).

198. S. Rangarajan, N. B. Bone, A. A. Zmijewska, S. Jiang, D. W. Park, K. Bernard, M. L. Locy, S. Ravi, J. Deshane, R. B. Mannon, E. Abraham, V. Darley-Usmar, V. J. Thannickal, J. W. Zmijewski, Metformin reverses established lung fibrosis in a bleomycin model, *Nat. Med.* **24**, 1121–1127 (2018).
199. S. J. Cho, J.-S. Moon, C.-M. Lee, A. M. K. Choi, H. W. Stout-Delgado, Glucose Transporter 1–Dependent Glycolysis Is Increased during Aging-Related Lung Fibrosis, and Phloretin Inhibits Lung Fibrosis, *Am. J. Respir. Cell Mol. Biol.* **56**, 521–531 (2017).
200. G. Leprivier, B. Rotblat, How does mTOR sense glucose starvation? AMPK is the usual suspect, *Cell Death Discov.* **6**, 27 (2020).
201. N. Sato, N. Takasaka, M. Yoshida, K. Tsubouchi, S. Minagawa, J. Araya, N. Saito, Y. Fujita, Y. Kurita, K. Kobayashi, S. Ito, H. Hara, T. Kadota, H. Yanagisawa, M. Hashimoto, H. Utsumi, H. Wakui, J. Kojima, T. Numata, Y. Kaneko, M. Odaka, T. Morikawa, K. Nakayama, H. Kohrogi, K. Kuwano, Metformin attenuates lung fibrosis development via NOX4 suppression, *Respir. Res.* **17**, 107 (2016).
202. A. G. Ladurner, Rheostat control of gene expression by metabolites., *Mol. Cell* **24**, 1–11 (2006).
203. R. M. Kottmann, E. Trawick, J. L. Judge, L. A. Wahl, A. P. Epa, K. M. Owens, T. H. Thatcher, R. P. Phipps, P. J. Sime, Pharmacologic inhibition of lactate production prevents myofibroblast differentiation, (available at http://ajplung.physiology.org/content/ajplung/309/11/L1305.full.pdf).
204. K. Bernard, N. J. Logsdon, S. Ravi, N. Xie, B. P. Persons, S.

Rangarajan, J. W. Zimjewski, K. Mitra, G. Liu, V. M. Darley-Usmar, V. J. Thannickal, J. W. Zmijewski, K. Mitra, G. Liu, V. M. Darley-Usmar, V. J. Thannickal, Metabolic Reprogramming is Required for Myofibroblast Contractility and Differentiation, *J. Biol. Chem.* **290**, jbc.M115.646984 (2015).
205. X. Yin, M. Choudhury, J.-H. Kang, K. J. Schaefbauer, M.-Y. Jung, M. Andrianifahanana, D. M. Hernandez, E. B. Leof, Hexokinase 2 couples glycolysis with the profibrotic actions of TGF-β., *Sci. Signal.* **12** (2019), doi:10.1126/scisignal.aax4067.
206. N. Xie, Z. Tan, S. Banerjee, H. Cui, J. Ge, R. M. Liu, K. Bernard, V. J. Thannickal, G. Liu, Glycolytic reprogramming in myofibroblast differentiation and lung fibrosis, *Am. J. Respir. Crit. Care Med.* **192**, 1462–1474 (2015).
207. H. Yang, D. G. Rudge, J. D. Koos, B. Vaidialingam, H. J. Yang, N. P. Pavletich, mTOR kinase structure, mechanism and regulation, *Nature* **497**, 217–223 (2013).
208. M. A. Malouf, P. Hopkins, G. Snell, A. R. Glanville, Everolimus in IPF Study Investigators, An investigator-driven study of everolimus in surgical lung biopsy confirmed idiopathic pulmonary fibrosis., *Respirology* **16**, 776–83 (2011).
209. C. C. Thoreen, L. Chantranupong, H. R. Keys, T. Wang, N. S. Gray, D. M. Sabatini, A unifying model for mTORC1-mediated regulation of mRNA translation., *Nature* **485**, 109–13 (2012).
210. J. K. Mouw, G. Ou, V. M. Weaver, Extracellular matrix assembly: a multiscale deconstruction, *Nat. Rev. Mol. Cell Biol.* **15**, 771–785 (2014).
211. J. L. Yecies, B. D. Manning, Transcriptional control of cellular metabolism by mtor signaling, *Cancer Res.* **71**, 2815–2820 (2011).
212. H. P. Harding, Y. Zhang, H. Zeng, I. Novoa, P. D. Lu, M.

Calfon, N. Sadri, C. Yun, B. Popko, R. Paules, D. F. Stojdl, J. C. Bell, T. Hettmann, J. M. Leiden, D. Ron, An Integrated Stress Response Regulates Amino Acid Metabolism and Resistance to Oxidative Stress, *Mol. Cell* **11**, 619–633 (2003).
213. K. Ameri, A. L. Harris, Activating transcription factor 4, *Int. J. Biochem. Cell Biol.* **40**, 14–21 (2008).
214. E. Timosenko, H. Ghadbane, J. D. Silk, D. Shepherd, U. Gileadi, L. J. Howson, R. Laynes, Q. Zhao, R. L. Strausberg, L. R. Olsen, S. Taylor, F. M. Buffa, R. Boyd, V. Cerundolo, Nutritional Stress Induced by Tryptophan-Degrading Enzymes Results in ATF4-Dependent Reprogramming of the Amino Acid Transporter Profile in Tumor Cells., *Cancer Res.* **76**, 6193–6204 (2016).
215. E. Zhao, J. Ding, Y. Xia, M. Liu, B. Ye, J. H. Choi, C. Yan, Z. Dong, S. Huang, Y. Zha, L. Yang, H. Cui, H. F. Ding, KDM4C and ATF4 Cooperate in Transcriptional Control of Amino Acid Metabolism, *Cell Rep.* **14**, 506–519 (2016).
216. M. S. Kilberg, J. Shan, N. Su, ATF4-dependent transcription mediates signaling of amino acid limitation, *Trends Endocrinol. Metab.* **20**, 436–443 (2009).
217. M. Korfei, C. Ruppert, P. Mahavadi, I. Henneke, P. Markart, M. Koch, G. Lang, L. Fink, R.-M. Bohle, W. Seeger, T. E. Weaver, A. Guenther, Epithelial endoplasmic reticulum stress and apoptosis in sporadic idiopathic pulmonary fibrosis., *Am. J. Respir. Crit. Care Med.* **178**, 838–46 (2008).
218. I. Ben-Sahra, G. Hoxhaj, S. J. H. Ricoult, J. M. Asara, B. D. Manning, mTORC1 induces purine synthesis through control of the mitochondrial tetrahydrofolate cycle., *Science* **351**, 728–33 (2016).
219. H. A. Baek, D. S. Kim, H. S. Park, K. Y. Jang, M. J. Kang, D. G. Lee, W. S. Moon, H. J. Chae, M. J. Chung, Involvement of

Endoplasmic Reticulum Stress in Myofibroblastic Differentiation of Lung Fibroblasts, *Am. J. Respir. Cell Mol. Biol.* **46**, 731–739 (2012).
220. N. J. Moerke, H. Aktas, H. Chen, S. Cantel, M. Y. Reibarkh, A. Fahmy, J. D. Gross, A. Degterev, J. Yuan, M. Chorev, J. A. Halperin, G. Wagner, Small-molecule inhibition of the interaction between the translation initiation factors eIF4E and eIF4G., *Cell* **128**, 257–67 (2007).
221. L. Chen, B. H. Aktas, Y. Wang, X. He, R. Sahoo, N. Zhang, S. Denoyelle, E. Kabha, H. Yang, R. Y. Freedman, J. G. Supko, M. Chorev, G. Wagner, J. A. Halperin, Tumor suppression by small molecule inhibitors of translation initiation., *Oncotarget* **3**, 869–81 (2012).
222. S. Willimott, D. Beck, M. J. Ahearne, V. C. Adams, S. D. Wagner, Cap-Translation Inhibitor, 4EGI-1, Restores Sensitivity to ABT-737 Apoptosis through Cap-Dependent and -Independent Mechanisms in Chronic Lymphocytic Leukemia, *Clin. Cancer Res.* **19**, 3212–3223 (2013).
223. E. M. O'Leary, Y. Tian, R. Nigdelioglu, L. J. Witt, R. Cetin-Atalay, A. Y. Meliton, P. S. Woods, L. M. Kimmig, K. A. Sun, G. A. Gökalp, G. M. Mutlu, R. B. Hamanaka, TGF-β Promotes Metabolic Reprogramming in Lung Fibroblasts via mTORC1-dependent ATF4 Activation, *Am. J. Respir. Cell Mol. Biol.* **63**, 601–612 (2020).
224. J. Ye, A. Mancuso, X. Tong, P. S. Ward, J. Fan, J. D. Rabinowitz, C. B. Thompson, Pyruvate kinase M2 promotes de novo serine synthesis to sustain mTORC1 activity and cell proliferation, *Proc. Natl. Acad. Sci.* **109**, 6904–6909 (2012).
225. T. Murakami, T. Nishiyama, T. Shirotani, Y. Shinohara, M. Kan, K. Ishii, F. Kanai, S. Nakazuru, Y. Ebina, Identification of two

enhancer elements in the gene encoding the type 1 glucose transporter from the mouse which are responsive to serum, growth factor, and oncogenes., *J. Biol. Chem.* **267**, 9300–6 (1992).
226. N. Samih, S. Hovsepian, A. Aouani, D. Lombardo, G. Fayet, Glut-1 translocation in FRTL-5 thyroid cells: role of phosphatidylinositol 3-kinase and N-glycosylation., *Endocrinology* **141**, 4146–55 (2000).
227. J. Aramburu, M. C. Ortells, S. Tejedor, M. Buxadé, C. López-Rodríguez, Transcriptional regulation of the stress response by mTOR., *Sci. Signal.* **7**, re2 (2014).
228. A. A. Goldberg, B. Nkengfac, A. M. J. Sanchez, N. Moroz, S. T. Qureshi, A. E. Koromilas, S. Wang, Y. Burelle, S. N. Hussain, A. S. Kristof, Regulation of ULK1 expression and autophagy by STAT1, *J. Biol. Chem.* **292**, jbc.M116.771584 (2016).
229. K. Düvel, J. L. Yecies, S. Menon, P. Raman, A. I. Lipovsky, A. L. Souza, E. Triantafellow, Q. Ma, R. Gorski, S. Cleaver, M. G. Vander Heiden, J. P. MacKeigan, P. M. Finan, C. B. Clish, L. O. Murphy, B. D. Manning, Activation of a metabolic gene regulatory network downstream of mTOR complex 1, *Mol. Cell* **39**, 171–183 (2010).
230. H. Pópulo, J. M. Lopes, P. Soares, The mTOR signalling pathway in human cancer., *Int. J. Mol. Sci.* **13**, 1886–918 (2012).
231. C. D. Cool, S. D. Groshong, P. R. Rai, P. M. Henson, J. S. Stewart, K. K. Brown, Fibroblast foci are not discrete sites of lung injury or repair: The fibroblast reticulum, *Am. J. Respir. Crit. Care Med.* **174**, 654–658 (2006).
232. R. Kalluri, The biology and function of fibroblasts in cancer, *Nat. Rev. Cancer* **16**, 582–598 (2016).
233. E. S. White, R. G. Atrasz, B. Hu, S. H. Phan, V. Stambolic, T.

W. Mak, C. M. Hogaboam, K. R. Flaherty, F. J. Martinez, C. D. Kontos, G. B. Toews, Negative Regulation of Myofibroblast Differentiation by PTEN (Phosphatase and Tensin Homolog Deleted on Chromosome 10), *Am. J. Respir. Crit. Care Med.* **173**, 112–121 (2006).

234. R. B. Hamanaka, R. Nigdelioglu, A. Y. Meliton, Y. Tian, L. J. Witt, E. O'Leary, K. A. Sun, P. S. Woods, D. Wu, B. Ansbro, S. Ard, J. M. Rohde, N. O. Dulin, R. D. Guzy, G. M. Mutlu, Inhibition of Phosphoglycerate Dehydrogenase Attenuates Bleomycin-induced Pulmonary Fibrosis, *Am. J. Respir. Cell Mol. Biol.* **58**, 585–593 (2018).

235. G. S. Ducker, L. Chen, R. J. Morscher, J. M. Ghergurovich, M. Esposito, X. Teng, Y. Kang, J. D. Rabinowitz, Reversal of Cytosolic One-Carbon Flux Compensates for Loss of the Mitochondrial Folate Pathway, *Cell Metab.* **23**, 1140–1153 (2016).

236. H. Patel, E. Di Pietro, R. E. MacKenzie, Mammalian fibroblasts lacking mitochondrial NAD+-dependent methylenetetrahydrofolate dehydrogenase-cyclohydrolase are glycine auxotrophs., *J. Biol. Chem.* **278**, 19436–41 (2003).

237. K. Bernard, N. J. Logsdon, G. A. Benavides, Y. Sanders, J. Zhang, V. M. Darley-Usmar, V. J. Thannickal, Glutaminolysis is required for transforming growth factor-β1–induced myofibroblast differentiation and activation, *J. Biol. Chem.* **293**, 1218–1228 (2018).

238. J. Ge, H. Cui, N. Xie, S. Banerjee, S. Guo, S. Dubey, S. Barnes, G. Liu, Glutaminolysis Promotes Collagen Translation and Stability via α-Ketoglutarate–mediated mTOR Activation and Proline Hydroxylation, *Am. J. Respir. Cell Mol. Biol.* **58**, 378–390 (2018).

239. A. Barbul, Proline precursors to sustain Mammalian collagen synthesis., *J. Nutr.* **138**, 2021S-2024S (2008).
240. T. Lung, T. Unit, S. Vincent, N. S. Wales, L. T. Program, An investigator-driven study of everolimus in surgical lung biopsy confirmed idiopathic pulmonary fibrosis, **2011**, 776–783 (2011).
241. H. Hua, Q. Kong, H. Zhang, J. Wang, T. Luo, Y. Jiang, Targeting mTOR for cancer therapy, *J. Hematol. Oncol.* **12**, 71 (2019).
242. D. Cervantes-Madrid, Y. Romero, A. Dueñas-González, Reviving Lonidamine and 6-Diazo-5-oxo-L-norleucine to Be Used in Combination for Metabolic Cancer Therapy., *Biomed Res. Int.* **2015**, 690492 (2015).
243. D. Singh, A. K. Banerji, B. S. Dwarakanath, R. P. Tripathi, J. P. Gupta, T. L. Mathew, T. Ravindranath, V. Jain, Optimizing Cancer Radiotherapy with 2-Deoxy-D-Glucose, *Strahlentherapie und Onkol.* **181**, 507–514 (2005).
244. B. K. Mohanti, G. K. Rath, N. Anantha, V. Kannan, B. S. Das, B. A. R. Chandramouli, A. K. Banerjee, S. Das, A. Jena, R. Ravichandran, U. P. Sahi, R. Kumar, N. Kapoor, V. K. Kalia, B. S. Dwarakanath, V. Jain, Improving cancer radiotherapy with 2-deoxy-d-glucose: phase I/II clinical trials on human cerebral gliomas, *Int. J. Radiat. Oncol.* **35**, 103–111 (1996).
245. N. Sun, I. E. Fernandez, M. Wei, M. Witting, M. Aichler, A. Feuchtinger, G. Burgstaller, S. E. Verleden, P. Schmitt-Kopplin, O. Eickelberg, A. Walch, Pharmacometabolic response to pirfenidone in pulmonary fibrosis detected by MALDI-FTICR-MSI., *Eur. Respir. J.* **52**, 1702314 (2018).

Publications

1. mTORC1 amplifies the ATF4-dependent de novo serine-glycine pathway to supply glycine during TGF-β1–induced collagen biosynthesis. B.Selvarajah, I. Azuelos… R.Chambers. Science Signaling 2019 May 21;12(582)

Prizes

1. ERS Lung Science Conference – Best Oral Presentation. “Metabolic Reprogramming in IPF” (March 2017)

2. ERS Lung Science Bursary (March 2017)

3. UCL Dean’s Research Prize – Postgraduate PhD research prize. “ Metabolic Reprogramming in IPF” (February 2017)

4. UCL Division of Medicine PhD seminar Prize – ‘Metabolic Reprogramming in IPF” (December 2016)

Appendix

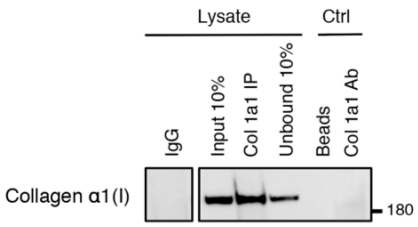

Appendix 1 Immunoprecipitation of collagen α1(I) : Confluent pHLFs were stimulated with TGF-β_1 prior to immunoprecipitation of collagen α1(I) from lysates. Immunoprecipitates, whole cell lysates, and flow-through were immunoblotted for collagen α1(I). Immunoprecipitation with an antibody against IgG, protein G agarose beads, and collagen type α1(I) antibody alone are negative controls. Data is representative of N= 3 independent experiments.

Appendix 2

Table 3.1 MetaCore pathways enriched in the rapamycin-insensitive mTOR module.

Pathway	P value	Genes
Glycine, serine, cysteine and threonine metabolism	5.45E-05	CBS,GARS,PHGDH,PISD,PSAT1,PSPH,SHMT2
Signal transduction_mTORC1 downstream signaling	0.000743439	CCND2,EIF4A2,EIF4EBP1,GRB10,MTHFD2,POLR3K, SLC2A1,SREBF2
L-Alanine and L-cysteine metabolism	0.000942113	CBS,GOT1,GPT2,PC
Translation_Insulin regulation of translation	0.002325036	EIF2B3,EIF2S2,EIF2S3,EIF4A2,EIF4EBP1,TSC1
Translation_Translation regulation by Alpha-1 adrenergic receptors	0.004874917	ADRA1B,EIF4A2,EIF4EBP1,GNB1,GNG11,RHOA
Tau pathology in Alzheimer disease	0.007691877	GPC1,GRIN2A,MARK1,SDC1,SDC2,TUBA1B,TUBB4B
Hypertrophy of asthmatic airway smooth muscle cells	0.009638728	EIF2B3,EIF2S2,EIF2S3,EIF4EBP1,IFNAR2,MAX
Immune response_Distinct metabolic pathways in naive and effector CD8+ T cells	0.011569384	EIF4EBP1,SLC1A5,SLC2A1,SLC7A5,TSC1
Translation_Opioid receptors in regulation of translation	0.013771852	EIF4EBP1,GNB1,GNG11,PENK
Apoptosis and survival_Endoplasmic reticulum stress response pathway	0.014249639	BAK1,BCL2L11,EIF2S2,EIF2S3,HERPUD1
Folic acid metabolism	0.016973265	ALDH1L2,MTHFD2,SHMT2
Stem cells_Excitotoxicity of Glutamate in glioblastoma	0.017731496	GNB1,GNG11,GOT1,GRIN2A
Regulation of lipid metabolism_Alpha-1 adrenergic receptors signaling via arachidonic acid	0.018431849	ADRA1B,GNB1,GNG11,PTGS1,RHOA
Fenofibrate in treatment of type 2 diabetes and metabolic syndrome X	0.01906206	ABCA1,ACSL4,RBP4
DeltaF508-CFTR traffic / Sorting endosome formation in CF	0.021286737	NSF,RAB7A,VPS25
Apoptosis and survival_Role of nuclear PI3K in NGF/ TrkA signaling	0.023647542	ACIN1,BCL2L11,NPM1
Role of ER stress in obesity and type 2 diabetes	0.024016297	ATF3,PCK2,SREBF2,TRIB3
Transcription_HIF-1 targets	0.025269769	ADRA1B,CCNG2,LOXL2,LOXL4,NPM1,SLC2A1
Cysteine-glutamate metabolism	0.027393787	CBS,GOT1
Muscle contraction_S1P2 receptor-mediated smooth muscle contraction	0.031496271	GNB1,GNG11,MYL7,RHOA
Proteolysis_Role of Parkin in the Ubiquitin-Proteasomal Pathway	0.032207644	PSMD11,SIAH2,TUBA1B,TUBB4B,UBE2G2
Sulfur metabolism	0.032360777	CBS,GOT1
Apoptosis and survival_Granzyme A signaling	0.033557078	ANP32A,APEX1,HIST1H2BD,HIST2H2BE

Neurophysiological process_Dynein-dynactin motor complex in axonal transport in neurons	0.037276388	DYNLRB2,IPO5,MAPRE3,RAB7A,TUBA1B,TUBB4B
Development_PIP3 signaling in cardiac myocytes	0.042916214	CCND2,EIF4EBP1,GNB1,GNG11,TSC1
Stem cells_Role of GSK3 beta in cardioprotection against myocardial infarction	0.043951681	ADM2,BDKRB2,PENK
Transcription_CoREST complex-mediated epigenetic gene silencing	0.045019326	ELAC2,GRIN2A,SIN3A,SMARCC1
Signal transduction_AKT signaling	0.04754385	BCL2L11,CCND2,EIF4EBP1,TSC1